Progress in Polymer Science 38 (2013) 462–502

Contents lists available at SciVerse ScienceDirect

Progress in Polymer Science

journal homepage: www.elsevier.com/locate/ppolysci

Macromolecular MRI contrast agents: Structures, properties and applications

Jianbin Tang[a], Yuqi Sheng[a], Hongjie Hu[b], Youqing Shen[a,*]

[a] Key Laboratory of Biomass Chemical Engineering of Ministry of Education, Center for Bionanoengineering, and Department of Chemical and Biological Engineering, Zhejiang University, Hangzhou, Zhejiang 310027, China
[b] Department of Radiology, Sir Run Run Shaw Hospital (SRRSH) of School of Medicine, Zhejiang University, Hangzhou, Zhejiang 310027, China

ARTICLE INFO

Article history:
Received 24 February 2012
Received in revised form 28 June 2012
Accepted 6 July 2012
Available online 16 July 2012

Keywords:
Magnetic resonance imaging
Contrast agent
Macromolecular contrast agent
Dendrimer
Blood pool agent
Tumor imaging

ABSTRACT

Stable gadolinium chelates are widely used as the contrast agents (CAs) for magnetic resonance imaging (MRI). Conjugation of the chelates onto macromolecular carriers forms macromolecular CAs (mCAs). Compared with small molecule MRI CAs, mCAs have advantages of high relaxivity and prolonged retention in blood circulation. Variants of mCAs have been synthesized and tested using animal models, showing their great potential applications in angiography, cancer imaging, kidney imaging, liver imaging, lymphatic imaging, and noninvasive visualization of drug delivery. Herein, the state of the art of mCAs, including their structures, properties, and applications is reviewed and future directions for developing mCAs are suggested.

Contents

* Corresponding author.
E-mail address: shenyq@zju.edu.cn (Y. Shen).

0079-6700/$ – see front matter © 2012 Elsevier Ltd. All rights reserved.
http://dx.doi.org/10.1016/j.progpolymsci.2012.07.001

1. Introduction

Magnetic resonance imaging (MRI) is a widely used medical imaging technique to visualize the structure and function of the body. Compared with other imaging techniques, such as computed tomography (CT), MRI has no radiation harm and provides great contrast between different soft tissues, making it widely used in neurological, musculoskeletal, cardiovascular, and oncological imaging [1]. To further improve the contrast of the imaging, MRI contrast agents (CAs) are generally needed to enhance the image contrast between normal and diseased tissues, and to indicate the status of organ function or blood flow. Currently, nearly half of all MRI studies are contrast enhanced, and the degree of contrast utilization is expected to increase in the future [2]. In 2006, contrast media (all imaging types) accounted for a total of $1.57 billion in revenue in the United States alone, $364 million (23%) of which was from sales of MRI CAs [2]. The development of novel MRI CAs remains an active area of research, with many new CAs currently in preclinical developments or in clinical trials [3].

Paramagnetic transition metal ion chelates (mainly gadolinium (Gd) chelates) and superparamagnetic iron oxide nanoparticles are the most widely studied and used MRI CAs. Paramagnetic transition metal ion chelates increase the signal intensity by decreasing the longitudinal (or spin-lattice) relaxation time (T_1) of H_2O. Many acyclic and macrocylic polyaminocarboxylate-Gd^{3+} chelates with various structures, shown in Fig. 1, have been clinically used [3]. In addition to them, a variety of chelates with different structures and functions have been reported as MRI CAs for various applications. The design, structure, theory, dynamics, and applications of small molecule MRI CAs with different ligands and transition metal ions can be found in recently published, high-quality reviews [1,4–7].

In contrast, the superparamagnetic nanoparticles that consist of specific iron oxide cores coated with macromolecular materials including dextran, carboxydextran, chitosan, starch, heparin, albumin and polystyrene, decrease the signal intensity by shortening transverse relaxation time of H_2O (T_2) [8]. Three iron oxide nanoparticle CAs including Feridex, Endorem, and Resovist have been approved for clinical use as liver-specific CAs. A detailed introduction of iron oxide nanoparticle CAs is available in recent reviews [9–11].

Currently, the development of MRI CAs is mainly focused on searching for CAs with high relaxivity, low toxicity, and tissue- or tumor-targeting capabilities. MRI CAs, i.e., Gd^{3+} chelates, conjugated with macromolecules, referred to as macromolecular CAs (mCAs), have shown great potential in improving contrast efficiency, providing tissue- or tumor-targeting capability, as well as conferring new functions for MRI. An increasing number of reports on the synthesis, structures, properties and applications of mCAs have been published [12–17], and several mCAs are undergoing clinical trials. The goal of this review is to summarize the research in this field and discuss the prospective directions for MRI mCAs.

2. Macromolecular effects on MRI CAs

2.1. Enhancing relaxivity (r_1)

Gd-based CAs play a role in MRI by increasing the longitudinal (or spin-lattice) relaxation rate ($1/T_1$) of H_2O protons, which is linearly dependant on the concentration of Gd chelates [Gd]. The capability of increasing the $1/T_1$ of H_2O protons for a CA is expressed in terms of relaxivity, r_1, which is defined as the slope of this dependence in a unit of $mM^{-1}\,s^{-1}$ (Eq. (1)). The r_1 is determined by both the nature of the CAs and the condition of the measurement [6].

$$\left(\frac{1}{T_1}\right)_{obsd} = \left(\frac{1}{T_1}\right)_{d} + r_1[\mathrm{Gd}] \quad (1)$$

The origin of paramagnetic relaxation enhancement is generally divided into two parts, inner-sphere and outer-sphere (Eq. (2)). The inner-sphere relaxation refers to the relaxation enhancement of H_2O directly coordinated to the transition metal, the outer-sphere relaxation refers to relaxation enhancement of H_2O in the second coordination sphere and beyond (i.e., bulk H_2O) [3,6].

$$\left(\frac{1}{T_1}\right)_{p} = \left(\frac{1}{T_1}\right)_{inner\ \ sphere} + \left(\frac{1}{T_1}\right)_{outer\ \ sphere} \quad (2)$$

The longitudinal relaxation contribution from the inner-sphere mechanism is determined by the number of H_2O molecules coordinated on Gd^{3+}, the exchange rate of H_2O molecules between the coordinated H_2O and bulk H_2O, and the relaxation time of the bound H_2O, as shown in Eq. (3) [3,6].

$$\left(\frac{1}{T_1}\right)_{inner\ \ sphere} = \frac{P_M q}{T_{1M} + \tau_M} \quad (3)$$

where P_M is the mole fraction of Gd^{3+}, T_{1M} is the relaxation time of the coordinated H_2O on Gd^{3+}, τ_M is the residence lifetime of the coordinated H_2O. The T_{1M} is given by the Solomon–Bloembergen equations, which represent

Nomenclature

$1/T_1$	longitudinal (or spin-lattice) relaxation rate
$1/T_2$	transverse relaxation rate
1B4M	2-(p-isothiocyanatobenzyl)-6-methyl-diethylenetriaminepenta acetic acid
A549	human lung carcinoma cell line
AIBN	azobisisobutyronitrile
BSA	bovine serum albumin
BxPC3	orthotopic pancreatic cancer model
CAs	contrast agents
CD	β-cyclodextrin
CMDA	dextran
CMHES	carboxymethyl hydroxyethyl starch
CP	conjugated polymer
DAB	poly(propylene imine) dendrimer with 1,4-diaminobutane
DACHPt	(1,2-diaminocyclohexane)platinum (II)
DCE	dynamic contrast-enhanced
DCE-MRI	dynamic contrast-enhanced MR imaging
DDS	drug delivery system
DNC	dendrimer nanocluster
DOTA-Gd^{3+}	1,4,7,10-tetraaza cyclododecane-1,4,7,10-tetraacetic acid Gd^{3+} chelate
DTPA-Gd^{3+}	diethylenetriaminepentaacetic acid Gd^{3+} chelate
DTPA-OSU	*N*-hydroxysuccinic acid DTPA ester
EA	esteramide
EPR	enhanced permeability and retention
G	generation
Gd	gadolinium
Gd-BOPTA	gadobenate dimeglumine
Gd-BT-DO_3A	gadobutrol
GDCC	(Gd-DTPA)-cystamine copolymers
GDCEP	(Gd-DTPA)-cystine diethyl ester copolymers
GDCP	(Gd-DTPA)-cystine copolymers
Gd-DOTA	gadoterate
Gd-DTPA	gadopentetate dimeglumine
Gd-DTPA-BMA	gadodiamide
Gd-DTPABMEA	gadoversetamide
Gd-EOB-DTPA	Eovist/Primovist
Gd-HP-DO_3A	gadoteridol
H22	hepatoma
HAS	human bovine serum albumin
HB	hyperbranched
Hela	human cervical carcinoma cell line
HOPO	1-Me-3,2-hydroxypyridinonate
HPMA	N-(2-hydroxypropyl)methacrylamide
HPTP	5-(p-carbonyloxy phenyl)-10,15,20-triphenylporphyrin
HSA	human serum albumin
IC-50	half maximal inhibitory concentration of a substance
K_{trans}	permeability values
Lu	letutium
mCA	macromolecular contrast agent
MIP	maximum intensity projection
MPEG-PL	PEG and polylysine block copolymer
MRA	magnetic resonance angiography
MRI	magnetic resonance imaging
MRL	micro-magnetic resonance lymphangiography
MVD	microvessel density
OAS	octasilsesquioxane
P(Glu)	poly(glutamic acid)
PAA	poly(acrylic acid)
PAMAM	poly(amidoamine) dendrimer
PEG	polyethylene glycol
PEI	poly(ethylene imine)
Peptide T7	sequenced HAIYPRH
PER	pentaerythritol
PG	poly(glutamic acid)
PG-*b*-PLA	poly(L-glutamic acid)-*b*-polylactide
PG-NH_2	amino-functionalized polyglycerol
PHPMA	poly[N-(2-hydroxypropyl)methacrylamide]
PL	polylysine
PLG	poly(L-glutamic acid)
PLL	poly(L-lysine)
PMA	poly(methylacrylate)
PMAA	poly(methacrylic acid)
PO	polyornithine
PPI	poly(propylene imine) dendrimers
$1/T_1$	longitudinal (or spin-lattice) relaxation rate
PSI	polysuccinimide derivatives
q	number of coordinated water
r_1	longitudinal (or spin-lattice) relaxivity
r_2	transverse relaxation relaxivity
RES	reticulo-endothelial system
SCK	shell-crosslinked nanoparticle
$t_{1/2}$	blood elimination half time
Tf	transferrin
Tf_R	transferrin receptor
THF	tetrahydrofuran
TREN	tris(2-aminoethyl)amine-2,3-dihydroxyterephthalamide disulfide
τ_M	exchange rate

the sum of dipolar ("through-space") and scalar, or contact ("through-bonds") contributions (Eq. (4)) [3,6].

$$\frac{1}{T_{1M}} = \frac{2}{15}\frac{\gamma_I^2 g^2 S((S+1)\beta^2)}{r^6}\left[\frac{7\tau_c}{(1+\omega_s^2\tau_c^2)} + \frac{3\tau_c}{(1+\omega_I^2\tau_c^2)}\right] + \frac{2}{3}S(S+1)\left(\frac{A}{\hbar}\right)^2\left[\frac{\tau_e}{(1+\omega_s{}^2\tau_c{}^2)}\right] \quad (4)$$

where γ_I is the proton gyromagnetic ratio, g is the electronic g-factor, S is the total electron spin of the metal ion, β is the Bohr Magneton, r is the proton–metal ion distance, ω_I and ω_s are the electronic and proton Larmor precession frequencies, respectively, and A/h is the electron–nuclear hyperfine coupling constant. The dipolar and scalar relaxation mechanisms are modulated by the correlation times τ_c and τ_e, as given by Eqs. (5) and (6):

$$\frac{1}{\tau_c} = \frac{1}{T_{1e}} + \frac{1}{\tau_M} + \frac{1}{\tau_R} \quad (5)$$

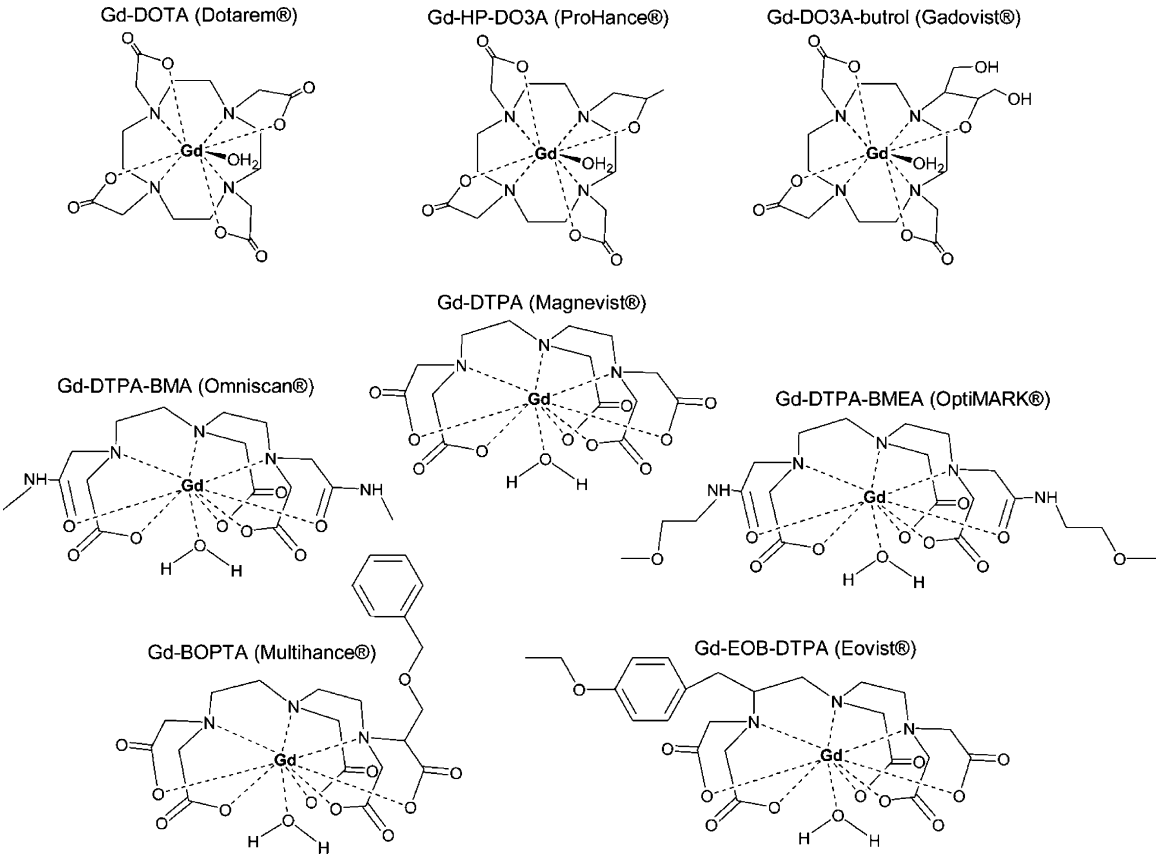

Fig. 1. Commercially available Gd^{3+} chelate MRI contrast agents. Reprinted from [3].

$$\frac{1}{\tau_e} = \frac{1}{T_{1e}} + \frac{1}{\tau_M} \tag{6}$$

where T_{1e} is the longitudinal electron spin relaxation time, τ_M is the H_2O residence time as mentioned above, and τ_R is the rotational tumbling time of the entire metal–H_2O unit. Rotation is perhaps the most critical variable in these equations. It was recognized early that the rotational correlation time of small Gd(III) chelates was the dominant contributor to the effective correlation time τ_c [3,6].

The conjugation of MRI CAs onto a macromolecule can efficiently retard the rotational motion of the complex and increase τ_R and thereby τ_c, substantially increasing r_1. For example, DTPA-Gd^{3+} conjugated to polylysine chains with the molecular weights ranging from 3.3 up to 102 kDa had a r_1 2.5 times higher than that of DTPA-Gd^{3+} alone (measured at 2.4 T), and the chain length did not significantly affect the r_1 [18]. The polymer property, especially, the rigidity, strongly affects the enhancement of the relaxivity for the mCAs. The rigid polymers can retard rotational motion of the complex more efficiently, and can therefore enhance the r_1 of CAs more significantly than the flexible polymers.

For instance, Langereis et al. conjugated DTPA-Gd^{3+} onto rigid poly(propylene imine) dendrimers (PPI, also abbreviated as DAB in some references, Fig. 2) [19,20] at different generations as mCAs. As shown in Fig. 3, the r_1 of the PPI-conjugated DTPA-Gd^{3+} increased as the PPI generation and thereby the rigidity increased. The fifth-generation (G5) PPI-CA displayed the highest ionic r_1 (per Gd) of 19.7 $mM^{-1}\,s^{-1}$, which was 4.7 times the ionic r_1 of DTPA-Gd^{3+} [21]. However, the flexible polyethylene glycol (PEG) had very little effect on the rotation correlation times of the Gd^{3+} chelates and therefore there was only a slight enhancement of their relaxivity, because the polymer contributed an almost negligible additional rigidity to the structure [22,23]. For example, the linear copolymers of Gd-DTPA-PEG with molecular weight ranging from 10 to 83 kDa had a r_1 of 6.0 $mM^{-1}\,s^{-1}$ at 37 °C and 20 MHz, only slightly higher than that of DTPA at same temperature and magnetic field.

Conjugation with polymers may reduce the number of the coordinated H_2O molecules (q) and slower the exchange rate between the coordinated H_2O and bulk H_2O (i.e., increase the τ_M of CAs). Therefore, polymer carriers, may actually decrease r_1 [24]. For example, when PEG was introduced to a rigid dendrimer conjugated with DOTA-Gd^{3+}, the PEG chains reduced the number of coordinated H_2O molecules and increase the τ_M of the dendritic mCA, and therefore, the r_1 decreased from 16.9 $mM^{-1}\,s^{-1}$ to 13.7 $mM^{-1}\,s^{-1}$ [24]. Doble et al. found

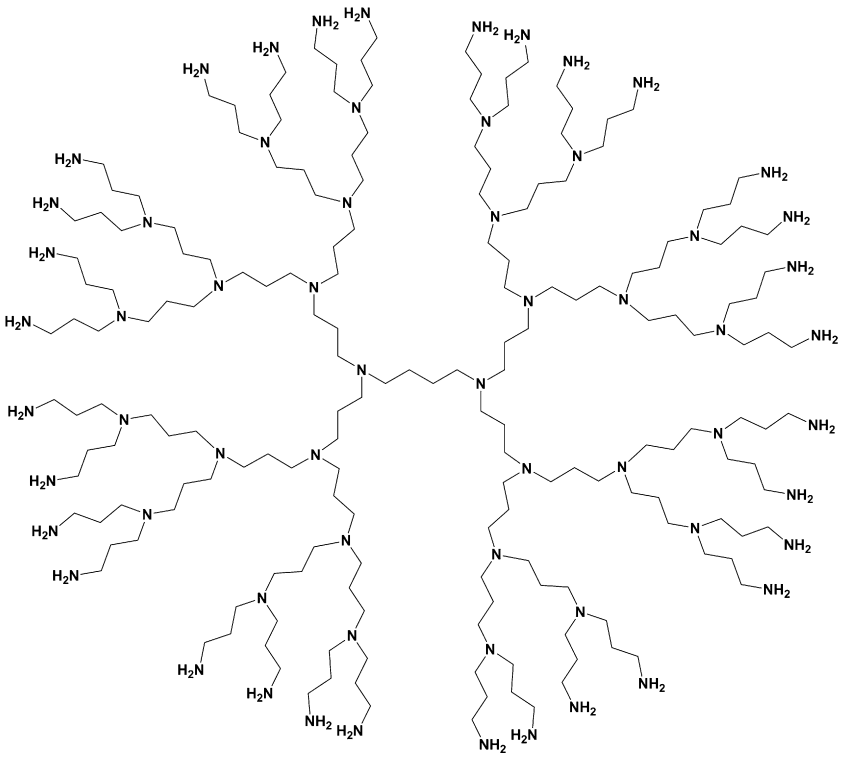

Fig. 2. PPI dendrimer with 1,4-diamine butane core (generation 4).

that in a non-polyaminocarboxylate Gd chelate, two H_2O molecules were coordinated to the Gd^{3+} ion. The chelate had an r_1 of 8.8 $mM^{-1}\,s^{-1}$, which was two times higher than that of a typical polyaminocarboxylate Gd chelate. When PEG chains of various molecular weights were grafted onto this chelate, the number of coordinated H_2O molecules decreased from two to one. As a result, the r_1 increase induced by the PEGylation was negligible [23].

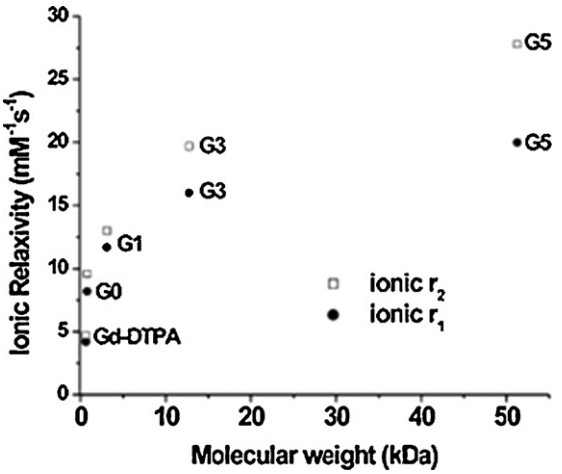

Fig. 3. The ionic relaxivities versus the generations (or molecular weight) of dendrimer-DTPA-Gd^{3+} CAs. Reprinted from [21].

2.2. Extending retention in blood circulation

Small molecule CAs are rapidly distributed into the extracellular fluid and excreted by glomerular filtration quickly after administration. For example, the distribution half-life and elimination half-life of DTPA-BMA-Gd^{3+} in a rat are 4.6 ± 1.7 and 18 ± 2.8 min, respectively [25]. However, cardiovascular and oncological MRIs require long blood pool retention, and long retention in the body can also provide a wider time frame for MRI [25]. Conjugation of CAs onto macromolecules can substantially increase the blood pool retention times of CAs since their large sizes prevent them from leaking out the blood vessel into the extracellular fluid and renal clearance [25].

The blood pharmacokinetics of mCAs is greatly affected by their size. Generally, the increment of blood circulation time is proportional to the molecular weight of the macromolecules [26–29]. For instance, Vexler et al. investigated the pharmacokinetics of the PLL-DTPA-Gd^{3+} (Fig. 4) in normal rats. The concentration of the small molecule DTPA-Gd^{3+} quickly decreased to a very low level after injection with a plasma clearance rate of 14.3 ± 3.8 mL/min/kg and a blood elimination half time ($t_{1/2}$) of 13.14 ± 2.39 min. In contrast, the PLL-DTPA-Gd^{3+} concentration decreased much more slowly and remained at a stable concentration for hours. The total plasma clearance rate of PLL-DTPA-Gd^{3+} decreased from 2.8 to 0.1 mL/min/kg as the molecular weight of the carrier PLL increased from 3.6 kDa to 480 kDa, and the $t_{1/2}$ increased from 65 to 429 min. Thus, the $t_{1/2}$ of a mCA can be easily tailored by changing the carrier's molecular weights [26]. In addition, the hydrophilicity, surface

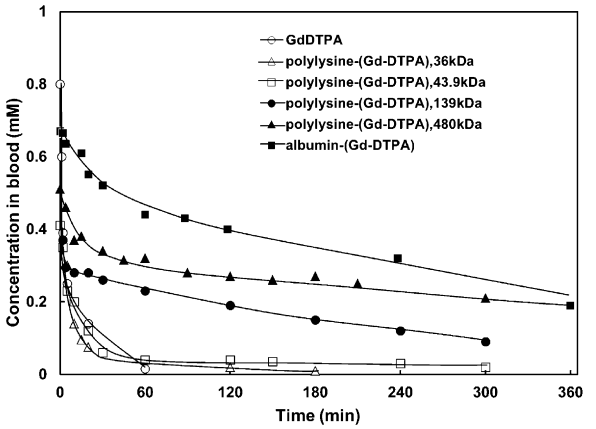

Fig. 4. Blood pharmacokinetic curves for PLL-DTPA-Gd^{3+}. Regenerated from [26].

modification, shape, and flexibility of mCAs also greatly affect their blood pharmacokinetics, which will be discussed in details in Section 4. In virtue of the variability of polymer structures, the pharmacokinetics and biodistribution of mCAs can be tailored according to various applications.

3. Structures and properties

A variety of mCAs have been reported, but they can be classified into four groups according to the position of the Gd^{3+} chelates in the carriers: (a) block, (b) graft, (c) dendritic, and (d) micellar mCAs, as illustrated in Fig. 5. For the block mCAs, the Gd chelates are incorporated into polymers by the condensation polymerization of DTPA dianhydride with diol or diamine monomers. As to the graft and dendritic mCAs, the Gd chelates are conjugated onto polymers through the reaction of bifunctional CAs with reactive groups such as amine group, carboxylic acid groups on the polymers. The micellar mCAs were made from emulsion polymerization or the assembly of the mCAs.

Various bifunctional polyaminocarboxylate ligands have been prepared for making mCAs. Their structures are shown in Fig. 6. In addition to the inherent carboxylic acid groups, the bifunctional CA ligands have other functional groups including anhydride [18], *N*-hydroxysuccinimide (NHS) activated carboxylic acid [18], isobutyl chloroformate activated carboxylic acid [30], amino [31–33], isothiocyanato [20,24,34–36], alkynyl [37–40], and squaric ester (SQ) groups [41] that can react with the reactive groups on polymers. The CA ligands with anhydride, NHS activated carboxylic acid, isobutyl chloroformate activated carboxylic acid, and SQ groups react with the amino groups on polymers, while those with amino groups react with the carboxylic acid group on polymers, and those with alkynyl react with azide group in polymers via a "click chemistry" reaction. Even through the CA ligands with anhydride, NHS activated carboxylic acid, isobutyl chloroformate activated carboxylic acid can be easily prepared, their conjugation reaction may cause the crosslinking of polymers. The conjugations with the CA ligands with isothiocyanato and alkynyl are efficient and have less side-reactions, but their synthesis is usually more complex [42]. An ideal conjugation method should have high efficiency and minimum side-reactions, and do not introduce harmful compounds into the mCAs.

The polyaminocarboxylate ligands are octadentate and thus they contain only one inner-coordination H_2O molecule ($q = 1$). Raymond et al., however, developed hexadentate oxygen donor chelators for Gd with the stabilities similar to those of the commercial polyaminocarboxylate CAs by utilizing the oxophilicity of gadolinium. These tris(2-aminoethyl)amine (TREN)-capped ligands, which contained either two

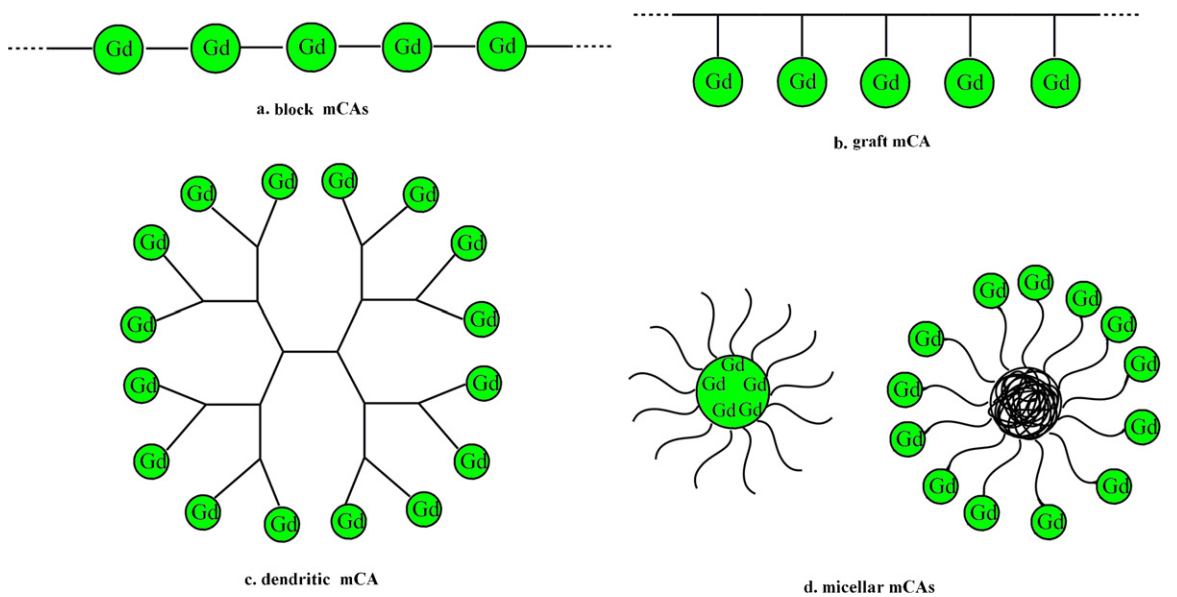

Fig. 5. The schematic structures of macromolecular contrast agents (mCAs).

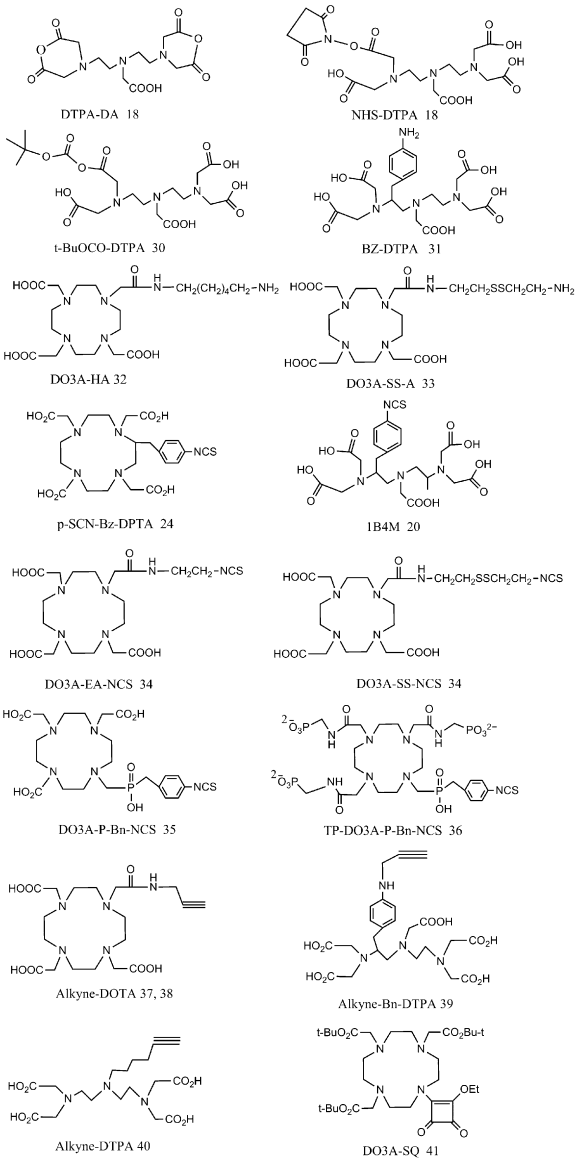

Fig. 6. The structures of the bifunctional MRI CA ligands.

1-Me-3,2-hydroxypyridinonate (HOPO) or two 1,2-HOPO rings and an amine-functionalized 2,3-dihydroxyterephthalamide (TAM) ring (Fig. 7) [43–47], had at least two coordinated H_2O molecules and exhibit high exchange rates, allowing for a much higher theoretical relaxivity than the small molecule amine-based chelators. The experiments indicated these complexes indeed had high r_1 (10–13 $mM^{-1}\,s^{-1}$) and thermodynamic complex stabilities (pGd ~ 17–18) [43,44]. A pendant amine was also introduced onto the 1-Me-3,2-HOPO-based ligands for conjugation with polymers (Fig. 7). Complex **1** had a short, rigid linker and a known q value of 2.2, Complex **2** had a longer, more flexible linkage incorporating a second ethylamine moiety, and Complex **3** had a branched linkage with a third ethylamine group. Complex **4**, which contained the 1,2-HOPO moiety, varied from these by its nitrogen substitution within the HOPO rings [48]. All these ligands were conjugated with polymers through the reaction between their amino group with the carboxylic acid groups on the polymers.

Most of the conjugates have the Gd^{3+} chelates conjugated onto the polymers by chemically stable bonds, which cannot degrade in vivo. In contrast, the polymers and Gd^{3+} chelates can also be connected by a biodegradable bond. The Gd^{3+} chelates can be cleaved from the polymer backbone in vivo, which can then be used to make excretable CAs [34]. For instance, in the conjugate shown in Fig. 8, the chelate DOTA-Gd^{3+} and the poly(L-glutamic acid) (PLG) polymer were linked by a disulfide bond, which could be broken by endogenous thiols. As a result, the DOTA-Gd^{3+} chelate could be cleaved from the PLG polymer chain in vivo and excreted out of the body, avoiding the systemic toxic problem due to the accumulation of Gd [33].

3.1. Block mCAs

The block mCAs are DTPA di-ester [49,50], or DTPA-bisamide [28,51–54] copolymers, in which Gd^{3+} chelates are inserted in the polymer backbones (Fig. 9). They were synthesized through the condensation polymerization of DTPA dianhydride with diol or diamine monomers and the following complexation with Gd^{3+}, and they could be further modified by grafting PEG onto them [53,55,56] (Fig. 9). In these mCAs, Gd^{3+} chelates were incorporated into the backbone of the polymers, which restricted the rotation of the CAs. Therefore, these mCAs had enhanced relaxivity due to the increase of τ_R, in comparison with the small molecule CAs. Their relaxivity properties of the reported block mCAs are summarized in Table 1. Since the value of r_1 is not only determined by the nature of the CAs, but also by the magnetic field and temperature for the measurement, when one compares the r_1s of the mCAs, it is necessary to pay attention to these measurement conditions. The r_1s of the DTPA-Gd^{3+} block mCAs were generally 1.5–2-fold of those for their corresponding small molecule CAs. The molecular weights of the polymers had a slight effect on their r_1s. For example, the r_1 of GDCP-Gd^{3+} increased from 5.4 to 6.8 $mM^{-1}\,s^{-1}$ as the molecular weight increased from 22 kDa to 62 kDa. The introduction of other polymer chains into the block mCAs had little effect on the r_1 [28]. For instance, GDCP-Gd^{3+} with and without grafting PEG had similar r_1s [53].

Most of the block mCAs were not biodegradable and thus might cause toxicity problems due to slow excretion. Lu et al. synthesized a series of biodegradable copolymers (GDCP, GDCEP, GDCC with the structures shown in Fig. 9) through the condensation polymerization of DTPA dianhydride with disulfide-functionalized diamine including cystamine, cystine, and cystine diethyl ester [28,52,53,56]. The disulfide bond could be broken in vivo through the reaction with the endogenous thiol-containing compounds including cysteine and glutathione [28,52,53,56]. For instance, the degradation of GDCC was very fast with a molecular weight reduction of approximately 28%, 33%, and 50% at 5, 15, and 60 min, respectively, in the incubation with 15 μM cysteine [29]. The degradation rate was significantly affected by the structures of the

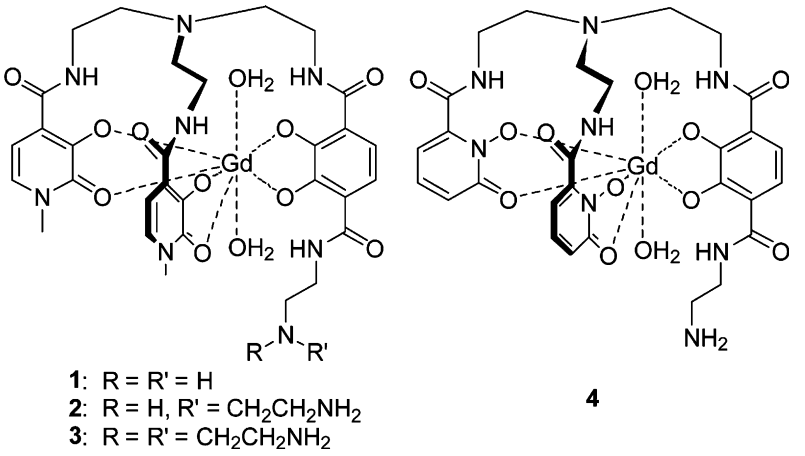

Fig. 7. Gd-TREN-bis(1-Me-3,2-HOPO)-TAM-ethylamine complexes **1**–**3** and Gd-TREN-bis(1,2-HOPO)-TAM-ethylamine complex. Reprinted from [48]. © 2011 with permission from ACS.

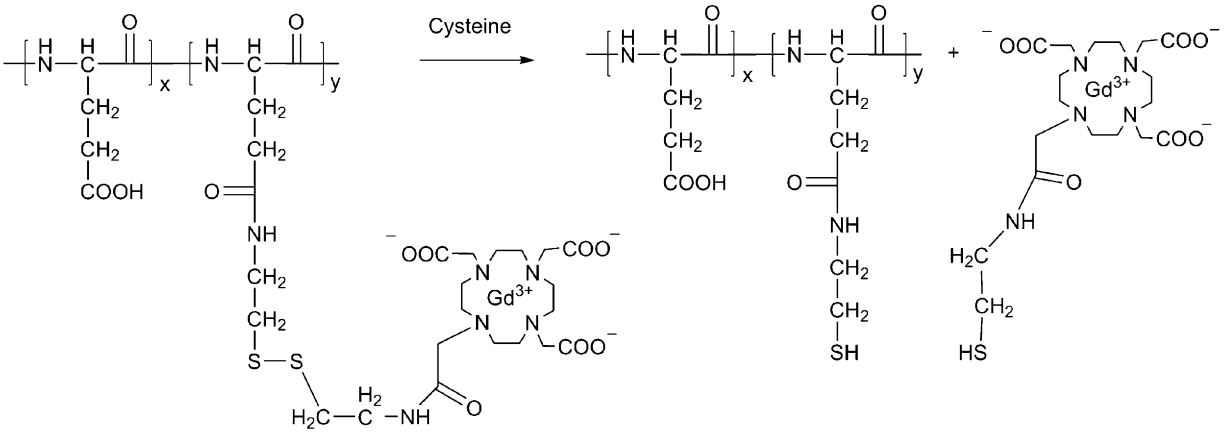

Fig. 8. Release of Gd(III)-DOTA from the conjugate by cysteine. Reprinted from [33]. © 2003 with permission from ACS.

copolymers. GDCEP with the ester substituent groups degraded slower than GDCC, with a molecular weight decrease of 6%, 11%, 15%, and 24% at 5, 15, 30, and 60 min, respectively. Even the GDCP with the carboxylic acid substituent groups showed no change in the molecular weight for 6 h under the same conditions [52]. The structure and biodegradability of the mCAs significantly affected their pharmacokinetics and blood pool

Table 1
The properties of block DTPA-Gd^{3+} copolymer agents.

mCA	Mw (kDa)	Ion r_1 ($mM^{-1}\,s^{-1}$)	Freq (MHz)	T (°C)	Ref.
HMD-DTPA-Gd^{3+}	7.9	8.2	10	25	[51]
CHD-DTPA-Gd^{3+}	8	9.5	10	25	[51]
PEG_{32}-DTPA-Gd^{3+}	22	6.0	20	40	[55]
GDCC-Gd^{3+}	17.7	4.42	64	37	[52]
	35	6.28			
GDCP-Gd^{3+}	62	6.8	128	25	[28]
	46	5.8			
	22	5.4			
GDCP-Gd^{3+}	28.1	8.31	128	21	[53]
GDCEP-Gd^{3+}	73	4.5	128	25	[28]
	48	4.8			
	34	4.6			
PEG_{2000}-GDCP-Gd^{3+}	37.8	8.73	128	21	[53,56]
PEG_{1000}-GDCP-Gd^{3+}	37.7	7.79	128	21	[53,56]
TA-DTPA-Gd^{3+}	18.6	4.7	400	310	[54]

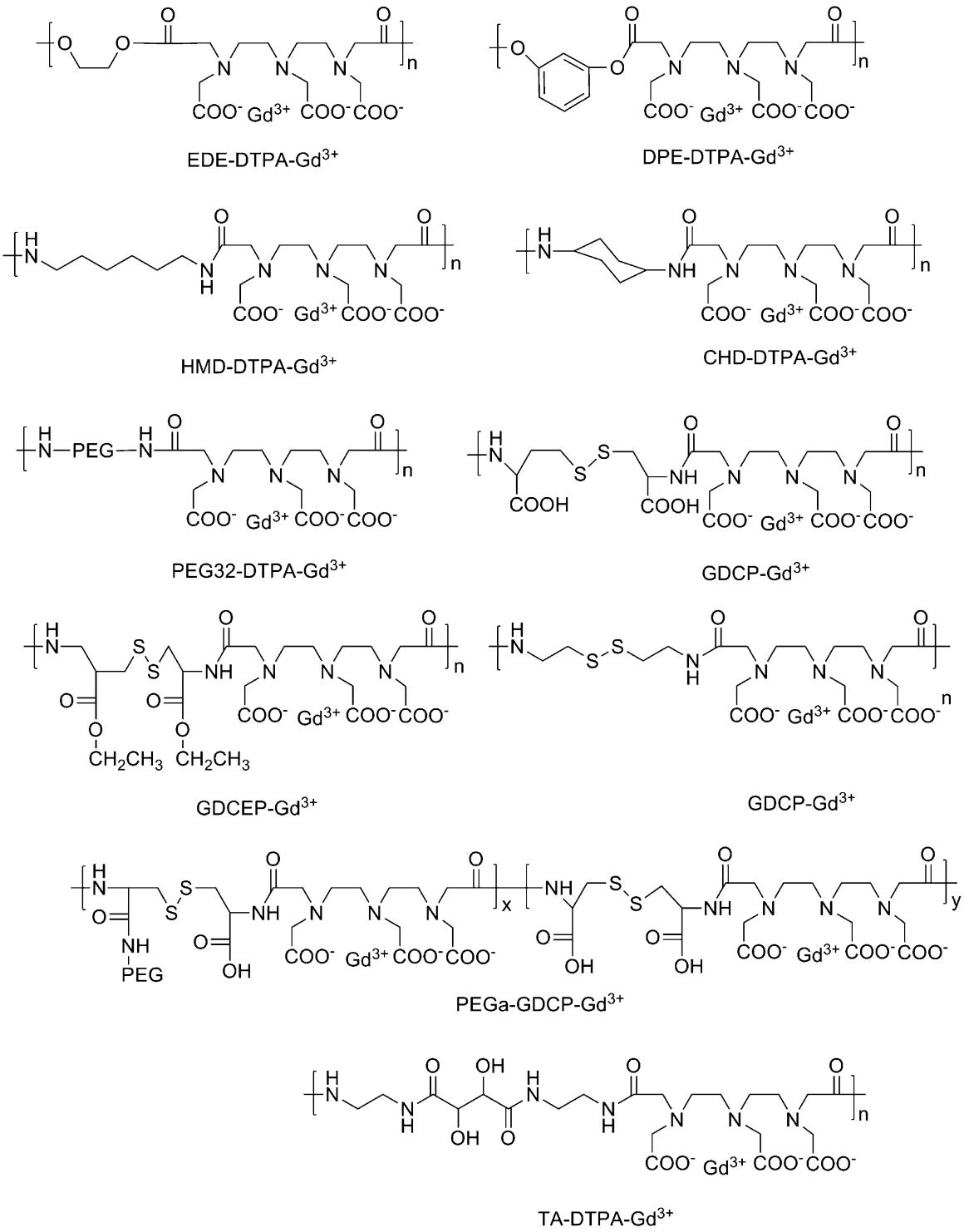

Fig. 9. The structures of the block DTPA-Gd^{3+} copolymers as CAs.

contrast enhancement. The GDCP and GDCEP had faster blood pool clearance than the non-biodegradable HMD-DTPA-Gd^{3+} with the structure shown in Fig. 9, and their long-term Gd(III) tissue retentions were substantially lower than the non-biodegradable mCAs. The negatively charged GDCP prolonged enhancement duration as compared with GDCEP [52], and the PEGylated GDCP was also prepared and showed further prolonged retention time as well as controllable degradation characteristics [53,56].

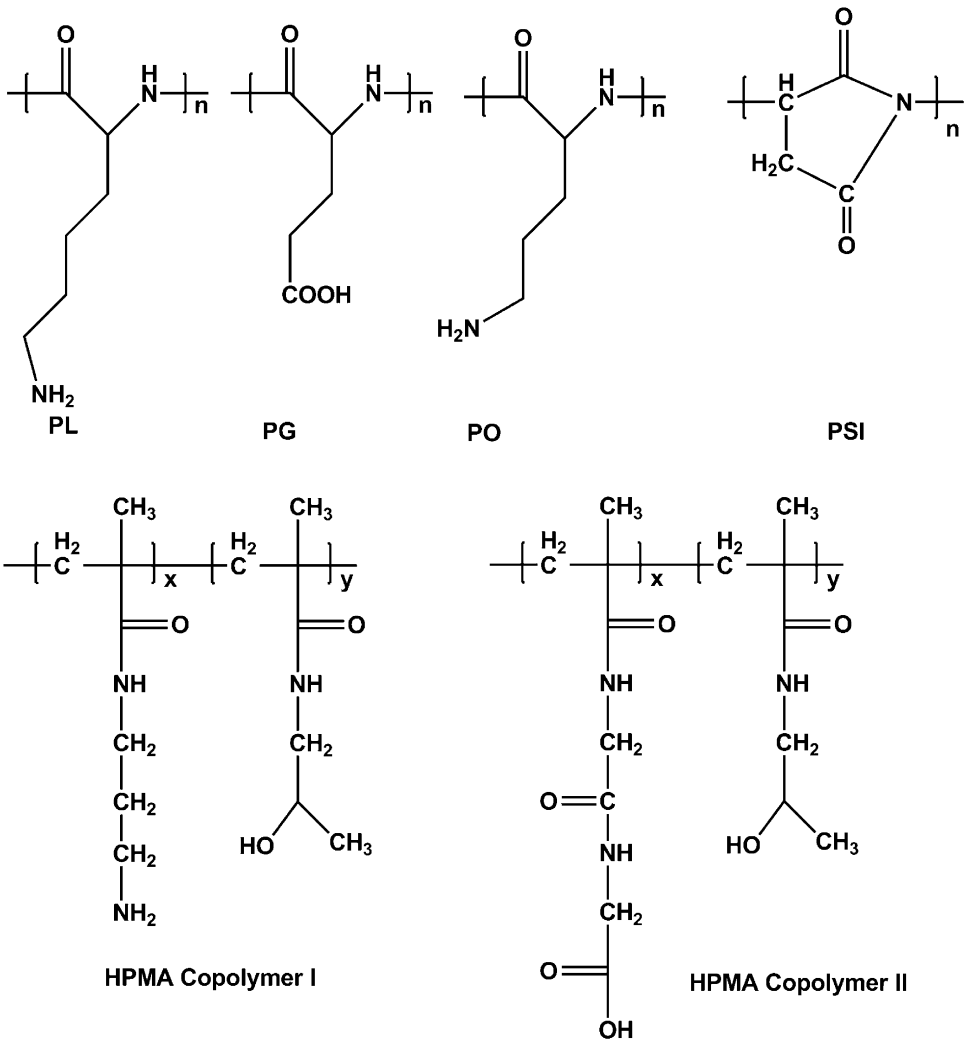

Fig. 10. The structures of the synthetic linear polymers used for making graft mCAs.

3.2. Graft mCAs

The graft mCAs are prepared through the conjugation of Gd^{3+} chelates onto the side groups of linear polymer carriers. The polymers used can be either synthetic or natural. The synthetic linear polymers used for making mCAs include polylysine (PL) [18,27,57–62], polyornithine (PO) [63,64], poly(glutamic acid) (PG) [5,31,33], poly[N-(2-hydroxypropyl)methacrylamide] (PHPMA) [31,65], poly(methacrylic acid) (PMAA) [66], polysuccinimide (PSI) derivatives [67], and other conjugated polymers. Their structures are shown in Fig. 10. PL is a synthetic cationic polypeptide with substantial amine groups to conjugate with CAs. PL conjugated with CAs not only show high r_1s, but also have low toxicity and immunogenicity [68]. PO has very similar structure and properties to PL [63,64]. In contrast, PG is an anionic synthetic polypeptide that can be readily degraded by lysosomal enzymes into its basic component, glutamic acid, a nontoxic natural compound [69,70], and it contains a large number of carboxyl acid groups for the CA attachment [5,31,33]. PSI is a poly(amino acid) derivative that has been used as drug carrier due to its biocompatibility and biodegradability, and it can be easily conjugated with CAs through its reaction with amino-functionalized CAs [71,72]. PHPMA is a neutral water-soluble polymer that has demonstrated good biocompatibility, and its conjugates with cancer drugs are currently under clinical trials for targeted cancer chemotherapy [73–75]. Since the hydroxyl groups in PHPMA have low reactivity, the copolymer of HPMA and other monomers with amino or carboxylic acid groups were prepared to introduce reactive groups for the conjugation with CAs [31,65]. The structures of HPMA copolymers are shown in Fig. 10. Recently, a conjugated polymer (CP) was also prepared and used as a CA carrier (Fig. 11). The conjugated polymer had a delocalized electronic structure, where the multiple and single bonds appear in turn along the backbone, making the CP more rigid than flexible polymers. This rigidity resulted in an increase in the τ_R and subsequently an increase in r_1. The

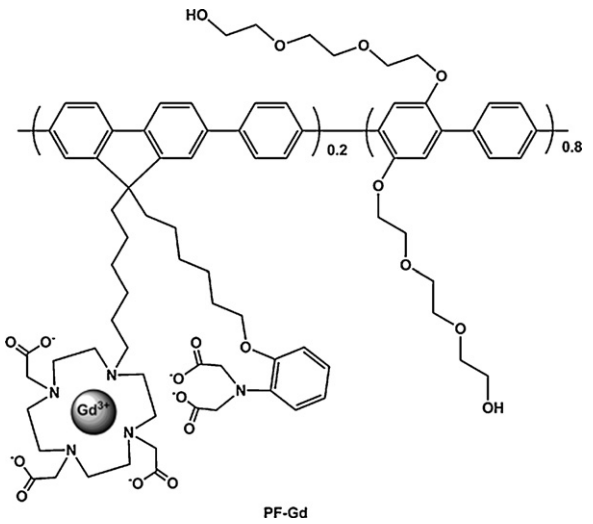

Fig. 11. The chemical structure of PF-Gd. Reprinted from [76]. © 2010 with permission from Elsevier.

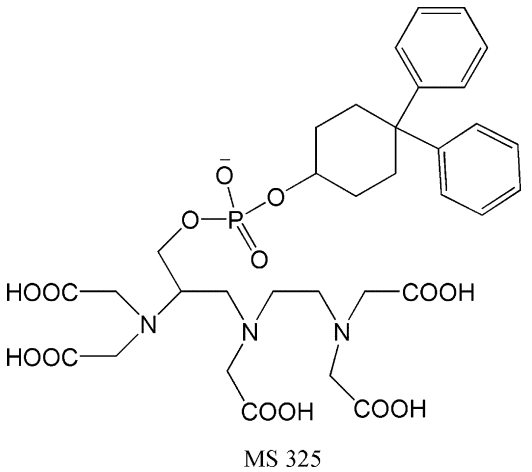

Fig. 12. The structure of MS-325 ligand.

r_1 of the CP conjugated with DOTA-Gd^{3+} (PF-Gd, shown in Fig. 11) was 12.57 mM^{-1} s^{-1}, higher than those of many other polymers with grafted DOTA-Gd^{3+} [76].

Different mCAs were prepared through the conjugation between these polymers and the various bifunctional ligands discussed above (Fig. 6). Their properties are summarized in Table 2. Generally, the r_1s increased 1–6-fold when the Gd^{3+} chelates were conjugated onto the linear polymers. Similarly to the linear mCAs, the molecular weights of these polymeric carriers had little effect on the r_1s [18]. However, the molecular weights of the carrier determined the pharmacokinetics of the mCAs (Fig. 4). For example, the blood elimination half-life time of PLL-DTPA-Gd^{3+} increased 7-fold as the molecular weight increased from 36 kDa to 480 kDa. Thus, PLL-DTPA-Gd^{3+} with a high molecular weight could provided almost constant tissue signal enhancement for a 60-min observation period [26]. However, the high molecular weight of the mCAs made them difficult to be excreted from body, which brought up toxic problems due to the metabolic release of toxic Gd(III) ions [27,68,77,78].

In addition, PEG chains were also grafted onto this type of mCA. The r_1s of the resulting mCAs decreased substantially as the grafted PEG hindered the H_2O exchange between the coordinated H_2O and bulk H_2O (Table 2). For example, the r_1s of PEG grafted PL CAs were only half of those of PL CAs. On the other hand, the PEG grafting made the mCAs more biocompatible and increased their retention time in the blood [58]. For example, the mCAs with 25-kDa PL and 5-kDa MPEG had a blood half-life of 12–24 h, depending on the modification degree and the size of the poly(amino acid), which were much higher than that of PL-DTPA-Gd^3. In comparison, the mCA comprised of a 25-kDa PL modified with 2-kDa MPEG chain was excreted more rapidly (blood half-life = 6 h). Thus, the blood half-lives of the mCAs can be tailored to specific needs by grafting with PEG of different molecular weights and modification degree [68].

In addition to the synthetic linear polymers, natural polymers have also received substantial research interest due to their good biocompatibility. Human or bovine serum albumin (HSA or BSA) and polysaccharides are two main natural polymers used to make mCAs. BSA or HSA have many amino groups on their side chains, which can be used to conjugate with the bifunctional DTPA or DOTA [18,57,79]. For example, up to about 30 DTPA ligands were readily introduced onto the polymer by the reaction of DTPA-dianhydride with BSA or HSA in buffered aqueous solution [57]. The conjugation rate increased to 100% when replacing DTPA-dianhydride with the NHS activated DTPA [18]. BSA/HSA-DTPA-Gd^{3+} is used as the "gold standard" blood pool agent to demonstrate the benefits of MR angiography [57,79]. The r_1 of BSA/HAS-DTPA-Gd^{3+} mCA is 14 mM^{-1} s^{-1}, 3 times higher than that of DTPA-Gd^{3+}.

Gd-chelates have also been introduced to endogenous HSA via non-covalent binding by forming adducts [80,81]. For example, the Gd-chelate MS-325 (Fig. 12) is a commercial CA (generic name: gadofosveset, trade name: Vasovist) approved in some countries to assess blockages in arteries. The MS-325 is reversibly bound to HSA via non-covalent binding. The r_1 of MS-325-Gd^{3+} bound to HSA is 9 times higher than MS-325-Gd^{3+} in buffer alone (without HSA).

Polysaccharides are attractive as carriers for drug delivery and imaging agents because they can be easily chemically functionalized and have both low toxicity and low immunogenicity. Dextran, inulin, carboxymethyl hydroxyethyl starch (CMHES), and cyclodextrin are the most widely investigated polysaccharides for MRI CAs [82–86]. Dextran, inulin, and starch conjugates with DTPA and DOTA are prepared via direct esterification of their hydroxyl groups using DTPA dianhydride [82], or a multistep method by first introducing an ethylenediamine spacer and then reacting with DTPA-dianhydride or the bifunctional DTPA and DOTA shown in Fig. 6 [83–86].

To date, a number of dextran-, inulin-, and CMHES-based mCAs with various molecular weights, spacer lengths and chelates have been reported [82–86]. Fig. 13 shows a general structure of a dextran-mCAs (CMDA*n*-DTPA-Gd^{3+}) with different spacer lengths. Recently, a "click

Table 2
The properties of the synthetic polymers grafted with Gd chelates.

mCAs	Mw (kDa)	Ion r_1 (mM^{-1} s^{-1})	Freq (MHz)	T (°C)	Ref.
PL-Gd-DTPA	48.7	13.1	20	39	[27]
PL-Gd-DTPA	50	10.8	10	37	[57]
PL-Gd-DTPA	238.1	11.74	100	37	[18]
PL-Gd-DTPA	89.9	11.58	100	37	[18]
PL-Gd-DTPA	56	10.56	100	37	[18]
PL-Gd-DTPA	7.7	11.67	100	37	[18]
PL-Gd-DOTA	65	13.03	10	37	[57]
MPEG-PL-Gd-DTPA	430	18	20	37	[68]
PG-Hex-DOTA	28–87	9.2–10.6	128	NA	[5]
PG-CA-DOTA	5.4	2.5	64	20	[33]
PG-Hex-DTPA-Gd	54	12	64	25	[31]
PG-Bz-DTPA-Gd	77	22	64	25	[31]
HPMA-Co-DOTA	52–58	21.8–24.9	64	20	[65]
PHPMA-GG-(Gd-DO_3A)	27.2–121	11.7–10.7	128	20	[66]
PHPMA-GFLG-(Gd-DO_3A)	28–121	11.9–11.5	128	20	[66]
PO-SQ-DO_3A-Gd^{3+}	35	31.0	20	20	[67]
PO-SQ-DO_3A-Gd^{3+}	5	15.6	20	20	[67]
PF-Gd	NA	12.57	3 T	NA	[76]

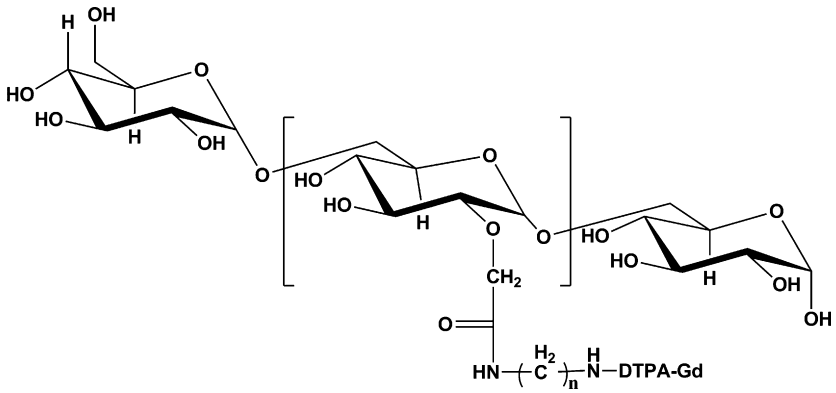

Fig. 13. The structure of dextran conjugate (CMDA*n*-DTPA) with different spacer lengths.

Table 3
The properties of CAs based on natural polymers.

mCA	MW (kDa)	ion r_1 (mM^{-1} s^{-1})	Freq (MHz)	T (°C)	Ref.
Albumin-DTPA-Gd	90	14	10	25	[57]
Albumin-MS325	NA	38.3	20	37	[80]
Inulin-DTPA-Gd	NA	8.3	100	25	[82]
Dextran-DTPA-Gd	9.4	8.7	100	25	[82]
Dextran-DTPA-Gd	40	8.1	100	25	[82]
Dextran-DTPA-Gd	71	7.1	100	25	[82]
Dextran-DTPA-Gd	487	5.8	100	25	[82]
CMHES-DOTA-Gd	70	14.1	20	39	[83]
Inulin-DTPA-Gd	23	20	20	37	[84]
CMDA-DTPA-Gd	345	9.8	20	37	[85]
CMDA*n*-Gd-DTPA where $n = 2$	NA	9.4	20	37	[86]
CMDA*n*-Gd-DTPA where $n = 3$	NA	9.5	20	37	[86]
CMDA*n*-Gd-DTPA where $n = 4$	NA	9.4	20	37	[86]
CMDA*n*-Gd-DTPA where $n = 6$	NA	8.9	20	37	[86]
β-CD-DOTA	5.5	12.2	60	37	[87]
β-CD-DPTA	5.5	6.2	400	37	[88]
Poly-β-CD-DOTA	NA	48.4	20	37	[89]

chemistry" reaction between the azide-functionalized β-cyclodextrin (β-CD) and the alkyne functionalized ligands DTPA/DOTA-Gd (Fig. 6) have been used to make a β-cyclodextrin-based mCAs [87,88]. The r_1s of the polysaccharide-based mCAs are summarized in Table 3. The r_1s of the polysaccharide-based mCAs ranges from 1.5 to 3 times that of DTPA-Gd^{3+}. The molecular weights of the carriers, as well as the type of chelates and spacer have little effect on their r_1s. β-CD has also been used to associate with DOTA-Gd and DTPA-Gd via a non-covalent host–guest interactions. The structure of the assembled CAs is shown in Fig. 14. The resulting mCAs exhibited a great relaxivity

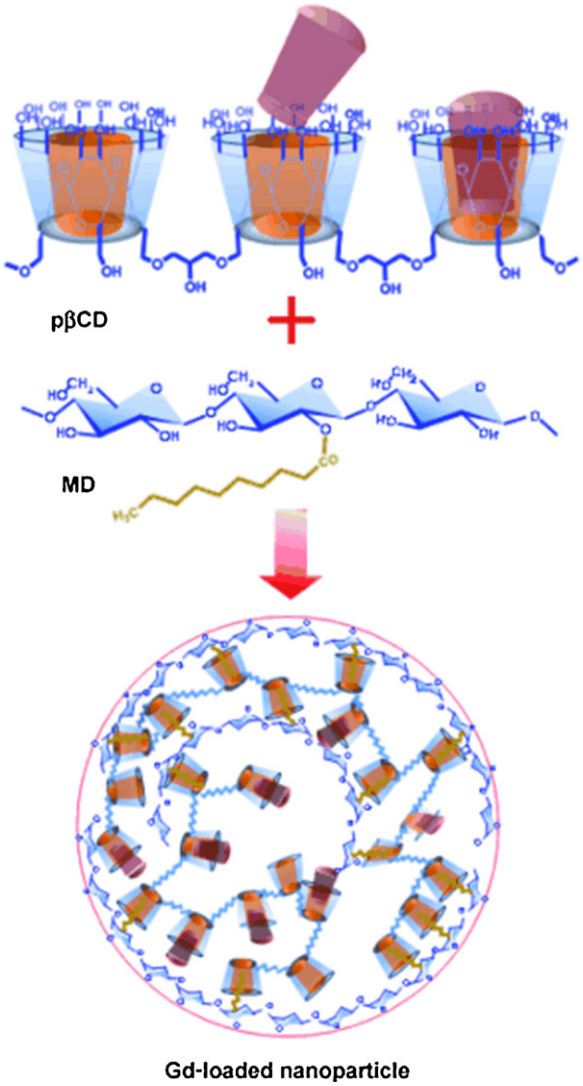

Fig. 14. Formation of Gd^{3+}-loaded nanoparticles through a supramolecular three-component assembly: Gd^{3+} chelate/pβCD/MD. The alkyl chains functionalizing dextran are in yellow, the Gd^{III} chelate is in violet. Reprinted from [89].

enhancement with an r_1 of 48.4 mM^{-1} s^{-1}, at 20 MHz and 37 °C, indicating that the host–guest method is a promising strategy for developing mCAs with high relaxivity [89,90].

3.3. Dendritic mCAs

Dendrimers are a family of nano-sized, three-dimensional polymers characterized by a unique tree-like branching architecture and compact spherical geometry when placed in solution [91]. As carriers for drugs and CAs, they have many advantages over other polymers because of their precise, spherical and highly branched structure, as well as their large modifiable surface functionality. Poly(propyleneimine) (PPI, Fig. 2), poly(amidoamine) (PAMAM, Fig. 15), and poly(L-lysine) dendrimers (Fig. 16) were the most commonly investigated CA carriers. They have substantial amino functional groups on their surface, which can be used to conjugate with DTPA and DOTA chelates. Similarly to the linear polymers, the dendrimers are conjugated with DTPA and DOTA chelates mainly through a reaction between the amino groups on their surface and the bifunctional ligands shown in Fig. 6.

The properties of the dendritic mCAs are summarized in Table 4. The dendrimers are inherently more rigid than their linear analogues, resulting in less freedom for the conjugated Gd-chelates to rotate. Thus, the contrast efficiencies of dendritic mCAs, in terms of r_1s, are higher than those of the linear analogues. The generation of dendrimers corresponding to their molecular weight, is the main parameter determining the r_1 of dendritic mCAs. For instance, the r_1s of the PAMAM-1B4M CAs has been shown to increase from 20 mM^{-1} s^{-1} to 29 mM^{-1} s^{-1} when the generation increases from 2 to 4 [19,20,92], with the eighth generation having the highest r_1 of 35 mM^{-1} s^{-1} [19]. The chemical structures of dendrimers and chelates have a minor effect on the r_1s of mCAs; however, grafting the PEG onto the dendritic mCAs decreases their r_1. For example, grafting PEG5000 onto PAMAM G3-DOTA-Gd^{3+} has been shown to decrease its r_1 from 14.9 to 13.8 mM^{-1} s^{-1} [24].

In addition, the biocompatibility of dendritic mCAs is an important issue when in vivo applications are considered [93]. Recently, in vitro studies showed that amine-terminated PPI and PAMAM dendrimers were cytotoxic, in particular at the higher generations. The IC50 of PPI with 64 terminal amino groups was less than 5 μg mL^{-1} [94,95]. Their cytotoxicity was due to the interactions between positively charged dendrimers and the negatively charged cell membranes [96]. PPI and PAMAM dendrimers functionalized with carboxylate end groups at the surface were neither cytotoxic nor haemolytic up to a concentration of 2 mg/mL [97]. Therefore, the overall toxicity of dendritic structures is strongly determined by their surface functional groups [97,98]. Gadomer-17 (shown in Fig. 17) is a dendritic mCA under phase II clinical development. The pharmacokinetics in many species (rat, rabbit, dog, monkey) indicated that after a single intravenous injection, the CA was rapidly and completely eliminated from the body, mainly via glomerular filtration, and no long-term accumulation or retention of the non-metabolized agent was detected in the organs or tissues [99,100]. The dendritic mCAs with high molecular weights (>40 kDa), however, are more difficult to excrete by the kidneys. As a result, the prolonged retention of these mCAs will place patients at high risk due to the high toxicity of free Gd^{3+} produced by the metabolization of dendritic mCAs [34].

Recently, a number of novel dendritic mCAs were prepared and evaluated in vitro and in vivo. Fu et al. synthesized a series of polylysine dendrimers with a PEG core and the corresponding dendritic mCAs via their reaction with the NHS-activated DTPA. Their structures are shown in Fig. 18. The dendritic mCAs had r_1s from 8.12 to 9.76 mM^{-1} s^{-1} at 2 T, and 37 °C, and showed a high degree of hydrophilicity, good stability in plasma, and lack of binding to proteins [101]. Lu et al. prepared mCAs from G1 to G3 polylysine dendrimers with a silsesquioxane core (Fig. 19). The dendritic mCAs had well-defined

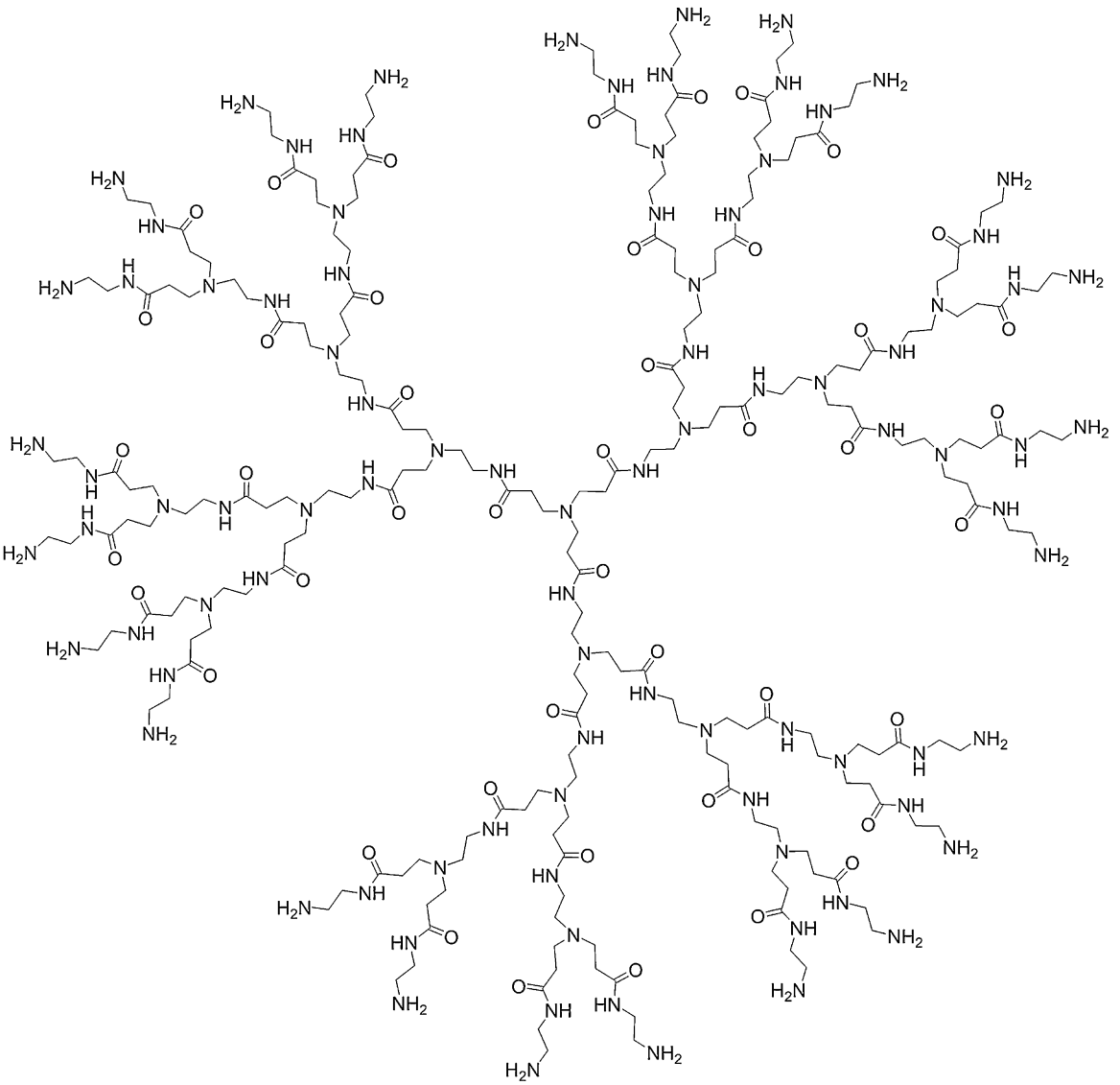

Fig. 15. PAMAM dendrimer with ammonia core (generation 4).

compact globular structures with high loadings of Gd-DOTA monoamide at their surface. The sizes of the G1, G2, and G3 dendritic mCAs were approximately 2.0, 2.4, and 3.2 nm, respectively and the corresponding r_1 values at 3 T were approximately 6.4, 7.2, and 10.0 $mM^{-1}\,s^{-1}$, respectively. The dendritic mCAs showed size-dependent vascular contrast enhancement. The G3 dendritic mCA produced more significant and prolonged vascular enhancement than the smaller dendritic mCAs. Moreover, these dendritic mCAs could significantly enhance the MRI of the xenografted tumor [102]. In order to avoid the toxic side effects of Gd based CAs, Gd^{3+} was also replaced by Mn^{2+} to make non-gadolinium(III) dendritic mCAs. The ionic r_1 values for the dendritic Mn(II)-DOTA monoamide mCAs of G2, G3 and G4 were 3.3, 2.8, and 2.4 $Mm^{-1}\,s^{-1}$ at 3 T, respectively. The dendritic macrocyclic Mn(II) chelate mCAs also showed good in vivo stability and were readily excreted via renal filtration [103].

Toth et al. prepared two dendritic mCAs from a hyperbranched poly(ethylene imine) (PEI), HB-PEI-[Gd(DOTA-pBn)$(H_2O)]_{32}$, and a hyperbranched polyglycerol, HB-PG-[Gd(DOTA-pBn)$(H_2O)]_{68}$, via a conjugation with 2-(4-isothiocyanatobenzyl)-1,4,7,10-tetraazacyclododecane-1,4,7,10-tetraacetic acid (DOTA-pBn-SCN) (Fig. 20), and investigated their r_1s in comparison with the CAs made from G4 polyamidoamine (PAMAM) at different frequencies [104]. Both hyperbranched structures were found to be as good scaffolds as regular PAMAM dendrimers in terms of the r_1s of the Gd^{3+} complexes. The two hyperbranched mCAs had high r_1s of 34.2 $mM^{-1}\,s^{-1}$ at 20 MHz, slightly higher than that based on PAMAM [104].

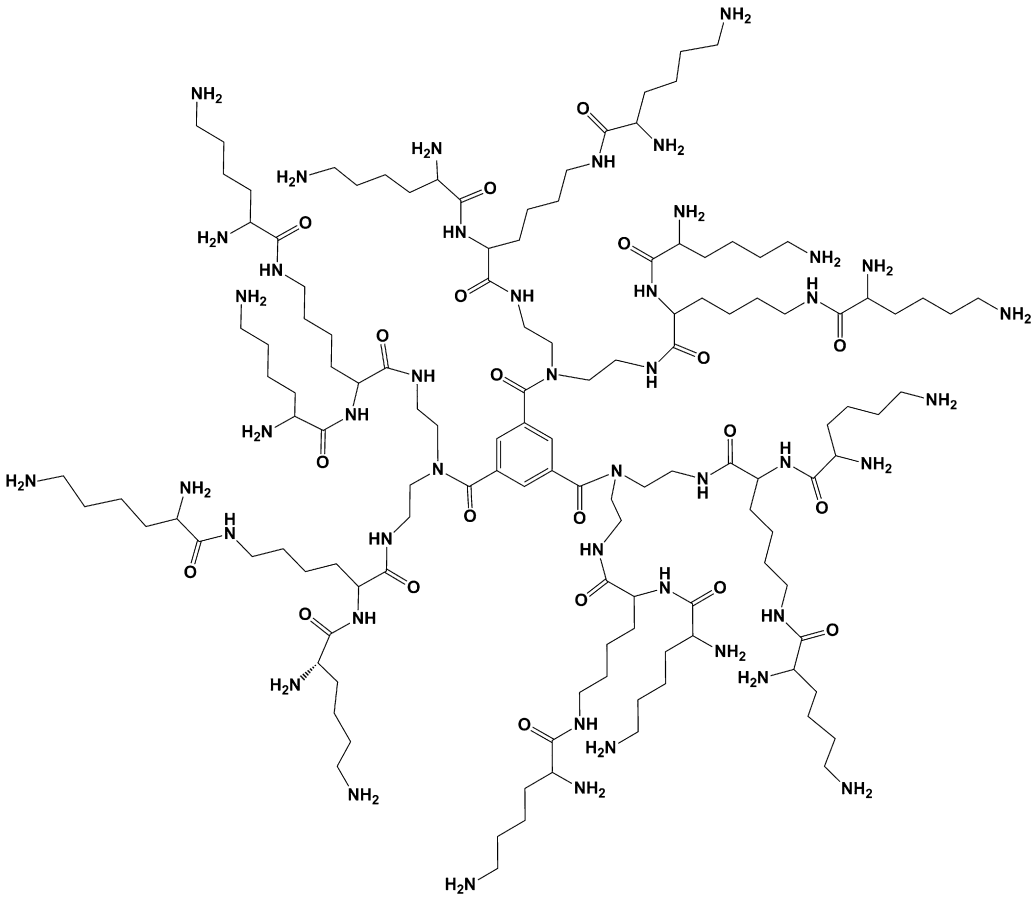

Fig. 16. PL dendrimer with aromatic core (generation 3).

Sideratou et al. prepared dendritic mCAs from a hyperbranched aliphatic polyester BH40 with EDTA or DTPA groups and poly(ethylene glycol) chains, with one of the latter chains bearing the folate targeting ligand at its end, i.e., BH40-EDTA-PEG-Folate and BH40-DTPA-PEG-Folate (Fig. 21). The r_1s determined for the Gd^{3+} complexes of BH40-EDTAPEG-Folate and BH40-DTPA-PEG-Folate were 7.10 ± 0.15 and $12.30 \pm 0.15\ mM^{-1}\ s^{-1}$, respectively. The cytotoxicity of the hyperbranched Gd complexes was comparatively assessed in a human lung carcinoma cell line (A549) not expressing folate receptors, and in a folate receptor-positive human cervical carcinoma cell line (HeLa). Preliminary studies revealed that the two dendritic Gd complexes were non-toxic and exhibited folate receptor specificity [105].

Shih et al. developed a dendritic mCA from a polyester dendrimer with PEG core bearing functional hydroxyl groups via conjugating folate and Gd chelates (Fig. 22). Its r_1 was tested using a NMR spectrometer at 20 MHz with a standard pulse program of inversion-recovery. The calculated r_1 of this dendritic mCA was $4.8\ mM^{-1}\ s^{-1}$. An in vivo experiment indicated that the PEG-cored dendrimer carrying gadolinium chelates and folates could be used in MR imaging to diagnose FR-positive tumors in a mouse xenograft model [106].

Raymond et al. synthesized and attached amine-functionalized TREN-bis(1,2-HOPO)-TAM-ethylamine and TREN-bis-(1-Me-3,2-HOPO)-TAM-ethylamine to biocompatible 40 kDa esteramide (EA)- and poly-L-lysine (PLL)-based dendrimers capable of binding up to eight gadolinium complexes. The structure of the dendrimers and chelates are shown in Fig. 23. One of the conjugates had an r_1 of up to $38.14\ mM^{-1}\ s^{-1}$, which was several times that of the small-molecule complexes. Moreover, both the structure of ligands and dendrimers had great effect on the r_1s of the dendritic mCAs. For example, the EA- and PLL-based dendrimers are conjugated with the same chelate. The resultant EA dendritic mCA had an r_1 of $38.14\ mM^{-1}\ s^{-1}$, while the PLL dendritic mCA had an r_1 of $21.0 \pm 0.6\ mM^{-1}\ s^{-1}$. The same EA dendrimer conjugated with 4 different chelates, shown in Fig. 23, had different r_1s of 38.14, 31.9 ± 0.1, 7.19 ± 0.07, and $20.2 \pm 0.6\ mM^{-1}\ s^{-1}$ [48].

An interesting pH-responsive dendritic mCA, shown in Fig. 24, was obtained by introducing pendant phosphonate groups onto the chelates. The pH-responsive properties are shown in Fig. 25. The r_1 of the mCA increased from $10.8\ mM^{-1}\ s^{-1}$ at pH 9 to $24.0\ mM^{-1}\ s^{-1}$ at pH 6 [36]. Similar pH-responsive r_1 was also found in PAMAM-based mCA using DO_3A-p-Bn-NCS (Fig. 6) as the ligand [35]. The

Table 4
The properties of the dendritic mCAs.

Dendritic polymers	Conjugated ligands	Core	Mw (kDa)	Ion r_1 ($mM^{-1}\,s^{-1}$)	Freq (MHz)	T (°C)	Ref.
PAMAM G8	1B4M	EDA	960	35	64	20	[19,20]
PAMAM G7	1B4M	EDA	58	28	64	20	[19]
PAMAM G6E	1B4M	EDA	238	33	64	20	[20]
PAMAM G6A	1B4M	Ammonia	175		64	20	[20]
PAMAM G5	DO_3A-bz-NCS	Ammonia	61.8	18.8	25	37	[24]
PAMAM G4	DO_3A-bz-NCS	Ammonia	37.4	16.9	20	37	[24]
PAMAM G3	DO_3A-bz-NCS	Ammonia	22.1	14.9	25	37	[24]
PAMAM G4	DO_3A-CS	Ammonia	59	28	128	NA	[34]
PAMAM G3	DO_3A-CS	Ammonia	29	25	128	NA	[34]
PAMAM G2	DO_3A-CS	Ammonia	14	20	128	NA	[34]
PAMAM G4	1B4M	EDA	59	29	64	20	[19,20,92]
PAMAM G3	1B4M	EDA	29	25	64	20	[19,20,92]
PAMAM G2	1B4M	EDA	15	20	64	20	[19,20,92]
PAMAM G3-PEG 5000	DO_3A-bz-NCS	Ammonia	69.3	13.8	20	37	[24]
PAMAM G3-PEG 2000	DO_3A-bz-NCS	Ammonia	33.3	13.7	20	37	[24]
PAMAM G2-PEG 5000	DO_3A-bz-NCS	Ammonia	23.8	12.4	20	37	[24]
PAMAM G2-PEG 2000	DO_3A-bz-NCS	Ammonia	20.6	11	20	37	[24]
PPI G5	1B4M	DAB	51	29	64	20	[19]
PPI G4	DO_3A-CS	DAB	51	29	128	NA	[34]
PPI G3	DO_3A-CS	DAB	25	17	128	NA	[34]
PPI G2	DO_3A-CS	DAB	12	12	128	NA	[34]
PPI G4	1B4M	DAB	51	29	64	NA	[19,92]
PPI G3	1B4M	DAB	25	17	64	NA	[19,92]
PPI G2	1B4M	DAB	12	12	64	NA	[19,92]
PPI G5	DTPA-B-NCO	DAB	51	27.8	64	20	[21]
PPI G3	DTPA-B-NCO	DAB	12.7	19.7	64	20	[21]
PPI G1	DTPA-B-NCO	DAB	3.1	13	64	20	[21]
PLL Gadomer 17	DO_3A-MA	Aromatic acid	17.5	17.3	20	39	[100]
PLL G4	NHS-DTPA	PEG3400	12.2.	8.12	2 T	37	[101]
PLL G5	NHS-DTPA	PEG3400	18.4	9.76	2 T	37	[101]
PLL G4	NHS-DTPA	PEG6000	14.2	8.88	2 T	37	[101]
PLL G4	NHS-DTPA	PEG1200	20.1	9.52	2 T	37	[101]
PLL G1	DOTA-MA	OAS	7.3	6.4	3 T	NA	[102]
PLL G2	DOTA-MA	OAS	14.8	7.2	3 T	NA	[102]
PLL G3	DOTA-MA	OAS	34.7	10.0	3 T	NA	[102]
PLL G2	HOPO	PER	NA	21.0 ± 0.6	60	37	[48]
EA G2	HOPO	PER	NA	38	60	37	[48]
HB PEI	DO_3A-bz-NCS	Ammonia	50	34.2	20	25	[104]
HB PG	DO_3A-bz-NCS	Glycerol	95	34.2	20	25	[104]
BH40-PEG-Folate	DTPA	2-Methylglycerol	NA	12.3	100	25	[105]
BH40-PEG-Folate	EDTA	2-Methylglycerol	NA	7.1	100	25	[105]
PEG-G3-$(Gd\text{-}DTPA)_{11}$-$(Folate)_5$	DTPA	PEG	12.6	4.8	20	37	[106]

EDA, 1,2-ethanediamine; DAB, 1,4-butanediamine; OAS, octasilsesquioxane; PER, pentaerythritol; NA, not available.

dendritic mCA showed enhanced r_1 at a pH below 6.0, and the inflection points in the r_1 pH dependence profile were at the pK_1s assigned to the protonation of the tertiary branching amines inside the dendrimers. Therefore, it was concluded that the r_1 enhancement in acidic solutions was a direct consequence of the protonation of the PAMAM inner-shell amines, which made the structure expand and consequently increase its rotational correlation time. This pH-responsive property is promising for developing MRI CAs to detect kidney disease and cancer, which both have a significant reduction in the extracellular pH [35,36].

3.4. Micellar MRI CAs

Assembly of mCAs into nano-sized micellar mCA is an important direction to develop high efficient MRI CAs as they have many advantages including a high Gd loading capacity and tunable sizes. The methods used to make micellar mCAs include emulsion polymerization and assembly of mCAs with the Gd chelates either in the core or shell of the micellar structures.

Li et al. reported the fabrication of micelle with shell-grafted DTPA-Gd^{3+} from a biodegradable poly(L-glutamic acid)-*b*-polylactide (PG-*b*-PLA) block copolymer. The structures of the copolymer grafted with DTPA-Gd^{3+} and the formed micelle are shown in Fig. 26. The resultant micelle in aqueous solution had an average diameter of 230 nm at pH 7.4. The DTPA-Gd^{3+} conjugated to the shell layer of the micelle showed an r_1 of 7.90 $mM^{-1}\,s^{-1}$ at 4.7 T, which was significantly higher than that of a small molecule MRI CA. Since the hydrophobic core of the micelle can load drugs, this polymeric micelle was proposed as a platform for the development of MRI–visible, targeted nano-scale drug delivery systems [107].

Reynolds et al. fabricated a Gd-loaded nanoparticle with a diameter of 120 nm via emulsion polymerization and succedent modification. The Gd loaded nanoparticle had a core–shell morphology where the interior comprised of a copolymer of ethylacrylate (48%), methacrylic acid

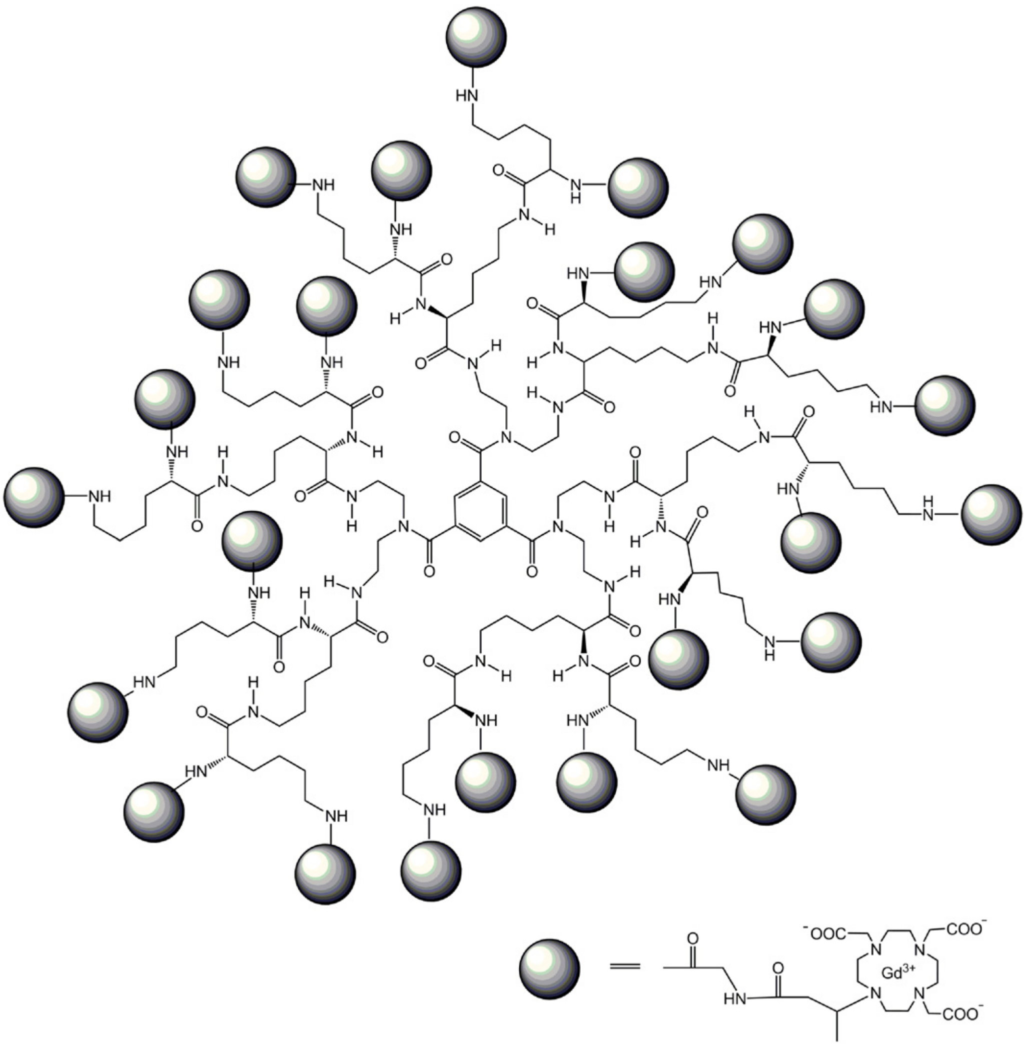

Fig. 17. The structure of Gadomer 17.

(48%), allylmethacrylate (4%), which provided high affinity for a specific metal, while the shell consisted of a porous hydrophobic copolymer of styrene (20%), ethylacrylate (70%), methacrylic acid (9%), allylmethacrylate (1%) that modulated the access to the core. This particle substantially reduced relaxation time in vitro, and provided excellent contrast when it was used to image the heart and gastrointestinal tract in a rat animal mode [108].

Wooley et al. made a Gd labeled shell-crosslinked nanoparticle (SCK) with a hydrodynamic diameter of 40 ± 3 nm, which was made from the aqueous assembly of poly(acrylic acid) (PAA) and poly(methylacrylate) (PMA) block copolymer and subsequent covalent crosslinking by amidation upon reaction with 2,2′-(ethylenedioxyl)bis(ethylamine) throughout the shell layer (Fig. 27). The Gd chelates were introduced onto the SCK via direct covalent conjugation of amino-functionalized DTPA-Gd chelates with the carboxylic acid groups in the hydrophilic shell layer of the SCK (Fig. 27). This SCK-based CAs demonstrated large ionic r_1s of 39 $mM^{-1}\,s^{-1}$ at 0.47 T and 40 °C due to the highly hydrated nature of the shell layer which allowed for rapid H_2O exchange [109].

Wang et al. prepared Gd-loaded particles via miniemulsion polymerization with amphiphilic Gd(III) complexes as metallosurfactants. As shown in Fig. 28, the miniemulsions were initially prepared by mixing cetyl alcohol, styrene, divinylbenzene and an aqueous dispersion of metallosurfactant (1 or 2) and cosurfactants followed by sonication at 180 W of power for 6 min. The polymerization was initiated at 75 °C by adding an oil-soluble initiator, azobisisobutyronitrile (AIBN), into the miniemulsion, and the polymerization stopped after 6 h. The resulting Gd(III)-based polymer latex was then dialyzed against deionized H_2O to remove excess surfactants and other low molecular weight impurities. The colloided nanoparticles with varied sizes (the hydrodynamic diameters ranging from 7.4 nm to 78 nm) and Gd-loading were prepared by adjusting: (i) the ratio of surfactants to monomers; (ii) the amount of co-surfactant; and (iii) the polymerization conditions.

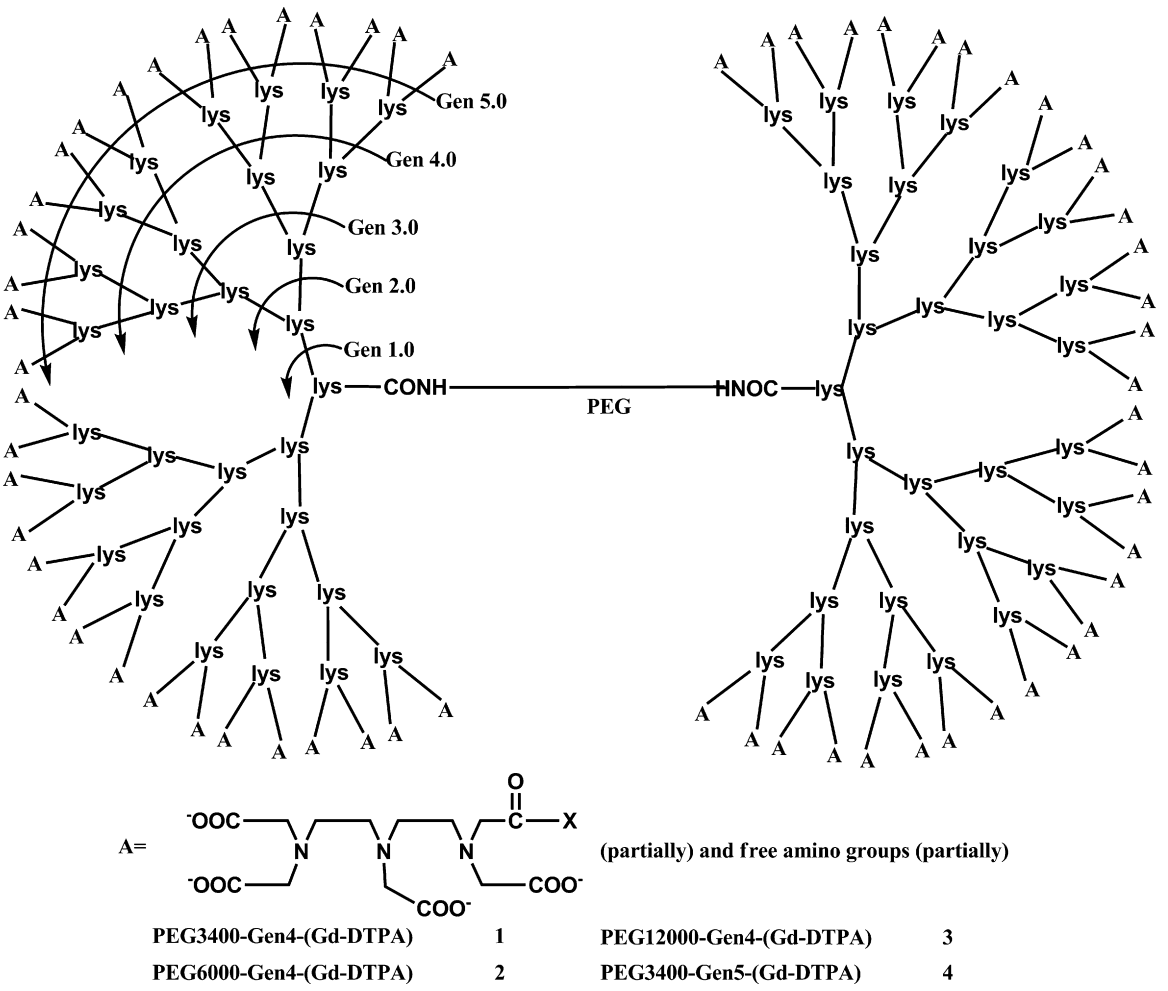

Fig. 18. Structure of Gd-based cascade polymeric MRI contrast media with PEG cores. Reprinted from [101].

All these Gd-loaded nanoparticles showed very high r_1s in 3 T imaging with the r_1s ranging from 7.5 $mM^{-1}\,s^{-1}$ to 20.4 $mM^{-1}\,s^{-1}$ [110].

Tsourkas et al. made Gd-conjugated dendrimer nanoclusters (DNCs) with a tumor-targeting group [111]. As shown in Fig. 29, the nanoclusters were fabricated by crosslinking G5 PAMAM using a bifunctional amine-reactive crosslinker. After the DNCs formation, paramagnetic Gd^{3+} ions were conjugated to the DNCs by DTPA. The resulting paramagnetic DNCs were further functionalized with a tumor-targeting ligand (folic acid) and a fluorescence dye (FITC). The gadolinium-conjugated DNCs had an r_1 of 12.3 $mM^{-1}\,s^{-1}$. This value was only slightly higher than gadolinium-labeled individual PAMAM (G5) dendrimers, which had an r_1 of 10.1 $mM^{-1}\,s^{-1}$ at the same condition. This marginal increase in r_1 can be attributed to a large amount of internal motions within the DNCs due to the PEG linkers [111].

Kataoka et al. developed a theranostic core–shell polymeric micelle based on the self-assembly of block copolymers with both MRI contrast and cancer therapy capacity. As shown in Fig. 30, the micelle incorporated Gd-DTPA and (1,2-diaminocyclohexane)platinum (II) (DACHPt), the parent complex of the potent anticancer drug oxaliplatin, in its core by reversible complexation between DACHPt, Gd-DTPA and poly(ethylene glycol)-*b*-poly(glutamic acid) (PEG-*b*-P(Glu). The r_1 of the micelle increased approximately 24 times compared to that of free Gd-DTPA. The extremely high r_1 of the Gd-DTPA/DACHPt-loaded micelle was ascribed to the combination of the τ_R increase and the optimization of the τ_m in the hydrophobic environment inside the micelle core [112].

Yokoyama et al. prepared a polymer micelle-based mCA with a pH-adaptable r_1. The polymer micelle was made from cationic polyallylamine or protamine and an anionic block copolymer poly(ethylene glycol)-*b*-poly(aspartic acid) conjugated with DTPA-Gd^{3+} chelates PEG-P(Asp(DTPA-Gd)) as follows. PEG-P(Asp(DTPA-Gd)) was firstly dissolved in 0.5 M NaCl aqueous solution, and then polyallylamine or protamine in 0.5 M NaCl aqueous

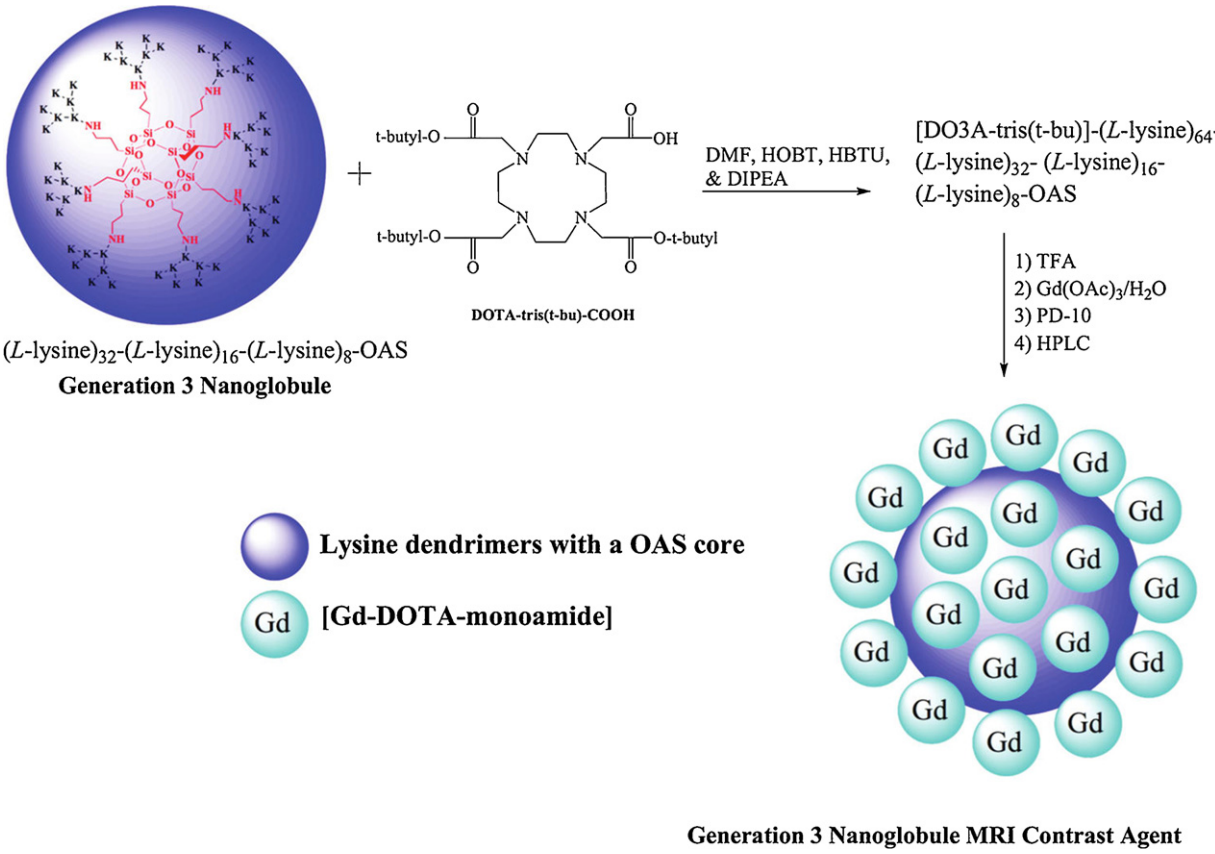

Fig. 19. Synthesis of dendritic MRI contrast agents with octasilsesquioxane core. Reprinted from [102].

solution was added to the solution. The anionic P(Asp) block complexed with the cationic polymer via the electrostatic interactions forming a micelle with the Gd chelates encapsulated inside the core. The micelle had a much lower r_1, only about 2.1–3.6 $mM^{-1}\,s^{-1}$, in contrast to the free PEG-P(Asp(DTPA-Gd)) with an r_1 of 10 $mM^{-1}\,s^{-1}$. The changeable r_1 make it promising for solid tumor imaging (Fig. 31). In normal tissue, the micelles cannot leak into tissues through the wall of blood vessel and exhibit low r_1. While in tumor tissue, the micelles accumulate via the enhanced permeability and retention (EPR) effect of solid tumors and then dissociate into free PEG-P(Asp(DTPA-Gd)) with high r_1 due to its acidic intracellular fluid, selectively enhancing the MRI in tumors [113].

Another pH responsive micellar CA was prepared through a similar method from poly(ethylene glycol)-*b*-poly(L-lysine) block copolymer (PEG-P(Lys)) partially conjugated with DOTA-Gd^{3+} and an oppositely charged polyanion, poly(methacrylic acid) or dextran sulfate. It also showed lower r_1 (3.8 $mM^{-1}\,s^{-1}$ at 9.4 T) than its parent polymeric CA, PEG-P(Lys)-DOTA-Gd^{3+} conjugate (6.2 $mM^{-1}\,s^{-1}$ at 9.4 T) [114]. In addition, the PEG-P(Lys)-DOTA conjugate partially chelated with Gd could form a micellar structure in an aqueous medium. The resultant micellar CAs showed long blood circulation time with 22.5 ± 2.9% of injected dose remaining in the blood for 24 h after the injection, and demonstrated a considerable amount (6.1 ± 0.3% of ID/g of the polymeric micelle) of accumulation in the solid tumor 24 h after intravenous injection, significantly enhancing the MRI of the tumor [115].

In summary, the micellar CAs with Gd chelates located in their shell have free access for H_2O molecules to the bound Gd ions. They, therefore, generally showed higher r_1 values than free mCAs as they have high τ_R due to the restricted rotation of their micellar structures. On the other hand, the micellar CAs with Gd chelates located in their interior have much lower r_1 values than the free mCAs because the inner core environment hinders the access of H_2O molecules to the bound Gd ions in the core, which increases the τ_M of CAs. Stimulus-responsive micellar CAs with changeable r_1 values can be achieved via designing environment-sensitive micellar structures, which change their morphology (e.g. from aggregated state to dissociated state) due to an external stimulus (e.g. change in pH) and consequently alter their r_1s. The micellar CAs also have different pharmacokinetics and biodistribution compared to mCAs due to their larger size. The micellar CAs also have longer blood retention times and accumulate more in tumors via the EPR effect. In addition, the structure and size of micellar CAs can also be tuned according to their applications.

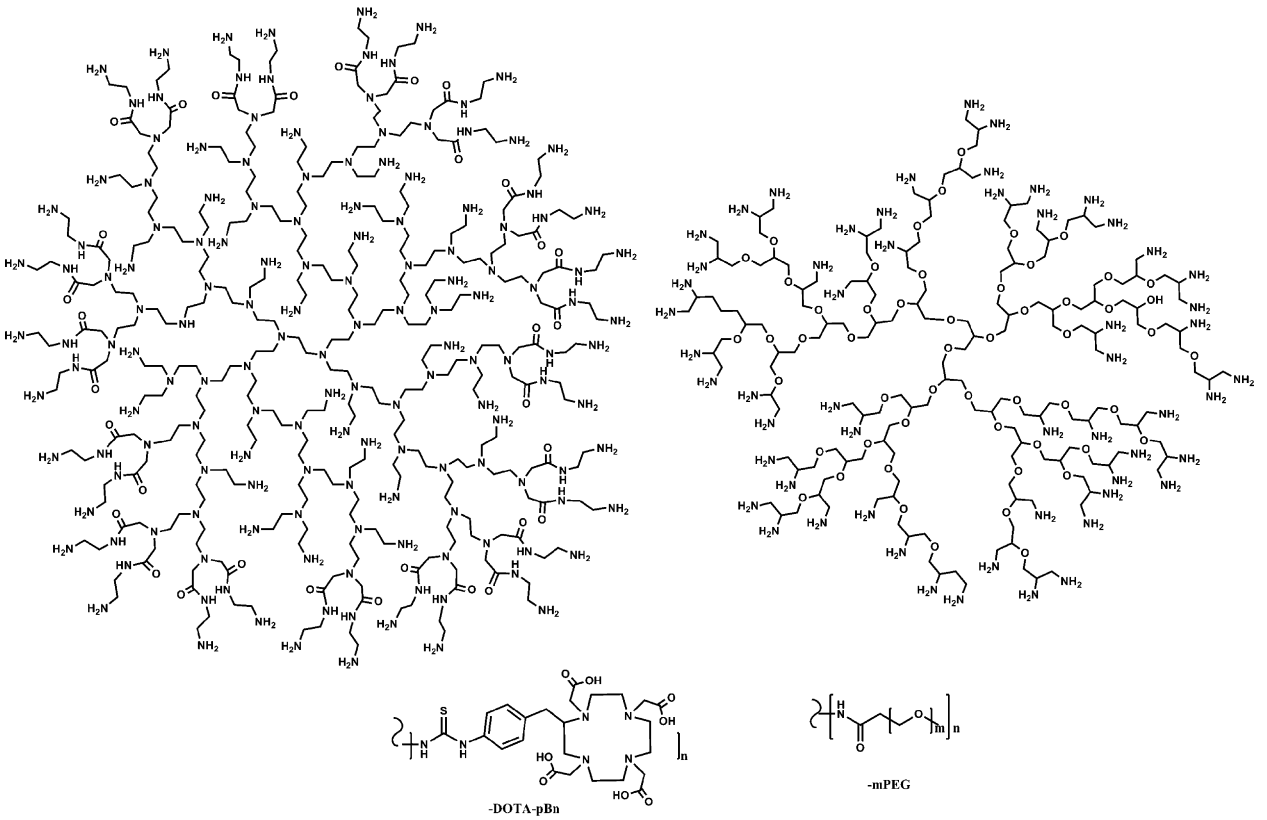

Fig. 20. Structures of the hyperbranched, ethylenediamine-cored poly(ethylene imine) (PEI), the hyperbranched, amino-functionalized polyglycerol (PEG-NH2) and the moieties attached to the respective dendrimers via amide or thiourea bonds. Reprinted from [104].

4. Clearance and pharmacokinetics

Since the accumulated mCAs in the body may be taken up by cells and metabolized into toxic Gd^{3+} and other harmful debris from the carriers, an ideal mCA not only should remain within the system for a sufficient time to produce desired effects such as tumor accumulation for oncologic imaging, but also should be effectively excreted from the body to minimize unwanted effects of foreign materials within body [116]. Nano-sized mCAs are cleared from the vascular compartment through three primary mechanisms: renal clearance with excretion into urine, hepatic clearance with biliary excretion, or uptake by macrophages into the reticuloendothelial system (RES) (liver, spleen, bone marrow) [116]. The renal clearance includes glomerular filtration or tubular excretion. Among all the modes of clearance, the glomerular filtration is the most desired route for mCA clearance from the body, as mCAs are excreted without cellular internalization or metabolism [116]. The size, hydrophilicity, surface modification, shape, and flexibility of mCAs have great effects on their clearance.

The pharmacokinetics and distribution of a mCA determine its specific applications. Organ-specific imaging can be achieved via adjusting the pharmacokinetics and distribution of mCAs by changing their size, shape, rigidity, and surface modification. For instance, as shown in Fig. 32, the sizes and hydrophilicity of the dendritic mCAs determined their pharmacokinetics and distribution and thus their specific applications [116]. G4-PAMAM CA with a size of 6 nm tends to accumulate in kidney and thus may be ideal for renal imaging [117,118]. G8-PAMAM CA with a size of 10 nm is taken up by the lymphatics and retained in lymphatic system more than 1 day, and thus may be used for lymphatic system imaging. G6-PAMAM CA with a size of 8 nm may be good for blood agent. In addtion, the more hydrophobic G4 PPI CA, which has higher accumulation in liver, may be suitable for liver imaging [116].

4.1. Size

Generally, macromolecules or particles smaller than 5.5 nm primarily undergo renal clearance, whereas those larger than 12 nm primarily undergo hepatic clearance, and those of intermediate size vary in terms of their properties. The pharmacokinetics and biodistribution of the G2 to G10 PAMAM dendrimers conjugated with 1B4M were evaluated by Kobayashi, et al. [119–121]. They found that the G2 to G4-based mCAs were quickly excreted via the kidney primarily during the first pass, while the G5 and G6-based mCAs were more slowly excreted. The G7 to G10-based mCAs, however, showed minimal excretion from the kidney. In addition, it was reported that the G2 and G3-based

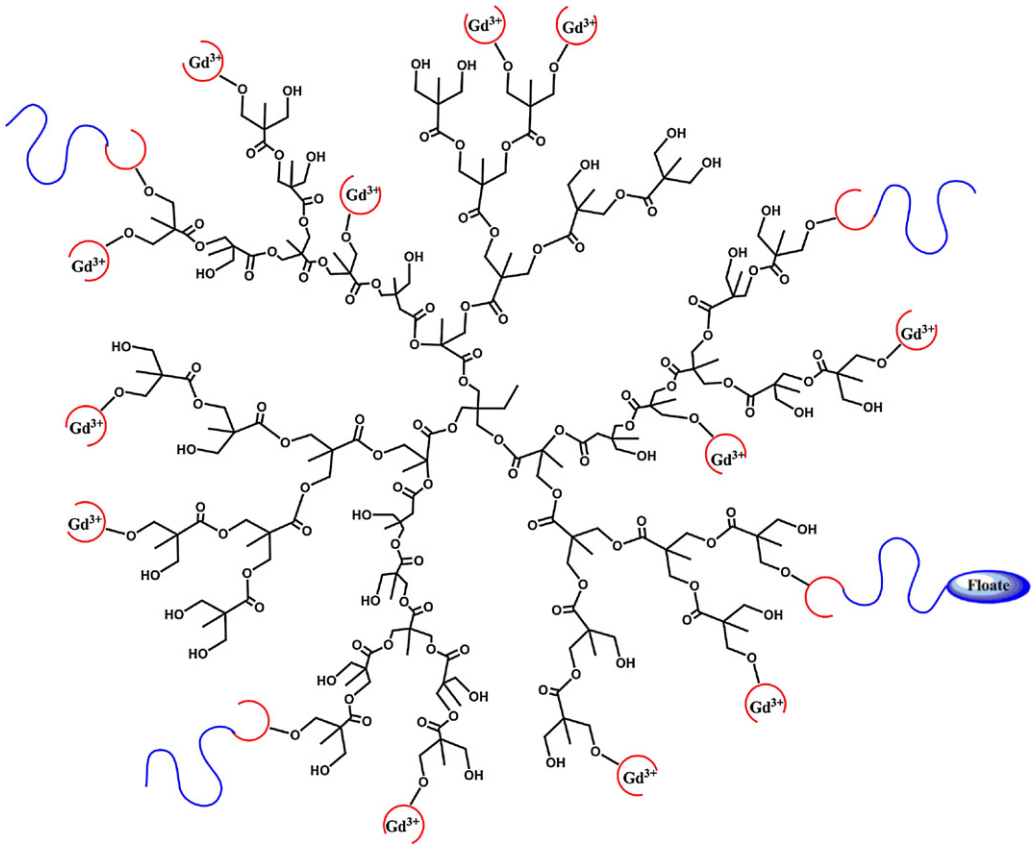

Fig. 21. Dendritic CAs based on aliphatic polyester with PEG and targeting group. Reprinted from [105].

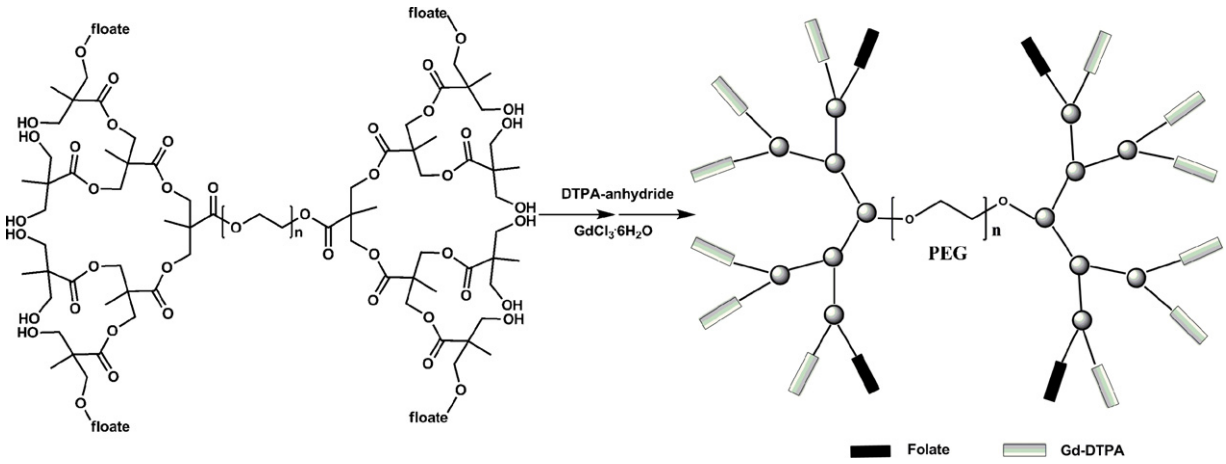

Fig. 22. Synthesis of the folate-targeting dendritic CA from PEG-cored polyester dendrimer. Reprinted from [106].

mCAs with sizes less than 5 nm in diameter were quickly distributed from the circulation into the soft tissue similarly to Gd-DTPA [120], indicating they could quickly leak out of the vasculature into surrounding tissues, even from normal vessels. In contrast, the slightly larger mCAs (i.e. G4 and G5-based mCAs) extravasated from the tumor vasculature but could not from normal blood vessels [122], while the mCAs larger than 8 nm diameter (i.e., G6 or higher generations-based mCAs) showed minimal leakage even from tumor vessels into surrounding tumor tissue [123–125]. Furthermore, the authors also found that the dendritic mCAs smaller than the G8-based mCAs were not recognized by the reticuloendothelial system, but the G9 and G10-based ones were quickly taken up and trapped in

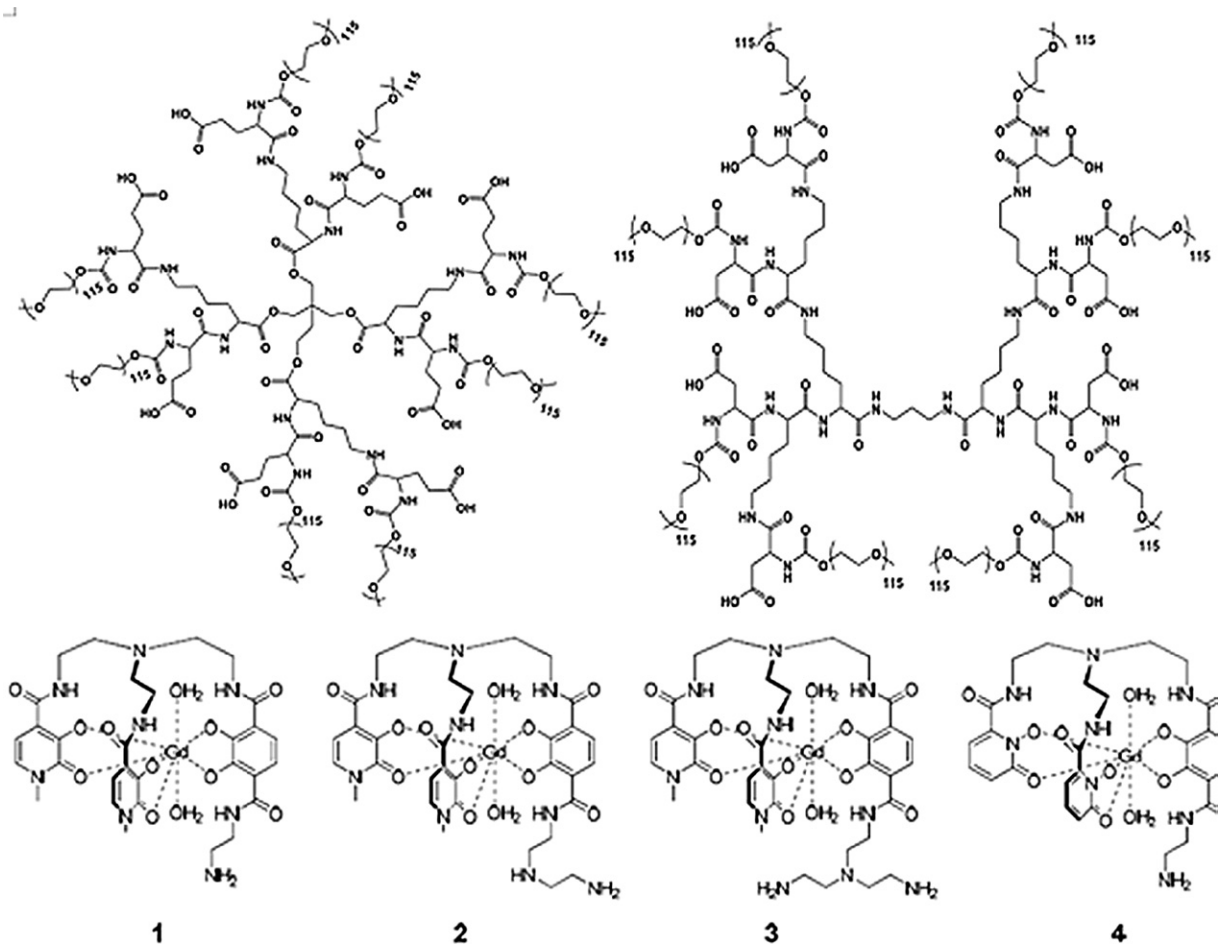

Fig. 23. The structures of the EA and PLL dendrimers, and Gd-TREN-bis(1-Me-3,2-HOPO)-TAM-ethylamine complexes **1**–**3** and Gd-TREN-bis(1,2-HOPO)-TAM-ethylamine complex **4**. Reprinted from [48].

the reticuloendothelial system, resulting in rapid clearance from the circulation [122].

4.2. Hydrophilicity

The hydrophilicity of polymers also greatly affects the pharmacokinetics and biodistribution of mCAs. For instance, Kobayashi et al. compared the pharmacokinetics and biodistribution of dendritic mCAs made from the G4 PPI or PAMAM, and 1B4M. PPI is more hydrophobic than PAMAM because it contains longer carbon chains and no amide groups. The PPI-G4-$(1B4M\text{-}Gd)_{64}$ had significantly faster blood clearance and accumulated significantly more in the liver and less in kidney than PAMAM-G4-$(1B4M\text{-}Gd)_{64}$. At 15 min after the injection, the blood concentrations of PAMAM-G4-$(1B4M\text{-}Gd)_{64}$, and PPI-G4-$(1B4M\text{-}Gd)_{64}$ were $2 \pm 0.1\%$ and $0.8 \pm 0.1\%$ ID/g, respectively. The whole body retention of PPI-G4-$(1B4M\text{-}Gd)_{64}$ was also significantly less than that of PAMAM-G4-$(1B4M\text{-}Gd)_{64}$ [126].

4.3. Surface modification

mCAs with high molecular weight like other nanoparticles or large macromolecules are often eleminated from the circulatory system by the reticuloendothelial system (RES) [127]. This process is initiated by opsonization, which is the process by which a foreign organism or particle becomes covered with opsonin protein, thereby making it more visible to phagocytic cells. Following opsonization, macrophages recognize, phagocytose, and then sequester the particles in the liver, spleen, and/or bone marrow. Avoiding or reducing opsonization is critical to prevent elimination by RES. One widely used method to slow opsonization is surface modification with hydrophilic polymers including polysaccharide, poly(vinylalcohol), poly(N-vinyl-2-pyrrolidone), PEG and PEG containing copolymer [116]. Of all the polymers tested to date, the most effective and most commonly used is PEG, which is very flexible, highly hydrophilic, charge neutral and biocompatible [127,128]. Bogdanov et al. prepared an mCA from PEG grafted polylysine copolymer (MPEG-PL), and found that

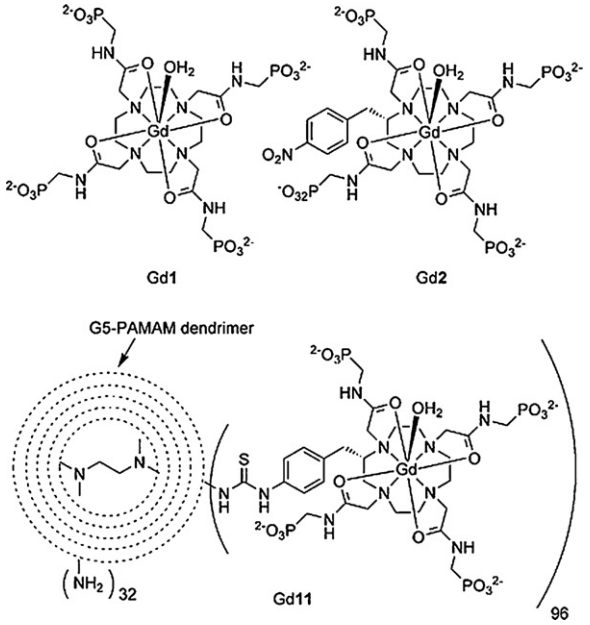

Fig. 24. The structure of pH-responsive PAMAM dendrimer CA. Reprinted from [36].
© 2008 with permission from Wiley.

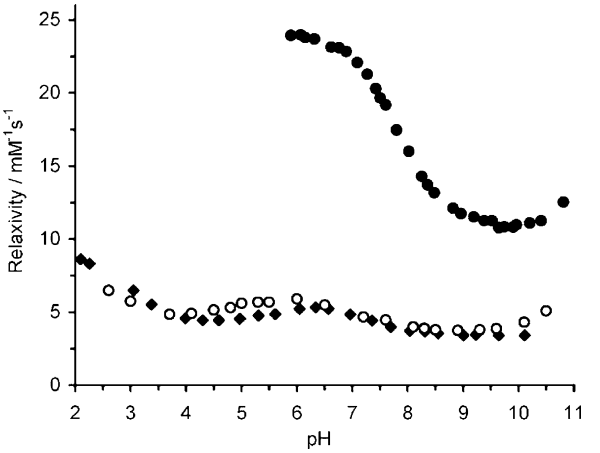

Fig. 25. Relaxivity pH profiles of Gd1 (♦), Gd2 (○) and Gd11 (●) recorded at 20 MHz and 25 °C (the structure of Gd1, Gd2 and Gd11 are shown in Fig. 24). Reprinted from [36].
© 2008 with permission from Wiley.

the $t_{1/2}$ of MPEG-PL-DTPA-Gd^{3+} with a molecular weight of 430 kDa reached 14 h, much higher than that of PLL-DTPA-Gd^{3+} even with a slightly higher molecular weight [68]. Kobayashi et al. made two PEGylated dendritic mCAs from G4 PAMAM via conjugation with 1B4M and one or two PEG chains, PEG_2-G_4PAMAM-$(1B4M\text{-}Gd)_{62}$ (MW: 96 kDa) and PEG_1-G_4PAMAM-$(1B4M\text{-}Gd)_{63}$ (MW: 77 kDa). The blood α phase half-lives of the two PEGylated mCAs and the one without PEGylation were 15 ± 4.2 min, 5.1 ± 1.6 min, and 3.2 ± 1.1 min, respectively, and their blood β phase half-lives were 162 ± 36 min, 119 ± 26 min, and 55 ± 24 min for PEG_2-G4D-$(1B4M\text{-}Gd)_{62}$, PEG_1-G4D-$(1B4M\text{-}Gd)_{63}$, and G4D-$(1B4M\text{-}Gd)_{64}$, respectively. It is evident that the two PEGylated dendritic mCAs remained in the blood significantly longer and accumulated significantly less in the liver and kidney than that without PEGylation [129].

4.4. Shape

The effect of shape, which has not yet been extensively explored, also significantly affect the clearance and pharmacokinetics of mCAs. The clearance and pharmacokinetics of linear copolymers and branched spherical PAMAM dendrimers were compared by Sadekar et al. [130]. They found that the G5 hydroxyl-terminated PAMAM (G5.0-OH) was retained in the kidney over 1 week, whereas the linear HPMA copolymer of comparable molecular weight was excreted into the urine and did not show persistent renal accumulation. In addition, the G6 hydroxyl-terminated PAMAM (G6.0-OH) was taken up by the liver to a higher extent, whereas the HPMA copolymer of comparable molecular weight was observed to have a plasma exposure three times that of this dendrimer due to much less uptake by the liver [130]. Kobayashi et al. compared the clearance and pharmacokinetics of dendrimers modified with PEG of different molecular weights. The dendritic mCAs modified with short PEG tails had spherical shapes, whereas those modified with one or two long PEG chain had non-spherical shapes. As a result, they showed very different

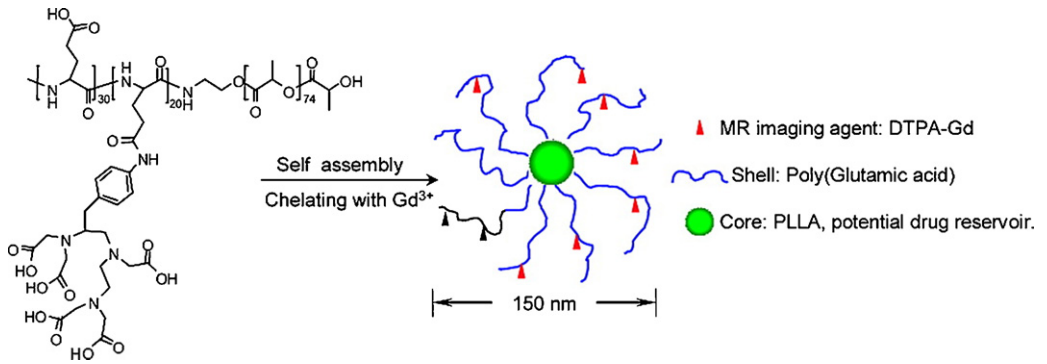

Fig. 26. Structure of PG(DTPA)-*b*-PLA (A) and schematic model of the micellar structure with DTPA-Gd chelated to the shell layer (B). Reprinted from [107].
© 2007 with permission from ACS.

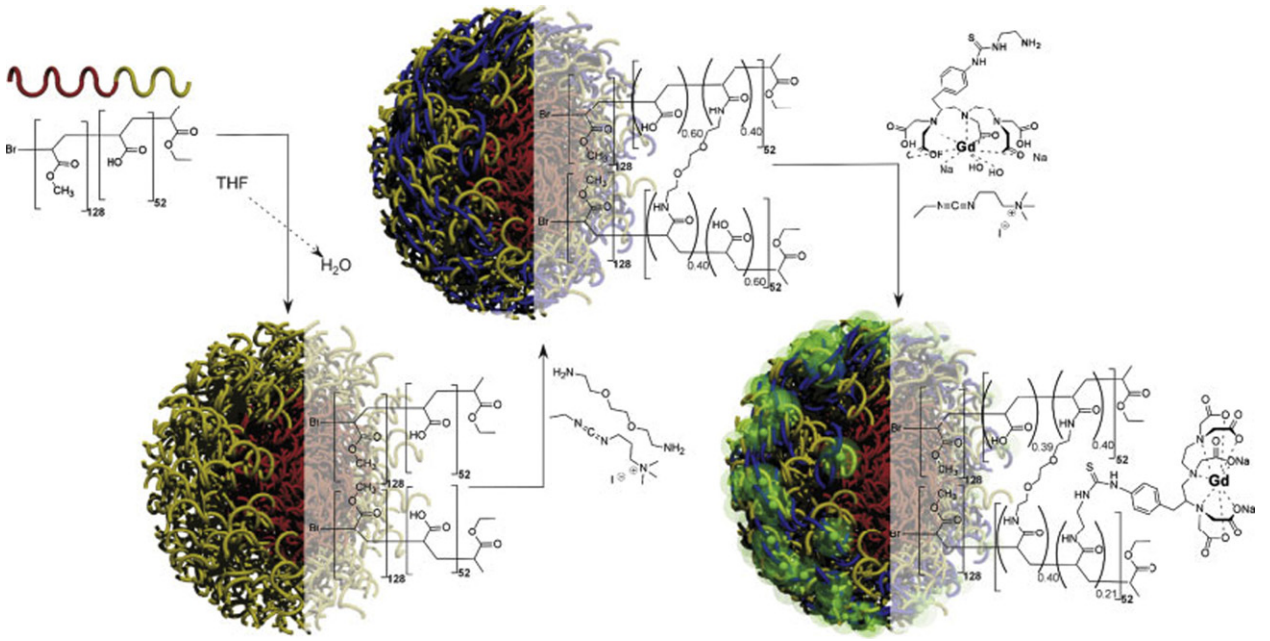

Fig. 27. Graphical representation of the synthesis of Gd^{III}-labeled SCK. Starting from a tetrahydrofuran (THF) solution of an amphiphilic diblock copolymer, PAA_{52}-*b*-PMA_{128}, self-assembly was induced by the controlled addition of H_2O to produce a multimolecular, micellar structure. Subsequent crosslinking of the shell layer upon amidation with a diamine produced a covalently stabilized SCK, which was then derivatized throughout the hydrophilic shell with a Gd^{3+}-coordinated, amino-functionalized DTPA analogue. Reprinted from [109].

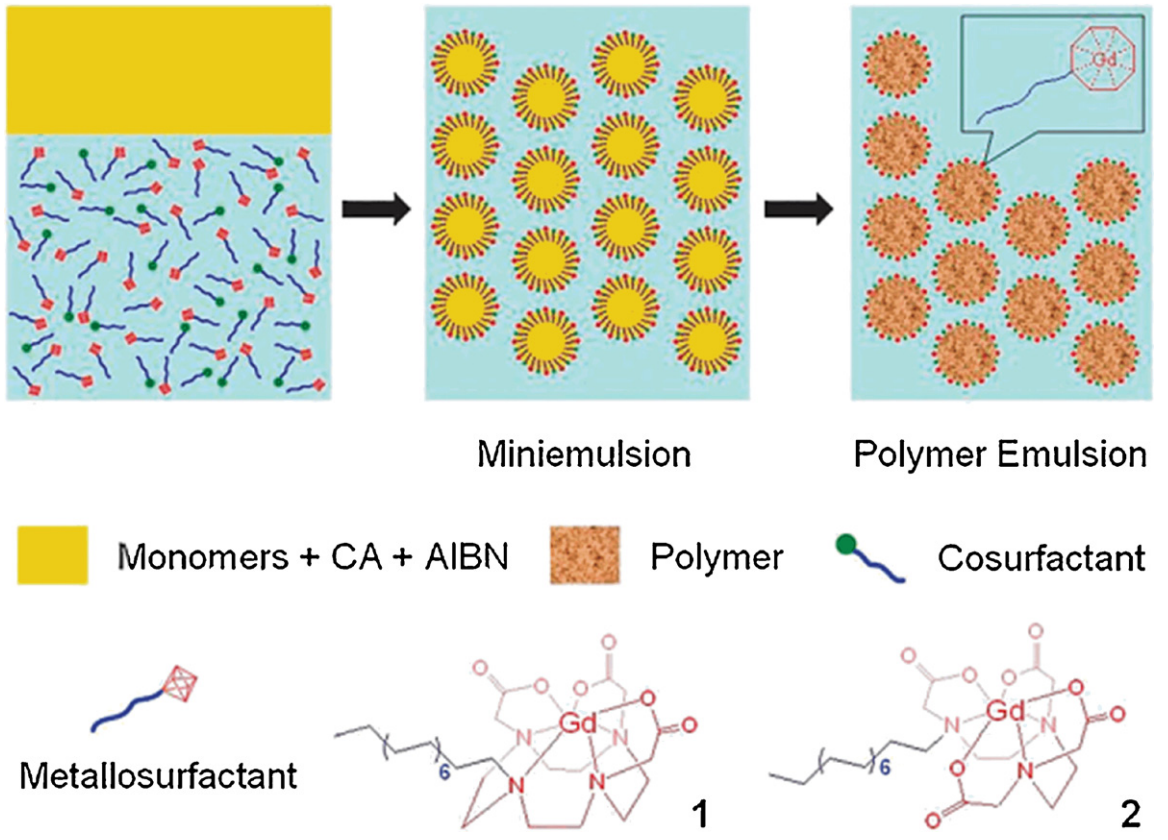

Fig. 28. Illustration of miniemulsion polymerization using gadolinium(III)-based metallosurfactants. Reprinted from [110].

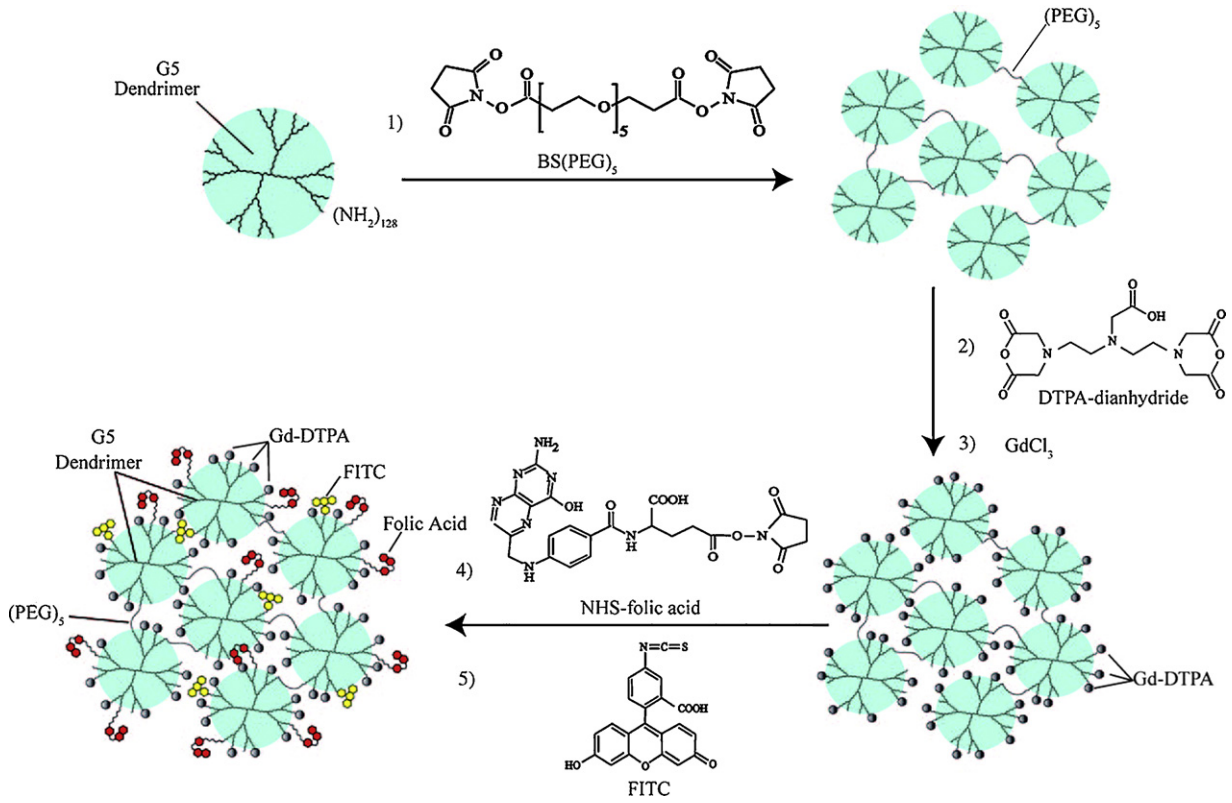

Fig. 29. Preparation of paramagnetic targeted dendrimer nanoclusters (DNCs). Reprinted from [111].

clearance and pharmacokinetics. The later with long PEGylated tails underwent relatively rapid renal clearance, while the former with short PEG tails did not show renal clearance (Fig. 33) [116,129]. The effect of nanoparticle shape on flow and drug delivery was also investigated by comparing linear polymer micelles known as filomicelles to spheres of the same chemistry in rodents. It was found that the filomicelles remained in circulation ten times longer than their chemically similar spherical counterparts, suggesting that the shape played a significant role in in vivo behavior [131].

4.5. Flexibility

The flexibility is also an important determinant of clearance and pharmacokinetics for mCAs. Generally, increasing flexibility of mCAs can increase the renal clearance of mCAs [116]. For example, Kobayashi et al. found that the dendritic mCA with more flexible interior of PAMAM dendrimer with ammonia core went through glomerular filtration more efficiently than those with less flexible interior of PAMAM dendrimer with ethylenediamine core, resulting faster clearance from the blood and higher renal accumulation, even though both of the two dendritic mCAs have almost similar molecular size and same chemical structure. The later remained in the blood significantly more than the former at 15 min post-injection and visualized the fine vessels longer than the former, whereas, the former showed higher signal intensity in the kidney on the dynamic MR images and brighter kidney images than the later [132].

5. Clinical applications

As discussed above, the mCAs have two main advantages over small molecular CAs: enhanced relaxivity and improved pharmacokinetics. The enhanced relaxivity makes it possible to reduce the risk of toxicity by lowering the dose of Gd^{3+} chelates. The different pharmacokinetics of mCAs makes them suitable for a variety of applications. The advantages of using mCAs in angiography, cancer imaging, kidney imaging, liver imaging, lymphatic imaging, and noninvasive visualization of drug delivery have been demonstrated by various studies.

5.1. Blood pool imaging

Blood pool CAs, also known as intravascular CAs, are used in vasculature imaging, also known as magnetic resonance angiography (MRA) or cardiovascular imaging to detect vascular diseases. Therefore, they are required to remain in the intravascular system for a prolonged time rather than diffuse quickly into interstitial space. mCAs show great potential for this application due to their long blood retention times and their inability to cross the vascular walls. Bogdanov et al. evaluated a PEG grafted polylysine-DTPA-Gd^{3+} mCA as a blood pool agent. The $t_{1/2}$

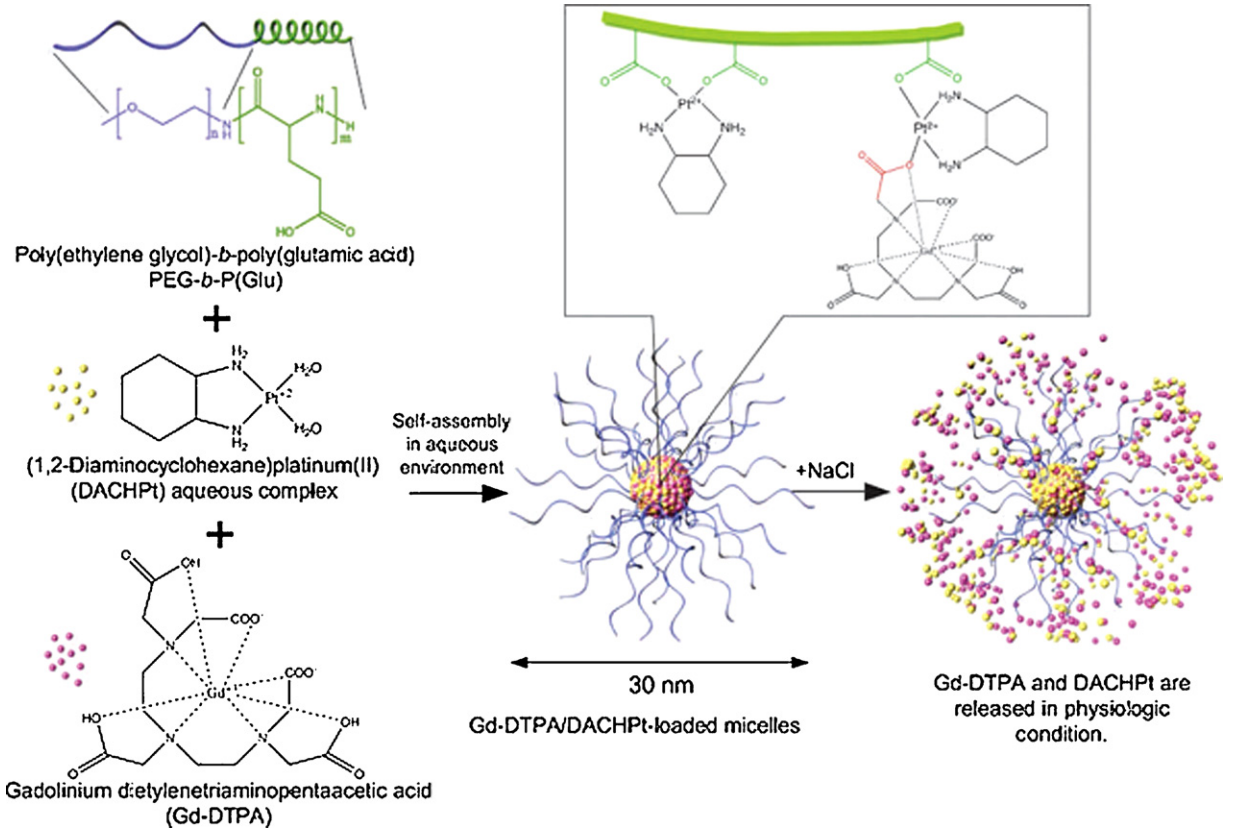

Fig. 30. Schematic diagram of proposed self-assembly of Gd-DTPA/DACHPt loaded micelles and release of Pt and Gd complexes from the micelles in chloride containing media. Reprinted from [112].

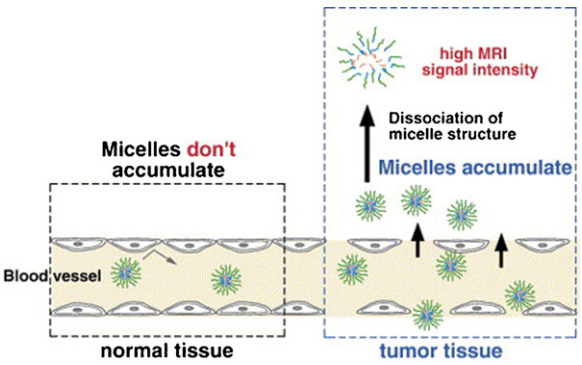

Fig. 31. The concept of polymeric micelle-type MRI contrast agent for tumor imaging. Reprinted from [113].

of the mCA was 14 h. A dose of 20 μmol of Gd per kg of body weight was sufficient to increase the vessel-muscle contrast ratio 4–5-fold [68]. Fig. 34 shows the maximum intensity projections (MIP) image from a 3D TOF sequence of a rat head before and after intravenous administration of 15 μmol/kg MPEG-PL-Gd-DTPA. While virtually no vessels were seen on the precontrast images, a considerable improvement in vessel delineation was evident on the postcontrast image. Not only the signal intensities of arteries but also those of veins became more readily discernible, even in the vessels of submillimeter diameters. Fig. 34 shows the right femur and tibia of the same rat. The iliac and femoral artery and vein are clearly demonstrated. Up to four orders of branching vessels could be identified [68].

The slow excretion, however, also increases the risks from the cellular uptake and metabolism of Gd chelates, resulting in long-term tissue accumulation of toxic Gd^{3+} ions. Two solutions have been proposed to solve this problem. One, is choosing the carriers with suitable molecular weights, which are large enough to have a much slower leakage of the mCAs through the normal functioning endothelium than small molecule CAs but still small enough than the renal clearance threshold for renal clearance via the kidneys. Gadomer 17, a dendritic mCA under phase II clinical development, which carries 24 Gd ions with a molecular weight of 17 kDa, is an example of this type of mCA [99]. While Gadomer 17 has a plasma half-life in rat of 1.4 h, more than 99% of the agent could be eliminated from the body after 7 days [59]. P792, shown in Fig. 35, is another mCA which is too large for capillary extravasation but is small enough for rapid renal elimination, which is currently under phase III clinical development [133].

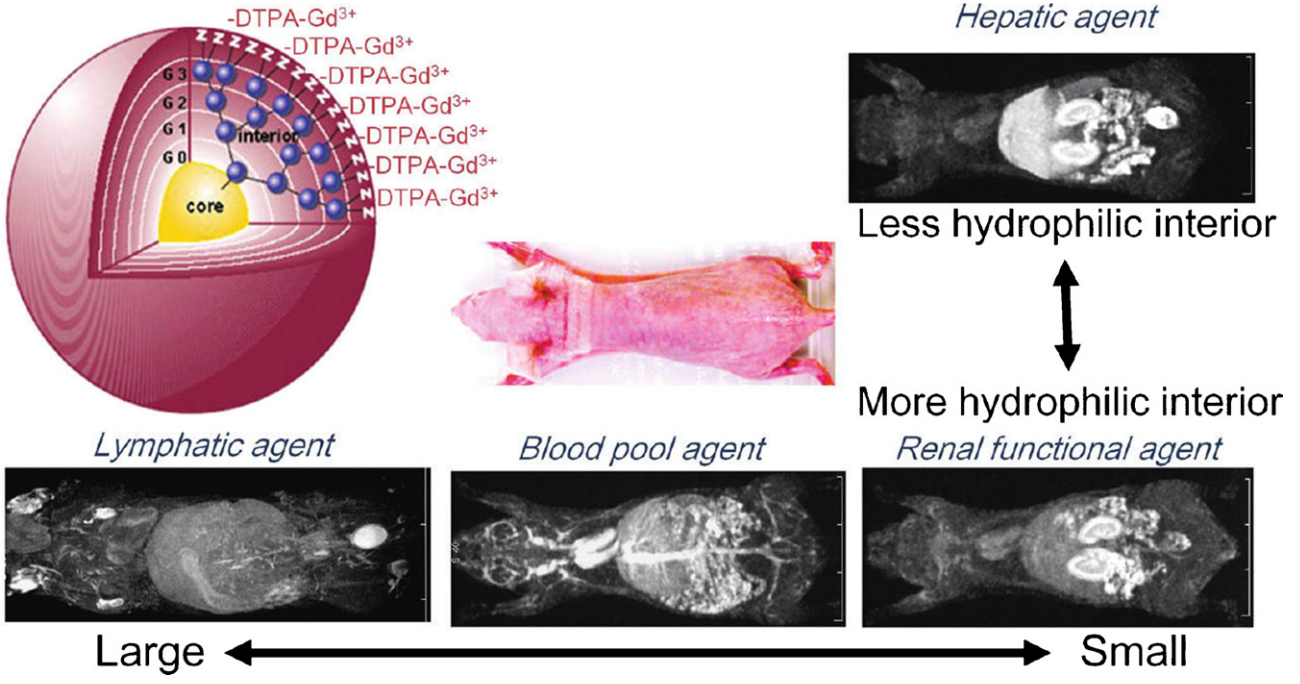

Fig. 32. Strategic use of dendrimer size to achieve organ-specific imaging. This schema depicts a generation 3 dendrimer, with core chemistry, shape, and surface modifications functionalized for use as an MRI contrast agent. Images of mice demonstrate that strategic selection of dendrimer size enables target organ-specific imaging. For example, PAMAM-G8 shows the lymphatic system; PAMAM-G6 shows the blood pool; PAMAM-G4 depicts renal function; and PPI/DAB-G4 depicts liver parenchyma. Reprinted from [116].

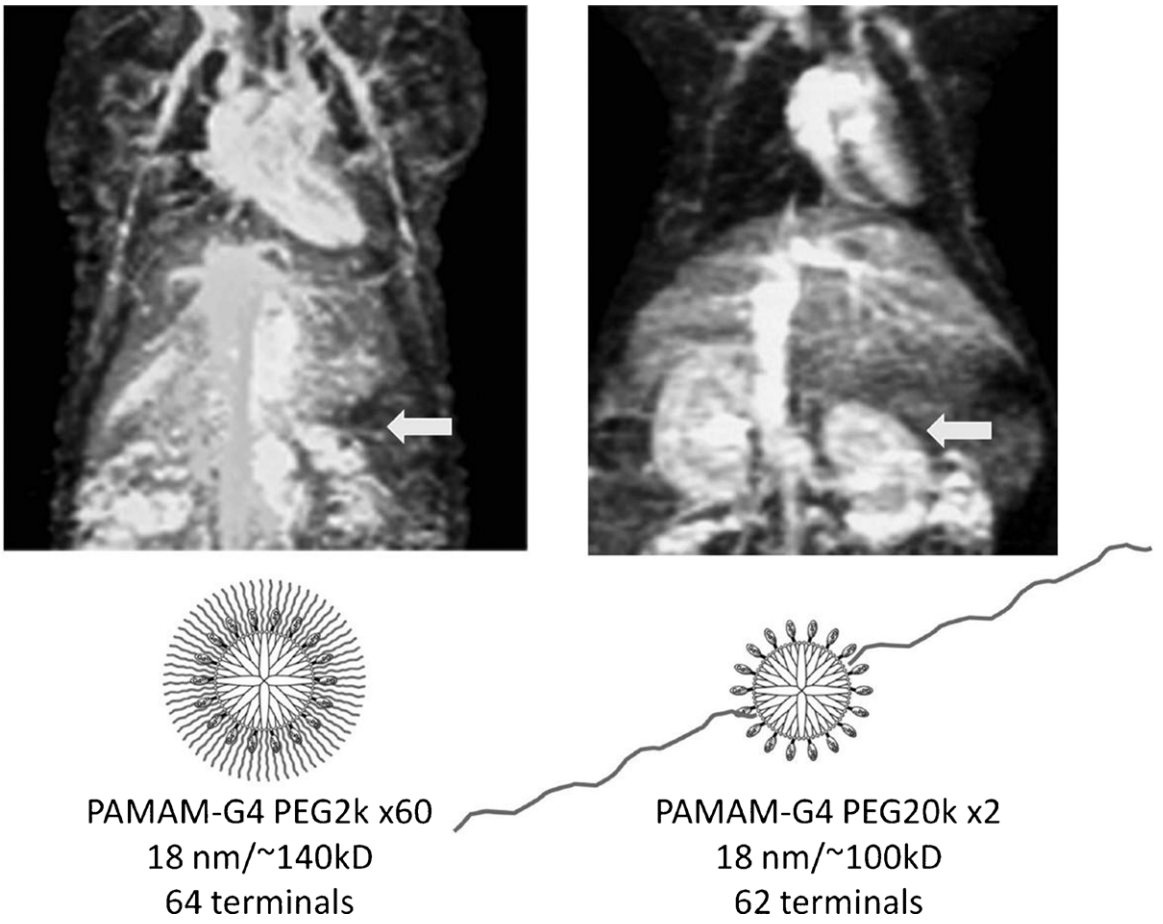

Fig. 33. Two long, linear PEG (20 kDa) conjugated PAMAM-G4-Gd shows renal excretion, whereas short PEG (2 kDa) conjugated PAMAM-G4-Gd of similar physical size shows no renal excretion. Reprinted from [116].

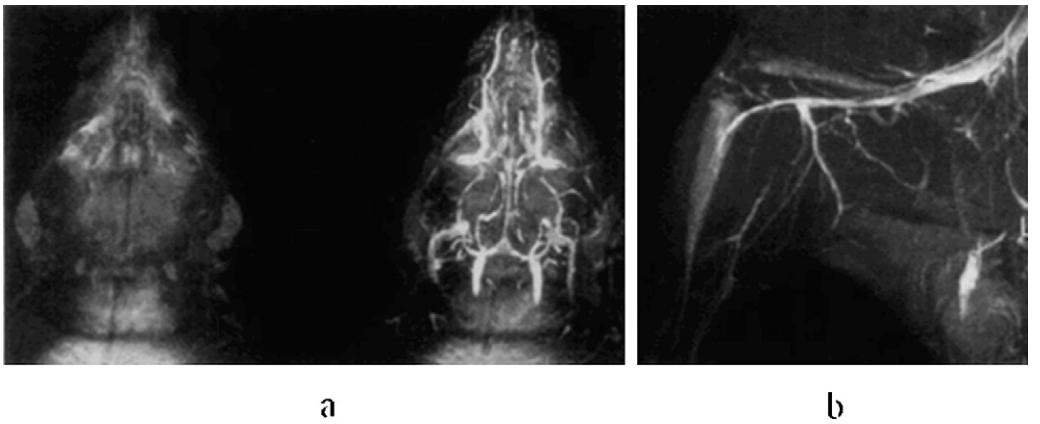

Fig. 34. MIP spoiled GRASS MR images of a rat head, obtained before (left) and after (right) intravenous administration of MPEG-PL-Gd-DTPA. The precontrast image was obtained at 60/8 (repetition time ms/echo time ms) with a flip angle of 20°. The postcontrast image was obtained at 60/8 with a flip angle of 60°. Veins and arteries are much better visualized after administration of the contrast medium. Vessels less than a millimeter in diameter are seen because of the high vessel-muscle ratio. Notice the areas of high vascularity in the whisker region. (b) Spoiled GRASS MR image (60/8; flip angle, 60°) obtained after administration of MPEG-PL-Gd-DTPA. The excellent vessel-muscle ratio facilitates delineation of four orders of vascularity. Reprinted from [68].

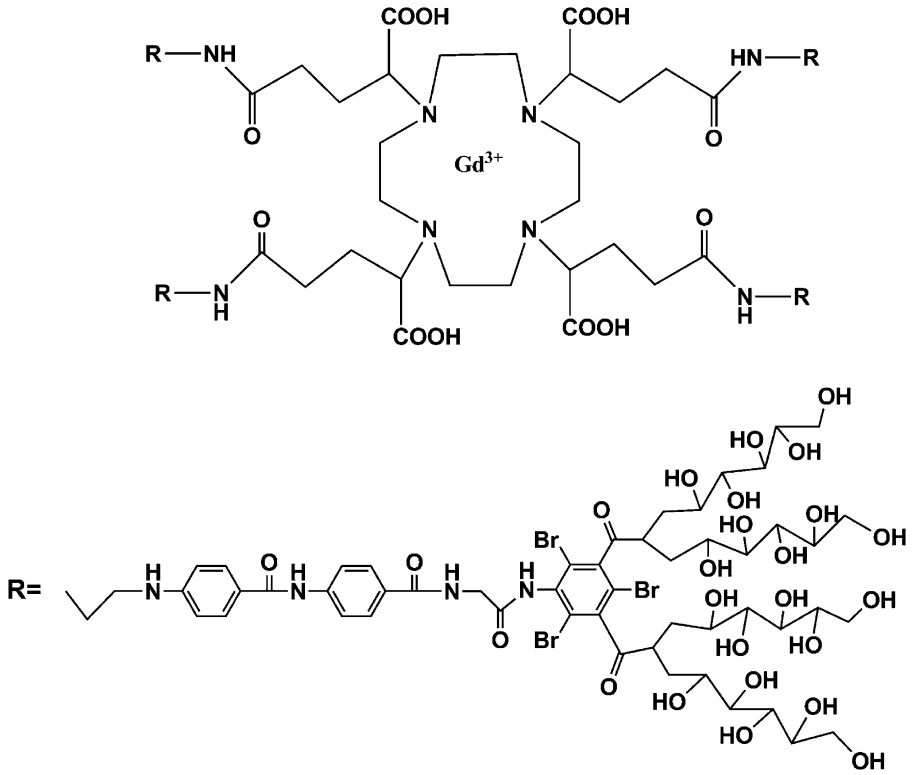

Fig. 35. The structure of P792.

An alternative method is to use biodegradable mCAs. These mCAs work as intravascular agents for blood pool imaging and then degrade into low molecular weight pieces to be excreted. Lu et al. developed a series of polydisulfide-based copolymers, shown in Fig. 9, which could be degraded into small pieces by cleaving the disulfide bonds in the polymer chains via disulfide-thiol exchange reaction with endogenous thiols. The smaller Gd(III) chelates can then be excreted rapidly by kidneys. These copolymers were evaluated as blood pool agents using different animal models, indicating that these copolymers had superior contrast enhancement in heart and blood vessels as compared to a low molecular weight control CA [52,53,56]. Fig. 36 demonstrates that GDCC markedly improved the visualization of the thoracic vessel branches and the heart for first-pass breath-hold imaging and the GDCC drastically improved blood signal-to-noise ratio compared to the precontrast images [134]. Moreover, the biodistributions of Gd(III) in the major organs and tissues, including the femur, heart, kidneys, liver, lungs, muscle, and spleen of rats 10 days after the injection of either GDCC, and control agent Gd-(DTPA-BMA), at a dose of 0.1 mmol Gd/kg were monitored. The accumulations of Gd(III) in the tissues measured were at the same minimal level for GDCC and the control agent [29].

5.2. Cancer imaging

Most solid tumors possess unique pathophysiological characteristics that are not observed in normal tissues or organs, such as extensive angiogenesis and hypervasculature, defective vascular architecture, and an impaired lymphatic drainage recovery system [135,136]. They also overproduce vascular permeability mediators to greatly enhance the permeability of their blood vessels. It was reported that even 1000 nm bacteria could diffuse out from these permeable vessels [137], which is known as the EPR effect [138]. mCAs are able to accumulate in tumors through the EPR effect, which makes them very promising for cancer imaging.

The applications of mCAs for tumor imaging mainly includes differentiating benign and malignant tumors [139], imaging the tumor aggressiveness [140,141], monitoring the early tumor responses to anti-angiogenesis drug therapy [142,143], and being used as a predictive biomarker for future tumor response [101,144]. The majority of reports focused on tumor angiogenesis imaging using dynamic contrast-enhanced MR imaging (DCE-MRI), which acquires a consecutive series of MR images before, during, and after administration of a CA. The results can be depicted numerically, or as color-encoded images. The measured DCE-MRI parameters were shown to correlate with the vascular permeability and hence the angiogenesis in the tumor tissue. A detailed description of DCE-MRI is available from previously published reviews [145,146].

Albumin, dextran and PAMAM or PPI dendrimers conjugated with DTPA/DOTA-Gd^{3+} chelates are the most frequently used mCAs for tumor imaging [145]. They have been successfully exploited for detecting and grading tumors, as well as detecting early responses to

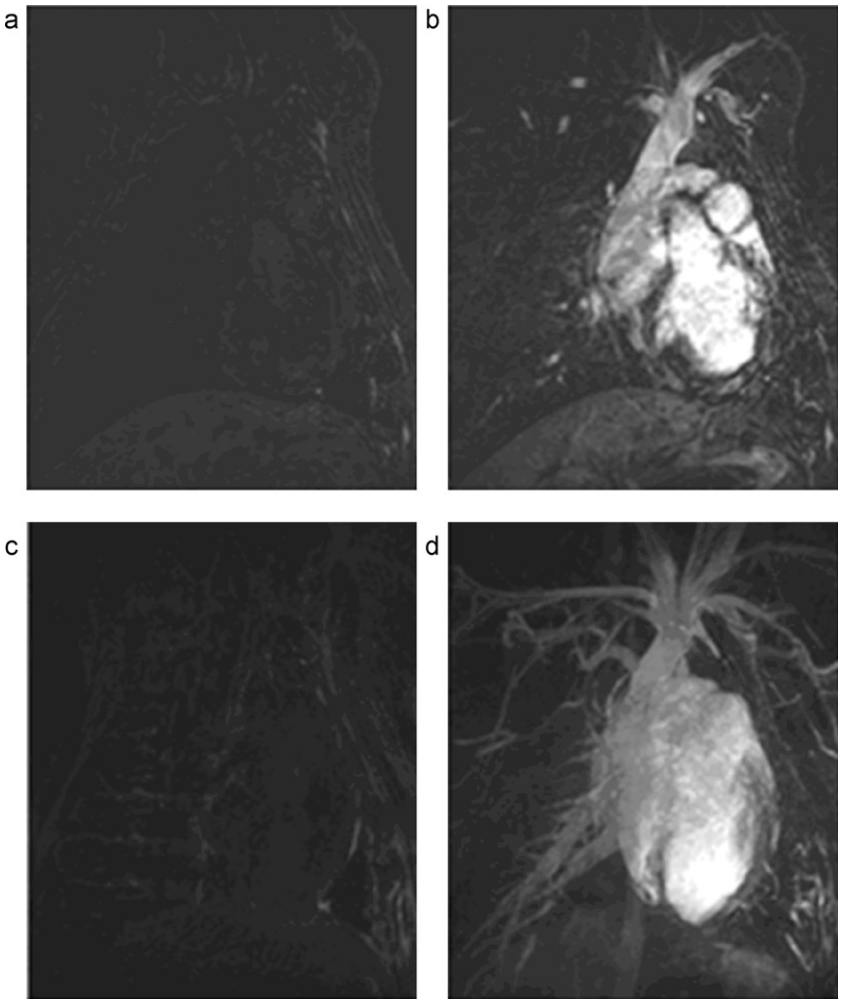

Fig. 36. First-pass breath-hold 3D MRA of the thorax. Source images acquired (A) pre-contrast, (B) post-GDCC. Corresponding MIP images acquired (C) pre-contrast, (D) post-GDCC. Reprinted from [134].

anti-angiogenesis drug therapy. Daldrup et al. developed a method to test the angiogenesis and grade tumor via measuring the tumor permeability using dynamic albumin-(DTPA-Gd-)-enhanced MRI. The tumor permeability for mCA was analyzed by testing the changes in the relaxation rate between the pre- and post-contrast tumor rim at different times. The results obtained from the dynamic albumin-(DTPA-Gd-)-enhanced MRI correlated closely with histological tumor analysis and grade [139]. The permeability values (K^{trans}) from albumin-(Gd-DTPA)-enhanced MRI measurement have been found effective for monitoring the response of anti-angiogenic therapy [139,147,148]. Kobayashi et al. evaluated the changes in the permeability of SCC VII tumor vessels after radiation treatment as a function of time by dynamic MRI with a generation-8 PAMAM dendrimer-based mCA, and found a significant transient image enhancement of the tumor tissue with a maximum occurring between 7 and 24 h after the radiation treatment [149].

Besides passive targeting via the EPR effect, tumor-targeting groups were also introduced onto mCAs to improve the tumor imaging. Monoclonal antibodies, peptides, or folate are the most commonly used targeting groups for tumor-targeting [150]. For example, the PAMAM-DTPA-Gd^{3+} mCA conjugated with folic acid as the targeting group was taken up specifically by tumor cells, leading to a specific increase of over 100% in the r_1 of tumor cells. When administrated in vivo, the folate conjugated mCA was found accumulated in xenografted ovarian tumors expressing the folate receptor and had a 33% increase in the contrast enhancement of ovarian tumors compared with a non-specific agent [151,152].

Torchilin et al. found that 2C5 (a monoclonal antibody capable of binding to the surface of a variety of cancer cells but not normal cells)-modified PEGylated liposome CA allowed for fast and specific tumor imaging as early as 4 h post-injection. The T_1 inversion recovery maps displayed a significant increase in the tumor-associated r_1

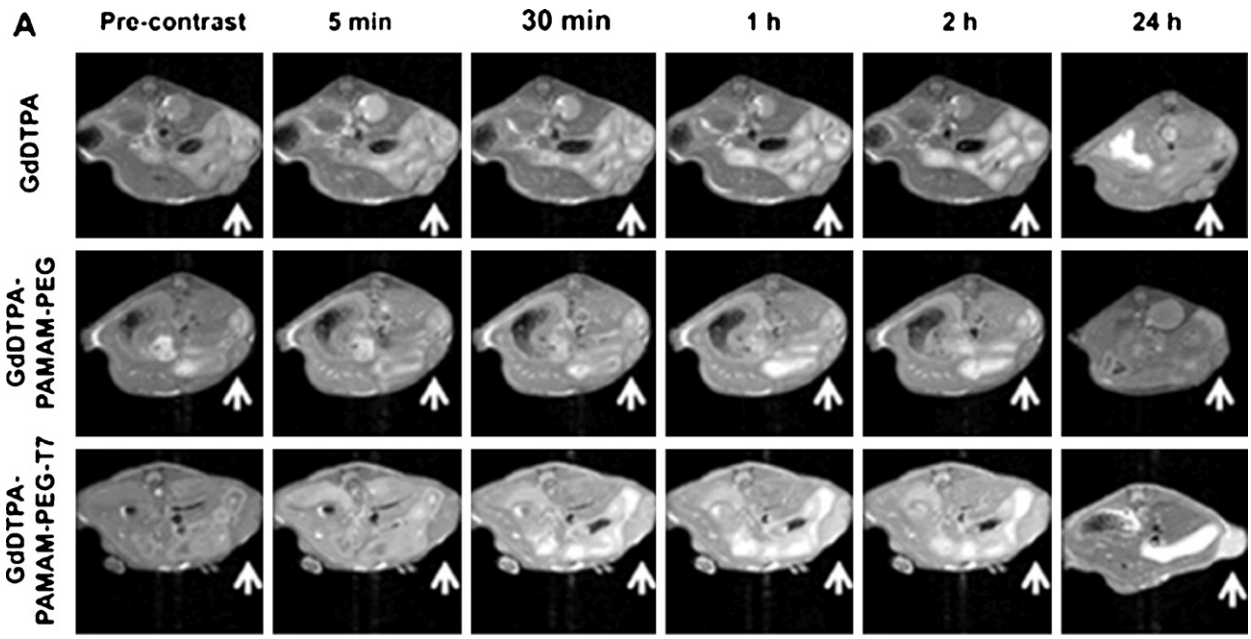

Fig. 37. MR imaging of mice with subcutaneous Bel-7402 xenograft. T1-weighted MR images of nude mice at various time after i.v. injection of Gd-DTPA (top row), Gd-DTPA-PAMAM-PEG (second row) and Gd-DTPA-PAMAM-PEG-T7 (bottom row). Images were acquired preinjection and 5, 30 min, 1, 2 and 24 h post-injection; white arrow shows location of subcutaneous Bel-7402 xenograft. Reprinted from [155].

in animals 4 h after injection of the targeted liposome CA and a gradual decrease thereafter consistent with the clearance of the agent from the tumor region. In the control animals injected with antibody-free liposome CA, the corresponding r_1 values at the investigated time points were significantly smaller [153]. Zhuo et al. prepared a tumor-selective mCA with 5-(p-carbonyloxy phenyl)-10,15,20-triphenylporphyrin (HPTP) as a targeting group and polyaspartamide as the carrier. The mCA containing HPTP moiety significantly enhanced the MRI contrast of hepatoma (H22) and Ehrlich ascites carcinoma after injection [30].

Transferrin receptors are highly expressed on both liver cancer cells and brain glioma cells. Peptide T7 (sequenced HAIYPRH) has been found to have high affinity for transferrin receptors (Tf_R) comparable to that of transferrin (Tf), with Kd of ~10 nM [154]. Thus, T7 has been explored as a ligand for targeting delivery of agents to target Tf_R highly expressed tumors. Jiang et al. prepared a tumor targeting mCA from T7-conjugated polyethylene glycol (PEG)-modified polyamidoamine (PAMAM) dendrimers (PAMAM-PEG-T7) after conjugation with DTPA-Gd. The mice with subcutaneous Bel-7402 xenografts were treated with GdDTPA-PAMAM-PEG-T7, GdDTPA and GdDTPA-PAMAM-PEG as controls to assess the specificity of GdDTPA-PAMAM-PEG-T7 (Fig. 37). Axial MR images were acquired pre-contrast and at various time after administration. As shown in Fig. 37, an image acquired pre-contrast, demonstrated that there was little intrinsic contrast between Bel-7402 tumor and surrounding muscle or organs. Five minutes after the injection of GdDTPA-PAMAM-PEG-T7, the subcutaneous Bel-7402 tumor appeared hyper intense, with the signal in the tumor lesion gradually increasing. After 24 h the image showed accurate delineation of the tumor boundary. The tumor signal enhancement by GdDTPA-PAMAM-PEG-T7 was evidently higher than that by GdDTPA and GdDTPA-PAMAM-PEG, and the signal enhancement by GdDTPA-PAMAMPEG-T7 could be retained for a much longer time [155].

5.3. Liver imaging

The presence of hydrophobic groups on the Gd^{3+} chelates can cause hepatocellular uptake and excretion into the bile ducts, gall bladder, and intestines, resulting in the visualization of a hyperintense/bright liver by the MRI. Thus, small molecule liver MRI CAs with hydrophobic groups enhance the signal of the normal liver parenchyma, and have been actively investigated for many years [156,157] with some being currently used in clinical practice [158–160]. The mCAs based on polymer carriers are also inclined to accumulate in the liver, and are therefore promising as liver MRI CAs [117]. For example, a PPI-G_5-dendrimer-based mCA was found to accumulate in the liver at 50% of the injected dose within 15 min after injection. The hydrophobicity of the carriers plays an important role in liver imaging using mCAs. The more hydrophobic PPI-based CAs accumulated more significantly in the liver and less in blood compared to the less hydrophobic PAMAM-based mCAs. The MRI enhanced by the PPI dendrimer mCA was able to visualize liver parenchyma and both portal and hepatic veins of 0.5 mm in diameter in mice (Fig. 38) [126]. Furthermore, the experiment on a mouse colon carcinoma liver metastasis model indicated that the dynamic micro-MRI with PPI-G_5-dendrimer-mCA could homogeneously

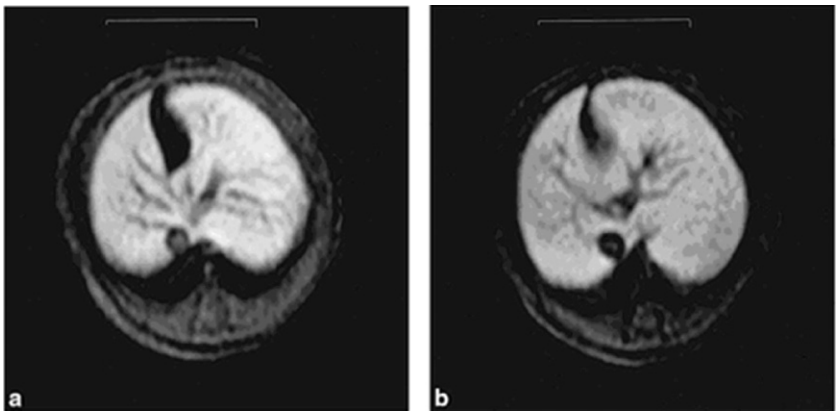

Fig. 38. Axial liver images of contrast-enhanced MRI at the level of the hepatic veins (A) and the portal veins (B) obtained 20 min after the injection of 0.033 mmol/kg of DAB-Am64-(1B4M-Gd)$_{64}$ are shown. The scale indicates 1 cm. The images showed a homogeneously high signal intensity in the liver parenchyma with negative contrast to both hepatic and portal veins. Reprinted from [126].

enhance the imaging of normal liver parenchyma and visualize the micrometastatic tumors of 0.3 mm in diameter in the mouse liver with a better contrast than that with Gd-DTPA [161].

Liver-targeting groups were also introduced into mCAs to increase their specificity to liver. For example, Zhuo et al. made liver-specific CAs by introducing D-galactose onto polylysine-DTPA/DOTA conjugates and found they could preferentially enhance liver imaging [162,163]. Ai et al. prepared liver-targeting dendritic mCAs via introduction of multiple galactosyl moieties onto dendritic mCAs. The dendritic mCAs provided better signal intensity (SI) enhancement in mouse liver, especially at 60 min post-injection, with the most efficient enhancement from the galactosyl moiety decorated G3 dendritic mCA [164].

5.4. Kidney imaging

Kidney imaging is mainly used to detect structural and functional abnormalities of the renal parenchyma [92]. Kobayashi et al. found a G4-dendrimer-based mCA could efficiently monitor renal injury caused by administration of cisplatin in mice [165]. Since then, PAMAM- and PPI dendrimer-based mCAs with molecular weight less than 60 kDa were synthesized and evaluated as an efficient mCA for imaging early renal tubular damage[20]. All the tested dendritic mCAs allowed MRI to visualize the renal functional anatomy in mice (Fig. 39) [92]. PPI-dendrimer-based mCAs were excreted more rapidly from the body than PAMAM-dendrimer-based mCAs at same generations, and the PPI-G_2 dendrimer mCA was found to be the best candidate for functional kidney imaging because it was cleared most rapidly but still enabled visualization of mild renal tubular injury at very early stages after injury [19,92].

5.5. Lymphatic imaging

Up to now, very few methods are available to visualize the deep lymphatic system [19]. Recently, mCAs, especially dendritic mCAs, have been shown to enable the clear visualization of even deep lymphatic vessels and lymph nodes using the micro-magnetic resonance lymphangiography (MRL) method [166–168], which can be used for diagnosing the impairment of lymphatic drainage function in a lymphedema, and distinguishing the appearance of infectious lymph nodes [20]. The core and size of dendritic mCAs affected their performances in visualizing the lymphatic system.

Kobayashi et al. compared different dendrimer-based mCAs for dynamic MRL in the context of lymphoma/lymphoproliferative disease, inflammation, and cancer metastasis, and found that PAMAM-G8-(1B4M-Gd)$_{1024}$, DAB-G5-(1B4M-Gd)$_{64}$, PAMAM-G4-(1B4M-Gd)$_{64}$, and Gadomer-17 enabled most of the deep lymph nodes to be visualized throughout the body of mice (Fig. 40) [169]. The large hydrophilic molecule, PAMAM-G8, was advantageous for visualizing lymphatic vessels. In contrast, the small hydrophobic DAB-G5, allowed specific visualization of the lymph nodes. The small hydrophilic PAMAM-G4, which showed intermediate characteristics between PAMAM-G8 and DAB-G5, appears to be the best compound for clinical use due to its quick clearance and low background signal [169].

5.6. Visible drug delivery system (visible DDS)

Visible DDS, also termed as theranostics, integrates therapy and diagnosis functions in one system. MRI guided DDS that carries both therapeutics and MRI CAs, is one of the most important theranostics used in clinical and preclinical study. The MRI guided theranostics could be polymeric colloids loaded with iron oxide nanoparticles and drugs [170–172], or polymer conjugates and polymeric colloids incorporating gadolinium chelates and drugs [5]. These MRI-guided DDSs can be used to noninvasively assess the biodistribution and the target site accumulation of therapeutics, to predict therapeutic responses, and to longitudinally monitor the efficacy of therapeutic interventions [173].

Kataoka et al. investigated the detection and treatment of pancreatic cancer using the previously introduced

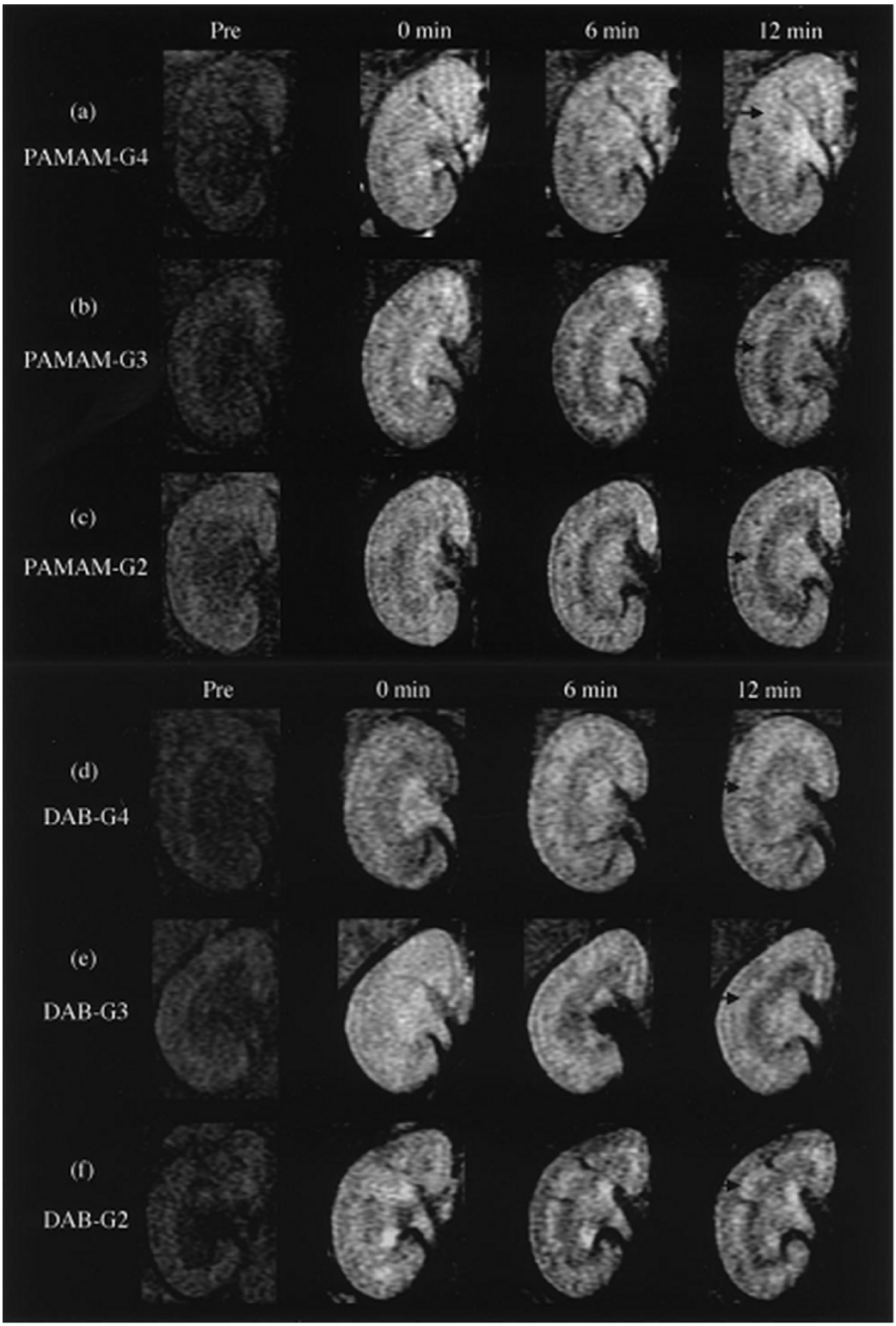

Fig. 39. Coronal high-resolution images of contrast enhanced dynamic micro-MRI at the center of the right kidney obtained preinjection, or 0, 6, and 12 min postinjection of 0.03 mmol/kg of CA: PAMAM-G4 (A), PAMAM-G3 (B), PAMAMG2 (C), DAB-G4 (D), DAB-G3 (E), DAB-G2. Reprinted from [92].

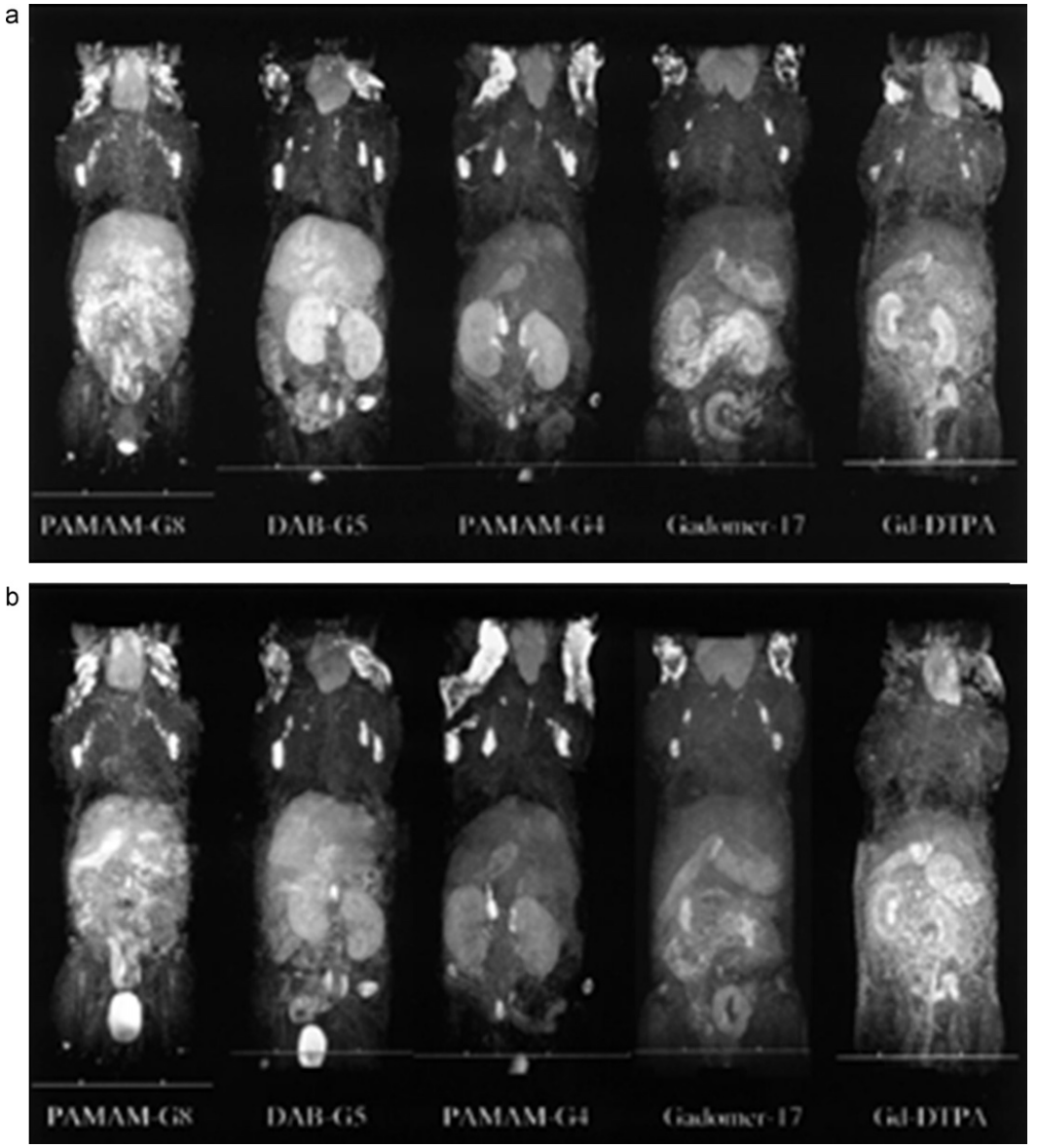

Fig. 40. Whole-body dynamic 3D-micro-MR lymphangiograms of mice injected intracutaneously into all four middle phalanges with 0.005 mmolGd/kg of PAMAM-G8-(1B4M-Gd)$_{1024}$, DAB-G5-(1B4M-Gd)$_{64}$, PAMAM-G4-(1B4M-Gd)$_{64}$, Gadomer-17, or Gd-DTPA are shown. MIPs obtained from images acquired at (A) 10 and (B) 45 min postinjection are shown for all five CAs. Reprinted from [169].

theranostic polymeric micelles with DTPA-Gd^{3+} and (1,2-diaminocyclohexane)platinum (II) (DACHPt), the parent complex of the potent anticancer drug oxaliplatin in the core (Fig. 30). The T_1-weighted MR images after intravenous administration of the Gd-DTPA/DACHPt-loaded micelles clearly showed specific contrast enhancement at the tumor area for more than 4 h (Fig. 41A and B), while the administration of free Gd-DTPA did not show any enhancement in the tumor region (Fig. 41A and B). The amount of Gd-DTPA delivered by the micelles in the orthotopic pancreatic tumor was 7 times higher than the accumulation of free Gd-DTPA (Fig. 41C). Accordingly, 3.5% of the total Gd dose from the micelles and 7.2% of the total Pt dose had accumulated in the tumor within 4 h after administration. The macroscopic observation of the orthotopic tumor-bearing mice that received Gd-DTPA/DACHPt-loaded micelles confirmed the position of every organ and the tumor (Fig. 41D, top and middle), while the histological study of the malignancy revealed a poorly differentiated histology of pancreatic adenocarcinoma with thick fibrosis and low vascularization (Fig. 41D, bottom) [112].

The antitumor activity of Gd-DTPA/DACHPt-loaded micelles was also evaluated by MRI. The mice treated with the micelles at 8 mg/kg on a Pt base achieved a significant reduction in the volume of orthotopic BxPC3 tumors

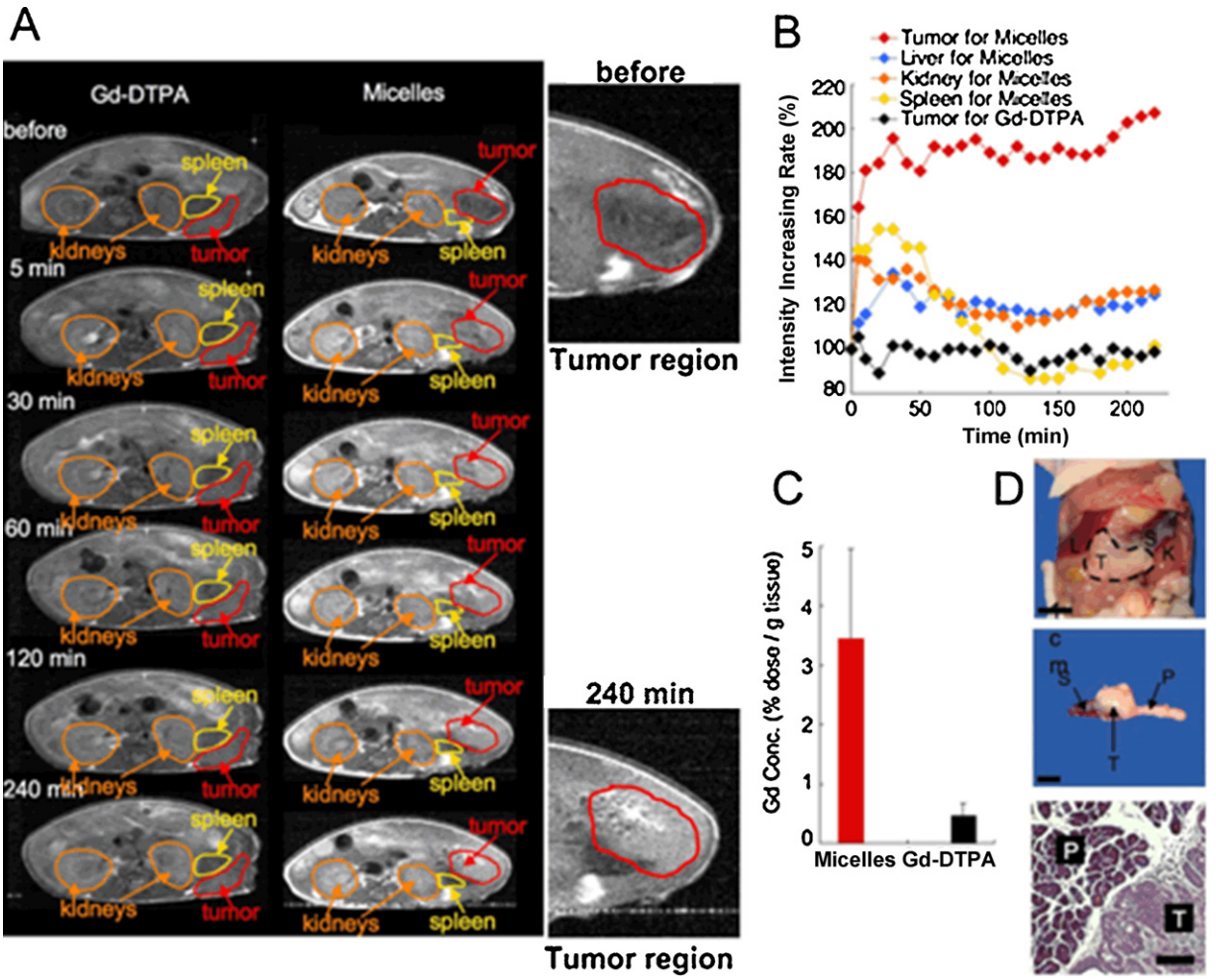

Fig. 41. In vivo behavior of Gd-DTPA/DACHPt-loaded micelles on an orthotopic pancreatic cancer (BxPC3). (A) In vivo MRI series of T_1-weighted transaxial slices of mice after i.v. injection of Gd-DTPA/DACHPt-loaded micelles or Gd-DTPA at 5 mol/kg. (B) Relative MRI intensity in each organ after i.v. injection of Gd-DTPA/DACHPt-loaded micelles at 5 μmol Gd-DTPA/kg or i.v. injection of Gd-DTPA at 5 μmol. (C) The Gd-DTPA/DACHPt-loaded micelles and Gd-DTPA accumulation in the BxPC3 tumor 4 h after i.v. administration ($n = 4$). (D) Top, Macroscopic findings of orthotopic BxPC3-bearing BALB/c nude mice after MRI acquisition. Bar = 1 cm. Pancreatic cancer (T), liver (L), kidney (K) and spleen (S). Middle, the pancreatic tumor after excision with spleen and normal pancreas. Bar = 0.5 cm. Bottom, microscopic findings (H&E staining) of the pancreatic cancer (T) and normal pancreatic tissue (P). Bar = 100 μm. Reprinted from [112].

(Fig. 42A). Likewise, the weight of the pancreas at day 18 of the micelle-treated animal was much lower than the mice that received only Gd-DTPA (Fig. 42B). Moreover, Gd-DTPA/DACHPt-loaded micelles were shown to enhance the signal intensity at the tumor region (Fig. 42C). Thus, Gd-DTPA/DACHPt-loaded micelle can be used to follow the micelle accumulation in the tumor and the tumor size by MRI [112].

Lu et al. synthesized pegylated and non-pegylated poly-(L-glutamic acid) conjugates containing mesochlorine6, a photosensitizer, and Gd(III)-DO_3A, an MRI CA. The effects of pegylation on the biodistribution and tumor targeting were non-invasively visualized in the mice bearing MDA-MB-231 tumor xenografts with MRI. MRI-guided photodynamic therapy was carried out in the tumor bearing mice, and the tumor response to photodynamic therapy was evaluated by dynamic contrast enhanced MRI and histological analysis. The pegylated conjugate had longer blood circulation, lower liver uptake and higher tumor accumulation than the non-pegylated conjugate as shown by the MRI. Site-directed laser irradiation of tumors resulted in higher therapeutic efficacy for the pegylated conjugate than that for the nonpegylated conjugate. Moreover, the animals treated with photodynamic therapy showed reduced vascular permeability on DCE-MRI and decreased microvessel density in the histological analysis [174].

Besides cancer detection and therapy, MRI-based theranostics can also be used for other diseases. Wang et al. found the Gd-DO_3A-modified poly(HPMA) effectively accumulated in the ankles of rats suffering from adjuvant-induced arthritis, whereas no accumulation was observed in the ankles of healthy rats [173], and the HPMA copolymer

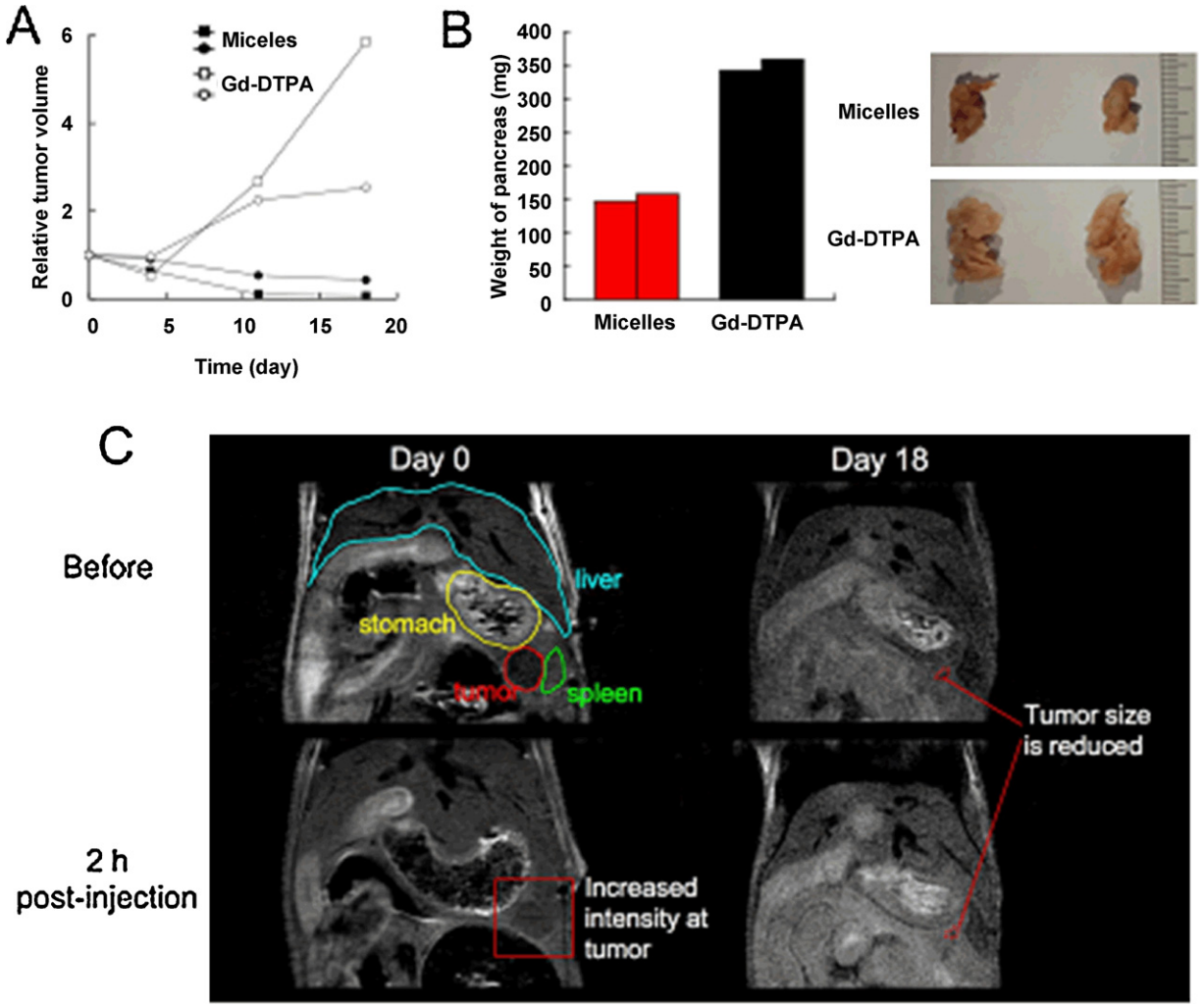

Fig. 42. In vivo antitumor activity of Gd-DTPA/DACHPt-loaded micelles on orthotopic pancreatic cancer model (BxPC3) assessed by volumetric MR imaging. (A) Effect of Gd-DTPA/DACHPt-loaded micelles (3 mg/kg on Pt basis) and oxaliplatin (8 mg/kg) injected i.v. 3 times at 2-day intervals on the growth of BxPC3 tumors. (B, left) Weight of the whole pancreas for mice treated with the micelles or Gd-DTPA at day 18 on the antitumor experiment. Right, macroscopies of the excised pancreas after treatment with the micelles or Gd-DTPA. (C) MR imaging at day 0 and day 18 of a tumor-bearing mouse treated with Gd-DTPA/DACHPt-loaded micelles. The tumor size was 89 mm^3 at day 0, and 5 mm^3 at day 18. Reprinted from [112].

conjugated with corticosteroid drug dexamethasone had long circulating and substantial improvement in disease inhibition [175–177].

6. Summary

This review presents the state of the art in mCAs. Compared with small molecule CAs, mCAs have two main favorable characteristics: enhanced relaxivity and extended retention in the blood circulation. Up to now, a variety of mCAs with various structures have been synthesized and studied in animal models, and demonstrated their great potential in angiography, cancer imaging, kidney imaging, liver imaging, lymphatic imaging, non-invasive visualization of drug delivery, to name a few. However, only few mCAs are currently under clinical trials. The kinetic and thermodynamic stability, basic pharmacokinetics, side effects and the costs of these agents limit their clinical translation. Since most of the mCAs are not biodegradable, they are difficult to excrete when their molecular weights are higher than their renal thresholds. Long-term retention of such mCAs imposes high risks to patients due to the high toxicity of free Gd^{3+} released by mCA metabolization. Thus, biodegradability of mCAs with high molecular weight must be considered. The future direction of mCAs may include: (1) further improving the r_1 of mCAs through self-assembly in order to reduce the dose of Gd^{3+} and hence minimize its side effects; (2) developing biodegradable and biocompatible mCAs; (3) developing tissue or tumor targeting/specific mCAs; (4) designing visible drug delivery systems and other multifunctional systems in combination with other imaging modes.

Acknowledgements

This work was financially supported by the National Nature Science Foundation of China (20904046, 21174128, 50888001, 21090352), the Doctoral Fund of Ministry of Education of China (20090101120159), the Qianjiang Talent Program of Zhejiang Province, China (2010R10050), and the Program for Changjiang Scholars and Innovative Research Team in University (IRT0942).

References

[1] Lin SP, Brown JJ. MR contrast agents: physical and pharmacologic basics. Journal of Magnetic Resonance Imaging 2007;25:884–99.
[2] Burns M. BIO-TECH report #260. The US market for medical imaging contrast media. Las Vegas, NV: Bio-tech Systems, Inc.; 2006. p. 1–9.
[3] Villaraza AJL, Bumb A, Brechbiel MW. Macromolecules, dendrimers, and nanomaterials in magnetic resonance imaging: the interplay between size, function, and pharmacokinetics. Chemical Reviews 2010;110:2921–59.
[4] Chan KWY, Wong WT. Small molecular gadolinium(III) complexes as MRI contrast agents for diagnostic imaging. Coordination Chemistry Reviews 2007;251:2428–51.
[5] Ye FR, Ke TY, Jeong EK, Wang XL, Sung YG, Johnson M, Lu ZR. Noninvasive visualization of in vivo drug delivery of poly(L-glutamic acid) using contrast-enhanced MRI. Molecular Pharmaceutics 2006;3:507–15.
[6] Caravan P, Ellison JJ, McMurry TJ, Lauffer RB. Gadolinium(III) chelates as MRI contrast agents: structure, dynamics, and applications. Chemical Reviews 1999;99:2293–352.
[7] Pan DPJ, Caruthers SD, Senpan A, Schmieder AH, Wickline SA, Lanza GM. Revisiting an old friend: manganese-based MRI contrast agents. Wires Nanomedicine and Nanobiotechnology 2011;3:162–73.
[8] Yan GP, Robinson L, Hogg P. Magnetic resonance imaging CAs: overview and perspectives. Radiography 2007;13:e5–19.
[9] Sun C, Lee JSH, Zhang MQ. Magnetic nanoparticles in MR imaging and drug delivery. Advanced Drug Delivery Reviews 2008;60:1252–65.
[10] Sosnovik DE, Nahrendorf M, Weissleder R. Magnetic nanoparticles for MR imaging: agents, techniques and cardiovascular applications. Basic Research in Cardiology 2008;103:122–30.
[11] Mornet S, Vasseur S, Grasset F, Duguet E. Magnetic nanoparticle design for medical diagnosis and therapy. Journal of Materials Chemistry 2004;14:2161–75.
[12] Adkins CT, Dobish JN, Brown CS, Mayrsohn B, Hamilton SK, Udoji F, Radford K, Yankeelov TE, Gore JC, Harth E. High relaxivity MRI imaging reagents from bimodal star polymers. Polymer Chemistry 2012;3:390–8.
[13] Kim JI, Chun C, Kim B, Hong JM, Cho JK, Lee SH, Song SC. Thermosensitive/magnetic poly(organophosphazene) hydrogel as a long-term magnetic resonance contrast platform. Biomaterials 2012;33:218–24.
[14] Okada S, Mizukami S, Kikuchi K. Switchable MRI contrast agents based on morphological changes of pH-responsive polymers. Bioorganic and Medicinal Chemistry 2012;20:769–74.
[15] Shi X, Liu X, Wu X, Lu ZR, Li SK, Jeong EK. Ocular pharmacokinetic study using T(1) mapping and Gd-chelate-labeled polymers. Pharmaceutical Research 2011;28:3180–8.
[16] Tallury P, Santra S, Sharma P, Matos BMD, Bengtsson N, Biswas S, Saha AK, Walter GA, Scott EA, Moudgil BM. Fluorescent and paramagnetic chitosan nanoparticles that exhibit high magnetic resonance relaxivity: synthesis, characterization and in vitro studies. Journal of Biomedical Nanotechnology 2011;7:724–9.
[17] Zhang WL, Li N, Huang J, Luo SF, Fan MX, Liu SY, Muir B, Yu JH. Gadolinium-conjugated folate poly(ethylene glycol)-polyamidoamine dendrimer-carboxyl nanoparticles as potential tumor-targeted, circulation-prolonged macromolecular magnetic resonance imaging contrast agents II. Journal of Applied Polymer Science 2011;121:3175–84.
[18] Spanoghe M, Lanens D, Dommisse R, Vanderlinden A, Alderweireldt F. Proton relaxation enhancement by means of serum-albumin and poly-L-lysine labeled with DTPA-Gd(III) – relaxivities as a function of molecular-weight and conjugation efficiency. Magnetic Resonance Imaging 1992;10:913–7.
[19] Kobayashi H, Brechbiel MW. Dendrimer-based macromolecular MRI contrast agents: characteristics and application. Molecular Imaging 2003;2:1–10.
[20] Kobayashi H, Brechbiel MW. Nano-sized MRI contrast agents with dendrimer cores. Advanced Drug Delivery Reviews 2005;57:2271–86.
[21] Langereis S, de Lussanet QG, van Genderen MHP, Backes WH, Meijer EW. Multivalent contrast agents based on gadolinium-diethylenetriaminepentaacetic acid-terminated poly(propylene imine) dendrimers for magnetic resonance imaging. Macromolecules 2004;37:3084–91.
[22] Toth E, van Uffelen I, Helm L, Merbach AE, Ladd D, Briley-Saebo K, Kellar KE. Gadolinium-based linear polymer with temperature-independent proton relaxivities: a unique interplay between the water exchange and rotational contributions. Magnetic Resonance in Chemistry 1998;36:S125–34.
[23] Doble DMJ, Botta M, Wang J, Aime S, Barge A, Raymond KN. Optimization of the relaxivity of MRI contrast agents: effect of poly(ethylene glycol) chains on the water-exchange rates of Gd-III complexes. Journal of the American Chemical Society 2001;123:10758–9.
[24] Margerum LD, Campion BK, Koo M, Shargill N, Lai JJ, Marumoto A, Sontum PC. Gadolinium(III) DO_3A macrocycles and polyethylene glycol coupled to dendrimers – effect of molecular weight on physical and biological properties of macromolecular magnetic resonance imaging contrast agents. Journal of Alloys and Compounds 1997;249:185–90.
[25] Oksendal AN, Hals PA. Biodistribution and toxicity of MR imaging contrast media. Journal of Magnetic Resonance Imaging 1993;3:157–65.
[26] Vexler VS, Clement O, Schmittwillich H, Brasch RC. Effect of varying the molecular-weight of the MR contrast agent Gd-DTPA-polylysine on blood pharmacokinetics and enhancement patterns. Journal of Magnetic Resonance Imaging 1994;4:381–8.
[27] Schuhmann-Giampieri G, Schmitt-Willich H, Frenzel T, Press WR, Weinmann HJ. In vivo and in vitro evaluation of Gd-DTPA-polylysine as a macromolecular contrast agent for magnetic resonance imaging. Investigative Radiology 1991;26:969–74.
[28] Zong Y, Guo J, Ke T, Mohs AM, Parker DL, Lu ZR. Effect of size and charge on pharmacokinetics enhancement of biodegradable and in vivo MRI contrast polydisulfide Gd(III) complexes. Journal of Controlled Release 2006;112:350–6.
[29] Wang XH, Feng Y, Ke TY, Schabel M, Lu ZR. Pharmacokinetics and tissue retention of (Gd-DTPA)-cystamine copolymers, a biodegradable macromolecular magnetic resonance imaging contrast agent. Pharmaceutical Research 2005;22:596–602.
[30] Yan GP, Zhuo RX, Yang YH, Li LY, Liu ML, Ye CH. Tumor-selective macromolecular MRI contrast agents. Journal of Bioactive and Compatible Polymers 2002;17:139–51.
[31] Wen XX, Jackson EF, Price RE, Kim EE, Wu QP, Wallace S, Charnsangavej C, Gelovani JG, Li C. Synthesis and characterization of poly(L-glutamic acid) gadolinium chelate: a new biodegradable MRI contrast agent. Bioconjugate Chemistry 2004;15:1408–15.
[32] Barge A, Tei L, Upadhyaya D, Fedeli F, Beltrami L, Stefania R, Aime S, Cravotto G. Bifunctional ligands based on the DOTA-monoamide cage. Organic & Biomolecular Chemistry 2008;6:1176–84.
[33] Lu ZR, Wang XH, Parker DL, Goodrich KC, Buswell HR. Poly(L-glutamic acid) Gd(III)-DOTA conjugate with a degradable spacer for magnetic resonance imaging. Bioconjugate Chemistry 2003;14:715–9.
[34] Xu RZ, Wang YL, Wang XL, Jeong EK, Parker DL, Lu ZR. In vivo evaluation of a PAMAM-cystamine-(Gd-DO_3A) conjugate as a biodegradable macromolecular MRI contrast agent. Experimental Biology and Medicine 2007;232:1081–9.
[35] Rudovsky J, Botta M, Hermann P, Hardcastle KI, Lukes I, Aime S. PAMAM dendrimeric conjugates with a Gd-DOTA phosphinate derivative and their adducts with polyaminoacids: the interplay of global motion, internal rotation, and fast water exchange. Bioconjugate Chemistry 2006;17:975–87.
[36] Ali MM, Woods M, Caravan P, Opina ACL, Spiller M, Fettinger JC, Sherry AD. Synthesis and relaxometric studies of a dendrimer-based pH-responsive MRI contrast agent. Chemistry: A European Journal 2008;14:7250–8.
[37] Viguier RFH, Hulme AN. A sensitized europium complex generated by micromolar concentrations of copper(I): toward the detection of copper(I) in biology. Journal of the American Chemical Society 2006;128:11370–1.
[38] Prasuhn DE, Yeh RM, Obenaus A, Manchester M, Finn MG. Viral MRI contrast agents: coordination of Gd by native virions and

attachment of Gd complexes by azide-alkyne cycloaddition. Chemical Communications 2007:1269–71.
[39] Mindt TL, Muller C, Stuker F, Salazar JF, Hohn A, Mueggler T, Rudin M, Schibli R. A "click chemistry" approach to the efficient synthesis of multiple imaging probes derived from a single precursor. Bioconjugate Chemistry 2009;20:1940–9.
[40] Bryson JM, Chu WJ, Lee JH, Reineke TM. A beta-cyclodextrin "click cluster" decorated with seven paramagnetic chelates containing two water exchange sites. Bioconjugate Chemistry 2008;19:1505–9.
[41] Aime S, Botta M, Crich SG, Giovenzana G, Palmisano G, Sisti M. Novel paramagnetic macromolecular complexes derived from the linkage of a macrocyclic Gd(III) complex to polyamino acids through a squaric acid moiety. Bioconjugate Chemistry 1999;10:192–9.
[42] Frullano L, Caravan P. Strategies for the preparation of bifunctional gadolinium(III) chelators. Current Organic Synthesis 2011;8:535–65.
[43] Werner EJ, Kozhukh J, Botta M, Moore EG, Avedano S, Aime S, Raymond KN. 1,2-Hydroxypyridonate/terephthalamide complexes of gadolinium(III): synthesis, stability, relaxivity, and water exchange properties. Inorganic Chemistry 2009;48:277–86.
[44] Datta A, Raymond KN. Gd-hydroxypyridinone (HOPO)-based high-relaxivity magnetic resonance imaging (MRI) contrast agents. Accounts of Chemical Research 2009;42:938–47.
[45] Pierre VC, Botta M, Aime S, Raymond KN. Substituent effects on Gd(III)-based MRI contrast agents: optimizing the stability and selectivity of the complex and the number of coordinated water molecules. Inorganic Chemistry 2006;45:8355–64.
[46] Pierre VC, Botta M, Raymond KN. Dendrimeric gadolinium chelate with fast water exchange and high relaxivity at high magnetic field strength. Journal of the American Chemical Society 2005;127:504–5.
[47] Xu J, Franklin SJ, Whisenhunt DW, Raymond KN. Gadolinium complex of tris(3-hydroxy-1-methyl-2-oxo-1,2-didehydropyridine-4-carboxamido)ethyl amine – a new class of gadolinium magnetic-resonance relaxation agents. Journal of the American Chemical Society 1995;117:7245–6.
[48] Floyd WC, Klemm PJ, Smiles DE, Kohlgruber AC, Pierre VC, Mynar JL, Mnar JL, Frechet JMJ, Raymond KN. Conjugation effects of various linkers on Gd(III) MRI contrast agents with dendrimers: optimizing the hydroxypyridinonate (HOPO) ligands with nontoxic, degradable esteramide (EA) dendrimers for high relaxivity. Journal of the American Chemical Society 2011;133:2390–3.
[49] Bai ZW, Zhuo RX. The synthesis and relaxivity of polyesteramide MRI contrast agent. Ion Exchange Adsorption 1996;12:332–8 (in Chinese).
[50] Ouyang M, Zhuo RX, Fu GC. Study on synthesis and relaxivity of paramagnetic polyester metal complexes for MRI. Chinese Journal of Reaction Polymer 1995;4:99–106.
[51] Duarte MG, Gil MH, Peters JA, Colet JM, Vander Elst L, Muller RN, Geraldes CFGC. Synthesis, characterization, and relaxivity of two linear Gd(DTPA)-polymer conjugates. Bioconjugate Chemistry 2001;12:170–7.
[52] Lu ZR, Parker DL, Goodrich KC, Wang XH, Dalle JG, Buswell HR. Extracellular biodegradable macromolecular gadolinium(III) complexes for MRI. Magnetic Resonance in Medicine 2004;51:27–34.
[53] Mohs AM, Zong YD, Guo JY, Parker DL, Lu ZR. PEG-g-poly(GdDTPA-co-L-cystine): effect of PEG chain length on in vivo contrast enhancement in MRI. Biomacromolecules 2005;6:2305–11.
[54] Lucas RL, Benjamin M, Reineke TM. Comparison of a tartaric acid derived polymeric MRI contrast agent to a small molecule model chelate. Bioconjugate Chemistry 2008;19:24–7.
[55] Ladd DL, Hollister R, Peng X, Wei D, Wu G, Delecki D, Snow RA, Toner JL, Kellar K, Eck J, Desai VC, Raymond G, Kinter LB, Desser TS, Rubin DL. Polymeric gadolinium chelate magnetic resonance imaging contrast agents: design, synthesis, and properties. Bioconjugate Chemistry 1999;10:361–70.
[56] Mohs AM, Wang XH, Goodrich KC, Zong YD, Parker DL, Lu ZR. PEG-g-poly(GdDTPA-co-L-cystine): a biodegradable macromolecular blood pool contrast agent for MR imaging. Bioconjugate Chemistry 2004;15:1424–30.
[57] Sieving PF, Watson AD, Rocklage SM. Preparation and characterization of paramagnetic polychelates and their protein conjugates. Bioconjugate Chemistry 1990;1:65–71.
[58] Desser TS, Rubin DL, Muller HH, Qing F, Khodor S, Zanazzi G, Young SW, Ladd DL, Wellons JA, Kellar KE, Toner JL, Snow RA. Dynamics of tumor imaging with Gd-DTPA polyethylene-glycol polymers – dependence on molecular-weight. Journal of Magnetic Resonance Imaging 1994;4:467–72.
[59] Adam G, Neuerburg J, Spuntrup E, Muhler A, Scherer K, Gunther RW. Dynamic contrast-enhanced MR-imaging of the upper abdomen – enhancement properties of gadobutrol, gadolinium-DTPA-polylysine, and gadolinium-DTPA-cascade-polymer. Magnetic Resonance in Medicine 1994;32:622–8.
[60] Bock JC, Kaufmann F, Felix R. Comparison of gadolinium-DTPA and macromolecular gadolinium-DTPA-polylysine for contrast-enhanced pulmonary time-of-flight magnetic resonance angiography. Investigative Radiology 1996;31:652–7.
[61] Mäurer J, Knollmann FD, Veuskens C, Ebert W, Bauer H, Felix R. Contrast enhanced high resolution MRI of cutaneous melanomas using Gd-DTPA and Gd-DTPA-polylysine: experimental results. Skin Research and Technology 1998;4:49–53.
[62] Uzgiris EE, Cline H, Moasser B, Grimmond B, Amaratunga M, Smith JF, Goddard G. Conformation and structure of polymeric contrast agents for medical imaging. Biomacromolecules 2004;5:54–61.
[63] Aime S, Botta M, Crich SG, Giovenzana G, Palmisano G, Sisti M. A macromolecular Gd(III) complex as pH-responsive relaxometric probe for MRI applications. Chemical Communications 1999:1577–8.
[64] Aime S, Fedeli F, Sanino A, Terreno E. A R2/R1 ratiometric procedure for a concentration-independent, pH-responsive, Gd(III)-based MRI agent. Journal of the American Chemical Society 2006;128:11326–7.
[65] Zarabi B, Nan A, Zhuo J, Gullapalli R, Ghandehari H. Macrophage targeted N-(2-hydroxypropyl)methacrylamide conjugates for magnetic resonance imaging. Molecular Pharmaceutics 2006;3:550–7.
[66] Wang YL, Ye FR, Jeong EK, Sun Y, Parker DL, Lu ZR. Noninvasive visualization of pharmacokinetics, biodistribution and tumor targeting of poly[N-(2-hydroxypropyl)methacrylamide] in mice using contrast enhanced MRI. Pharmaceutical Research 2007;24:1208–16.
[67] Lee HY, Jee HW, Seo SM, Kwak BK, Khang G, Cho SH. Diethylenetriaminepentaacetic acid-gadolinium (DTPA-Gd)-conjugated polysuccinimide derivatives as magnetic resonance imaging contrast agents. Bioconjugate Chemistry 2006;17:700–6.
[68] Bogdanov AA, Weissleder R, Frank HW, Bogdanova AV, Nossif N, Schaffer BK, Tsai E, Papisov MI, Brady TJ. A new macromolecule as a contrast agent for MR-angiography – preparation, properties, and animal studies. Radiology 1993;187:701–6.
[69] Li C, Wallace S. Polymer–drug conjugates: recent development in clinical oncology. Advanced Drug Delivery Reviews 2008;60:886–98.
[70] Li C. Poly(L-glutamic acid) – anticancer drug conjugates. Advanced Drug Delivery Reviews 2002;54:695–713.
[71] Jain GL, Ray AR. Syntheses and characterization of random copolymers of aspartic-acid with lactic-acid and glycolic acid. Makromolekulare Chemie 1981;182:2557–61.
[72] Giammona G, Carlisi B, Palazzo S. Reaction of alpha,beta-poly(n-hydroxyethyl)-DL-aspartamide with derivatives of carboxylic-acids. Journal of Polymer Science Part A: Polymer Chemistry 1987;25:2813–8.
[73] Kopecek J, Kopeckova P. HPMA copolymers: origins, early developments, present, and future. Advanced Drug Delivery Reviews 2010;62:122–49.
[74] Ulbrich K, Subr V. Structural and chemical aspects of HPMA copolymers as drug carriers. Advanced Drug Delivery Reviews 2010;62:150–66.
[75] Duncan R, Vicent MJ. Do HPMA copolymer conjugates have a future as clinically useful nanomedicines? A critical overview of current status and future opportunities. Advanced Drug Delivery Reviews 2010;62:272–82.
[76] Xu QL, Zhu LT, Yu MH, Feng FD, An LL, Xing CF, Wang S. Gadolinium(III) chelated conjugated polymer as a potential MRI contrast agent. Polymer 2010;51:1336–40.
[77] Zong YD, Wang XH, Goodrich KC, Mohs AM, Parker DL, Lu ZR. Contrast-enhanced MRI with new biodegradable macromolecular Gd(III) complexes in tumor-bearing mice. Magnetic Resonance in Medicine 2005;53:835–42.
[78] Franano FN, Edwards WB, Welch MJ, Brechbiel MW, Gansow OA, Duncan JR. Biodistribution and metabolism of targeted and non-targeted protein-chelate-gadolinium complexes – evidence for gadolinium dissociation in vitro and in vivo. Magnetic Resonance Imaging 1995;13:201–14.
[79] Casali C, Janier M, Canet E, Obadia JF, Benderbous S, Corot C, Revel D. Evaluation of Gd-DOTA-labeled dextran polymer as an intravascular MR contrast agent for myocardial perfusion. Academic Radiology 1998;5:S214–8.
[80] Caravan P, Parigi G, Chasse JM, Cloutier NJ, Ellison JJ, Lauffer RB, Luchinat C, McDermid SA, Spiller M, McMurry TJ. Albumin binding,

relaxivity, and water exchange kinetics of the diastereoisomers of MS-325, a gadolinium(III)-based magnetic resonance angiography contrast agent. Inorganic Chemistry 2007;46:6632–9.
[81] Ou MH, Tu CH, Tsai SC, Lee WT, Liu GC, Wang YM. Synthesis and physicochemical characterization of two gadolinium(III) TTDA-like complexes and their interaction with human serum albumin. Inorganic Chemistry 2006;45:244–54.
[82] Armitage FE, Richardson DE, Li KC. Polymeric contrast agents for magnetic resonance imaging: synthesis and characterization of gadolinium diethylenetriaminepentaacetic acid conjugated to polysaccharides. Bioconjugate Chemistry 1990;1:365–74.
[83] Helbich TH, Gossman A, Mareski PA, Raduchel B, Roberts TPL, Shames DM, Muhler M, Turetschek K, Brasch RC. A new polysaccharide macromolecular contrast agent for MR imaging: biodistribution and imaging characteristics. Journal of Magnetic Resonance Imaging 2000;11:694–701.
[84] Lebduskova P, Kotek J, Hermann P, Elst LV, Muller RN, Lukes I, Peters JA. A gadolinium(III) complex of a carboxylic-phosphorus acid derivative of diethylenetriamine covalently bound to inulin, a potential macromolecular MRI contrast agent. Bioconjugate Chemistry 2004;15:881–9.
[85] Rebizak R, Schaefer M, Dellacherie E. Polymeric conjugates of Gd(III)-diethylenetriaminepentaacetic acid and dextran. 1. Synthesis, characterization, and paramagnetic properties. Bioconjugate Chemistry 1997;8:605–10.
[86] Rebizak R, Schaefer M, Dellacherie E. Polymeric conjugates of Gd(III)-diethylenetriaminepentaacetic acid and dextran. 2. Influence of spacer arm length and conjugate molecular mass on the paramagnetic properties and some biological parameters. Bioconjugate Chemistry 1998;9:94–9.
[87] Song Y, Kohlmeir EK, Meade TJ. Synthesis of multimeric MR contrast agents for cellular imaging. Journal of the American Chemical Society 2008;130:6662–3.
[88] Bryson JM, Chu WJ, Lee JH, Reineke TM. A beta-cyclodextrin "Click Cluster" decorated with seven paramagnetic chelates containing two water exchange sites. Bioconjugate Chemistry 2008;19:1505–9.
[89] Battistini E, Gianolio E, Gref R, Couvreur P, Fuzerova S, Othman M, Aime S, Badet B, Durand P. High-relaxivity magnetic resonance imaging (MRI) contrast agent based on supramolecular assembly between a gadolinium chelate, a modified dextran, and poly-beta-cyclodextrin. Chemistry: A European Journal 2008;14:4551–61.
[90] Aime S, Gianolio E, Uggeri F, Tagliapietra S, Barge A, Cravotto G. New paramagnetic supramolecular adducts for MRI applications based on non-covalent interactions between Gd(III)-complexes and beta- or gamma-cyclodextrin units anchored to chitosan. Journal of Inorganic Biochemistry 2006;100:931–8.
[91] Medina SH, El-Sayed MEH. Dendrimers as carriers for delivery of chemotherapeutic agents. Chemical Reviews 2009;109:3141–57.
[92] Kobayashi H, Jo SK, Kawamoto S, Yasuda H, Hu XZ, Knopp MV, Brechbiel MW, Choyke PL, Star RA. Polyamine dendrimer-based MRI contrast agents for functional kidney imaging to diagnose acute renal failure. Journal of Magnetic Resonance Imaging 2004;20:512–8.
[93] Boas U, Heegaard PMH. Dendrimers in drug research. Chemical Society Reviews 2004;33:43–63.
[94] Zinselmeyer BH, Mackay SP, Schatzlein AG, Uchegbu IF. The lower-generation polypropylenimine dendrimers are effective gene-transfer agents. Pharmaceutical Research 2002;19:960–7.
[95] Malik N, Wiwattanapatapee R, Klopsch R, Lorenz K, Frey H, Weener JW, Meijer EM, Paulus W, Duncan R. Dendrimers: relationship between structure and biocompatibility in vitro, and preliminary studies on the biodistribution of ^{125}I-labelled polyamidoamine dendrimers in vivo. Journal of Controlled Release 2000;65:133–48.
[96] Rittner K, Benavente A, Bompard-Sorlet A, Heitz F, Divita G, Brasseur R, Jacobs E. New basic membrane-destabilizing peptides for plasmid-based gene delivery in vitro and in vivo. Molecular Therapy 2002;5:104–14.
[97] Roberts JC, Bhalgat MK, Zera RT. Preliminary biological evaluation of polyamidoamine (PAMAM) Starburst (TM) dendrimers. Journal of Biomedical Materials Research 1996;30:53–65.
[98] Svenson S, Tomalia DA. Commentary – dendrimers in biomedical applications – reflections on the field. Advanced Drug Delivery Reviews 2005;57:2106–29.
[99] Misselwitz B, Schmitt-Willich H, Ebert W, Frenzel T, Weinmann HJ. Pharmacokinetics of Gadomer-17, a new dendritic magnetic resonance contrast agent. Magnetic Resonance Materials in Physics, Biology and Medicine 2001;12:128–34.
[100] Dong Q, Hurst DR, Weinmann HJ, Chenevert TL, Londy FJ, Prince MR. Magnetic resonance angiography with gadomer-17 – an animal study original investigation. Investigative Radiology 1998;33:699–708.
[101] Fu YJ, Raatschen HJ, Nitecki DE, Wendland MF, Novikov V, Fournier LS, Cyran C, Rogut V, Shames DM, Brasch RC. Cascade polymeric MRI contrast media derived from poly(ethylene glycol) cores: initial syntheses and characterizations. Biomacromolecules 2007;8:1519–29.
[102] Kaneshiro TL, Jeong EK, Morrell G, Parker DL, Lu ZR. Synthesis and evaluation of globular Gd-DOTA-monoamideconjugates with precisely controlled nanosizes for magnetic resonance angiography. Biomacromolecules 2008;9:2742–8.
[103] Tan M, Ye Z, Jeong EK, Wu X, Parker DL, Lu ZR. Synthesis and evaluation of nanoglobular macrocyclic Mn(II) chelate conjugates as non-gadolinium(III) MRI contrast agents. Bioconjugate Chemistry 2011;22:931–7.
[104] Jaszberenyi Z, Moriggi L, Schmidt P, Weidensteiner C, Kneuer R, Merbach AE, Helm L, Toth E. Physicochemical and MRI characterization of Gd^{3+}-loaded polyamidoamine and hyperbranched dendrimers. Journal of Biological Inorganic Chemistry 2007;12:406–20.
[105] Sideratou Z, Tsiourvas D, Theodossiou T, Fardis M, Paleos CM. Synthesis and characterization of multifunctional hyperbranched polyesters as prospective contrast agents for targeted MRI. Bioorganic and Medicinal Chemistry Letters 2010;20:4177–81.
[106] Chen WT, Thirumalai D, Shih TTF, Chen RC, Tu SY, Lin CI, Yang PC. Dynamic contrast-enhanced folate-receptor-targeted MR imaging using a Gd-loaded PEG-dendrimer-folate conjugate in a mouse xenograft tumor model. Molecular Imaging and Biology 2010;12:145–54.
[107] Zhang G, Zhang R, Wen X, Li L, Li C. Micelles based on biodegradable poly(L-glutamic acid)-b-polylactide with paramagnetic Gd ions chelated to the shell layer as a potential nanoscale MRI–visible delivery system. Biomacromolecules 2007;9:36–42.
[108] Reynolds CH, Annan N, Beshah K, Huber JH, Shaber SH, Lenkinski RE, Wortman JA. Gadolinium-loaded nanoparticles: new contrast agents for magnetic resonance imaging. Journal of the American Chemical Society 2000;122:8940–5.
[109] Turner JL, Pan DPJ, Plummer R, Chen ZY, Whittaker AK, Wooley KL. Synthesis of gadolinium-labeled shell-crosslinked nanoparticles for magnetic resonance imaging applications. Advanced Functional Materials 2005;15:1248–54.
[110] Gong P, Chen ZY, Chen YY, Wang W, Wang XS, Hu AG. High-relaxivity MRI contrast agents prepared from miniemulsion polymerization using gadolinium(III)-based metallosurfactants. Chemical Communications 2011;47:4240–2.
[111] Cheng ZL, Thorek DLJ, Tsourkas A. Gadolinium-conjugated dendrimer nanoclusters as a tumor-targeted T-1 magnetic resonance imaging contrast agent. Angewandte Chemie International Edition 2010;49:346–50.
[112] Kaida S, Cabral H, Kumagai M, Kishimura A, Terada Y, Sekino M, Aoki I, Nishiyama N, Tani T, Kataoka K. Visible drug delivery by supramolecular nanocarriers directing to single-platformed diagnosis and therapy of pancreatic tumor model. Cancer Research 2010;70:7031–41.
[113] Nakamura E, Makino K, Okano T, Yamamoto T, Yokoyama M. A polymeric micelle MRI contrast agent with changeable relaxivity. Journal of Controlled Release 2006;114:325–33.
[114] Shiraishi K, Kawano K, Maitani Y, Yokoyama M. Polyion complex micelle MRI contrast agents from poly(ethylene glycol)-b-poly(L-lysine) block copolymers having Gd-DOTA; preparations and their control of T(1)-relaxivities and blood circulation characteristics. Journal of Controlled Release 2010;148:160–7.
[115] Shiraishi K, Kawano K, Minowa T, Maitani Y, Yokoyama M. Preparation and in vivo imaging of PEG-poly(L-lysine)-based polymeric micelle MRI contrast agents. Journal of Controlled Release 2009;136:14–20.
[116] Longmire MR, Ogawa M, Choyke PL, Kobayashi H. Biologically optimized nanosized molecules and particles: more than just size. Bioconjugate Chemistry 2011;22:993–1000.
[117] Kobayashi H, Brechbiel MW. Dendrimer-based nanosized MRI contrast agents. Current Pharmaceutical Biotechnology 2004;5:539–49.
[118] Choyke PL, Kobayashi H. Functional magnetic resonance imaging of the kidney using macromolecular contrast agents. Abdominal Imaging 2006;31:224–31.
[119] Wiener EC, Brechbiel MW, Brothers H, Magin RL, Gansow OA, Tomalia DA, Lauterbur PC. Dendrimer-based metal-chelates – a new class

of magnetic-resonance-imaging contrast agents. Magnetic Resonance in Medicine 1994;31:1–8.
[120] Sato N, Kobayashi H, Hiraga A, Saga T, Togashi K, Konishi J, Brechbiel MW. Pharmacokinetics and enhancement patterns of macromolecular MR contrast agents with various sizes of polyamidoamine dendrimer cores. Magnetic Resonance in Medicine 2001;46:1169–73.
[121] Kobayashi H, Sato N, Hiraga A, Saga T, Nakamoto Y, Ueda H, Konishi J, Togashi K, Brechbiel MW. 3D-micro-MR angiography of mice using macromolecular MR contrast agents with polyamidoamine dendrimer core with reference to their pharmacokinetic properties. Magnetic Resonance in Medicine 2001;45:454–60.
[122] Kobayashi H, Kawamoto S, Saga T, Sato N, Hiraga A, Konishi J, Togashi K, Brechbiel MW. Micro-MR angiography of normal and intratumoral vessels in mice using dedicated intravascular MR contrast agents with high generation of polyamidoamine dendrimer core: reference to pharmacokinetic properties of dendrimer-based MR contrast agents. Journal of Magnetic Resonance Imaging 2001;14:705–13.
[123] Kobayashi H, Sato N, Kawamoto S, Saga T, Hiraga A, Ishimori T, Togashi K, Konishi J, Brechbiel MW. 3D MR angiography of intratumoral vasculature using a novel macromolecular MR contrast agent. Magnetic Resonance in Medicine 2001;46:579–85.
[124] Shirakawa K, Kobayashi H, Heike Y, Kawamoto S, Brechbiel MW, Kasumi F, Lwanaga T, Konishi F, Terada M, Wakasugi H. Hemodynamics in vasculogenic mimicry and angiogenesis of inflammatory breast cancer xenograft. Cancer Research 2002;62:560–6.
[125] Kobayashi H, Shirakawa K, Kawamoto S, Saga T, Sato N, Hiraga A, Watanabe L, Heike Y, Togashi K, Konishi J, Brechbiel MW, Wakasugi H. Rapid accumulation and internalization of radiolabeled herceptin in an inflammatory breast cancer xenograft with vasculogenic mimicry predicted by the contrast-enhanced dynamic MRI with the macromolecular contrast agent G6-(1B4M-Gd)(256). Cancer Research 2002;62:860–6.
[126] Kobayashi H, Kawamoto S, Saga T, Sato N, Hiraga A, Ishimori T, Akita Y, Mamede MH, Togashi K, Konishi J. Novel liver macromolecular MR contrast agent with a polypropylenimine diaminobutyl dendrimer core: comparison to the vascular MR contrast agent with the polyamidoamine dendrimer core. Magnetic Resonance in Medicine 2001;46:795–802.
[127] Owens 3rd DE, Peppas NA. Opsonization, biodistribution, and pharmacokinetics of polymeric nanoparticles. International Journal of Pharmaceutics 2006;307:93–102.
[128] Kaminskas LM, Boyd BJ, Karellas P, Krippner GY, Lessene R, Kelly B, Porter CJH. The impact of molecular weight and PEG chain length on the systemic pharmacokinetics of PEGylated poly L-lysine dendrimers. Molecular Pharmaceutics 2008;5:449–63.
[129] Kobayashi H, Kawamoto S, Saga T, Sato N, Hiraga A, Ishimori T, Togashi K, Konishi J, Brechbiel MW. Positive effects of polyethylene glycol conjugation to generation-4 polyamidoamine dendrimers as macromolecular MR contrast agents. Magnetic Resonance in Medicine 2001;46:781–8.
[130] Sadekar S, Ray A, Janat-Amsbury M, Peterson CM, Ghandehari H. Comparative biodistribution of PAMAM dendrimers and HPMA copolymers in ovarian-tumor-bearing mice. Biomacromolecules 2011;12:88–96.
[131] Geng Y, Dalhaimer P, Cai S, Tsai R, Tewari M, Minko T, Discher DE. Shape effects of filaments versus spherical particles in flow and drug delivery. Nature Nanotechnology 2007;2:249–55.
[132] Kobayashi H, Sato N, Kawamoto S, Saga T, Hiraga A, Haque TL, Ishimori T, Konishi J, Togashi K, Brechbiel MW. Comparison of the macromolecular MR contrast agents with ethylenediamine-core versus ammonia-core generation-6 polyamidoamine dendrimer. Bioconjugate Chemistry 2001;12:100–7.
[133] Vander Elst L, Raynal I, Port M, Tisnes P, Muller RN. In vitro relaxometric and luminescence characterization of P792 (Gadomelitol, Vistarem((R))), an efficient and rapid clearance blood pool MRI contrast agent. European Journal of Inorganic Chemistry 2005: 1142–8.
[134] Nguyen TD, Spincemaille P, Vaidya A, Prince MR, Lu ZR, Wang Y. Contrast-enhanced magnetic resonance angiography with biodegradable (Gd-DTPA)-cystamine copolymers: comparison with MS-325 in a swine model. Molecular Pharmaceutics 2006;3:558–65.
[135] Maeda H, Wu J, Sawa T, Matsumura Y, Hori K. Tumor vascular permeability and the EPR effect in macromolecular therapeutics: a review. Journal of Controlled Release 2000;65:271–84.
[136] Hanahan D, Weinberg RA. Hallmarks of cancer: the next generation. Cell 2011;144:646–74.
[137] Zhao M, Yang M, Li XM, Jiang P, Baranov E, Li SK, Xu MX, Penman S, Hoffman RM. Tumor-targeting bacterial therapy with amino acid auxotrophs of GFP-expressing *Salmonella typhimurium*. Proceedings of the National Academy of Sciences of the United States of America 2005;102:755–60.
[138] Fang J, Nakamura H, Maeda H. The EPR effect: unique features of tumor blood vessels for drug delivery, factors involved, and limitations and augmentation of the effect. Advanced Drug Delivery Reviews 2011;63:136–51.
[139] Daldrup H, Shames DM, Wendland M, Okuhata Y, Link TM, Rosenau W, Lu Y, Brasch RC. Correlation of dynamic contrast-enhanced MR imaging with histologic tumor grade: comparison of macromolecular and small-molecular contrast media. American Journal of Roentgenology 1998;171:941–9.
[140] Gossmann A, Okuhata Y, Shames DM, Helbich TH, Roberts TPL, Wendland MF, Huber S, Brasch RC. Prostate cancer tumor grade differentiation with dynamic contrast-enhanced MR imaging in the rat: comparison of macromolecular and small-molecular contrast media – preliminary experience. Radiology 1999;213:265–72.
[141] Feng Y, Jeong EK, Mohs AM, Emerson L, Lu ZR. Characterization of tumor angiogenesis with dynamic contrast-enhanced MRI and biodegradable macromolecular contrast agents in mice. Magnetic Resonance in Medicine 2008;60:1347–52.
[142] Gossmann A, Helbich TH, Kuriyama N, Ostrowitzki S, Roberts TPL, Shames DM, van Bruggen N, Wendland MF, Israel MA, Brasch RC. Dynamic contrast-enhanced magnetic resonance imaging as a surrogate marker of tumor response to anti-angiogenic therapy in a xenograft model of glioblastoma multiforme. Journal of Magnetic Resonance Imaging 2002;15:233–40.
[143] Pham CD, Roberts TPL, van Bruggen N, Melnyk O, Mann J, Ferrara N, Cohen RL, Brasch RC. Magnetic resonance imaging detects suppression of tumor vascular permeability after administration of antibody to vascular endothelial growth factor. Cancer Investigation 1998;16:225–30.
[144] Cyran CC, Fu YJ, Raatschen HJ, Rogut V, Chaopathomkul B, Shames DM, Wendland MF, Yeh BM, Brasch RC. New macromolecular polymeric MRI contrast agents for application in the differentiation of cancer from benign soft tissues. Journal of Magnetic Resonance Imaging 2008;27:581–9.
[145] Barrett T, Kobayashi H, Brechbiel M, Choyke PL. Macromolecular MRI contrast agents for imaging tumor angiogenesis. European Journal of Radiology 2006;60:353–66.
[146] Barrett T, Brechbiel M, Bernardo M, Choyke PL. MRI of tumor angiogenesis. Journal of Magnetic Resonance Imaging 2007;26:235–49.
[147] Turetschek K, Huber S, Floyd E, Helbich T, Roberts TPL, Shames DM, Tarlo KS, Wendland MF, Brasch RC. MR imaging characterization of microvessels in experimental breast tumors by using a particulate contrast agent with histopathologic correlation. Radiology 2001;218:562–9.
[148] vanDijke CF, Brasch RC, Roberts TPL, Weidner N, Mathur A, Shames DM, Mann JS, Demsar F, Lang P, Schwickert HC. Mammary carcinoma model: correlation of macromolecular contrast-enhanced MR imaging characterizations of tumor microvasculature and histologic capillary density. Radiology 1996;198:813–8.
[149] Kobayashi H, Reijnders K, English S, Yordanov AT, Milenic DE, Sowers AL, Citrin D, Krishna MC, Waldmann TA, Mitchell JB, Brechbiel MW. Application of a macromolecular contrast agent for detection of alterations of tumor vessel permeability induced by radiation. Clinical Cancer Research 2004;10:7712–20.
[150] Byrne JD, Betancourt T, Brannon-Peppas L. Active targeting schemes for nanoparticle systems in cancer therapeutics. Advanced Drug Delivery Reviews 2008;60:1615–26.
[151] Konda SD, Aref M, Wang S, Brechbiel M, Wiener EC. Specific targeting of folate-dendrimer MRI contrast agents to the high affinity folate receptor expressed in ovarian tumor xenografts. Magnetic Resonance Materials in Physics, Biology and Medicine 2001;12:104–13.
[152] Wiener EC, Konda S, Shadron A, Brechbiel M, Gansow O. Targeting dendrimer-chelates to tumors and tumor cells expressing the high-affinity folate receptor. Investigative Radiology 1997;32:748–54.
[153] Erdogan S, Medarova ZO, Roby A, Moore A, Torchilin VP. Enhanced tumor MR imaging with gadolinium-loaded polychelating polymer-containing tumor-targeted liposomes. Journal of Magnetic Resonance Imaging 2008;27:574–80.
[154] Lee JH, Engler JA, Collawn JF, Moore BA. Receptor mediated uptake of peptides that bind the human transferrin receptor. European Journal of Biochemistry 2001;268:2004–12.
[155] Han LA, Li JF, Huang SX, Huang RQ, Liu SH, Hu X, Yi PW, Shan D, Wang XX, Lei H, Jiang C. Peptide-conjugated polyamidoamine

dendrimer as a nanoscale tumor-targeted T1 magnetic resonance imaging contrast agent. Biomaterials 2011;32:2989–98.
[156] Schuhmanngiampieri G, Schmittwillich H, Frenzel T. Biliary-excretion and pharmacokinetics of a Gadolinium chelate used as a liver-specific contrast agent for magnetic-resonance-imaging in the rat. Journal of Pharmaceutical Sciences 1993;82:799–803.
[157] Schuhmanngiampieri G, Schmittwillich H, Press WR, Negishi C, Weinmann HJ, Speck U. Preclinical evaluation of Gd-EOB-DTPA as a contrast agent in MR imaging of the hepatobiliary system. Radiology 1992;183:59–64.
[158] Hamm B, Staks T, Muhler A, Bollow M, Taupitz M, Frenzel T, Wolf KJ, Weinmann HJ, Lange L. Phase-I clinical-evaluation of Gd-EOB-DTPA as a hepatobiliary MR contrast agent – safety, pharmacokinetics, and MR-imaging. Radiology 1995;195:785–92.
[159] Reimer P, Rummeny EJ, Shamsi K, Balzer T, Daldrup HE, Tombach B, Hesse T, Berns T, Peters PE. Phase II clinical evaluation of Gd-EOB-DTPA: dose, safety aspects, and pulse sequence. Radiology 1996;199:177–83.
[160] Vogl TJ, Kummel S, Hammerstingl R, Schellenbeck M, Schumacher G, Balzer T, Schwarz W, Muller PK, Bechstein WO, Mack MG, Sollner O, Felix R. Liver tumors: comparison of MR imaging with Gd-EOB-DTPA and Gd-DTPA. Radiology 1996;200:59–67.
[161] Kobayashi H, Saga T, Kawamoto S, Sato N, Hiraga A, Ishimori T, Konishi J, Togashi K, Brechbiel MW. Dynamic micro-magnetic resonance imaging of liver micrometastasis in mice with a novel liver macromolecular magnetic resonance contrast agent DAB-Am64-(1B4M-Gd)(64). Cancer Research 2001;61:4966–70.
[162] Fu YJ, Zhuo RX. Studies on hepatocyte-targeting magnetic resonance imaging macromolecular contrast media. Chemical Research in Chinese Universities 1997;13:336–43.
[163] Zhuo RX, Fu YJ, Liao J. Synthesis, relaxivity and biodistribution of novel magnetic resonance imaging (MRI) contrast agents: polylysine (Gd-DTPA/DOTA) with pendent galactose moieties as hepatocyte-targeting groups. Chinese Chemical Letters 1997;8:157–60.
[164] Luo K, Liu G, He B, Wu Y, Gong QY, Song B, Ai H, Gu ZW. Multifunctional gadolinium-based dendritic macromolecules as liver targeting imaging probes. Biomaterials 2011;32:2575–85.
[165] Kobayashi H, Kawamoto S, Jo SK, Sato N, Saga T, Hiraga A, Konishi J, Hu S, Togashi K, Brechbiel MW, Star RA. Renal tubular damage detected by dynamic micro-MRI with a dendrimer-based magnetic resonance contrast agent. Kidney International 2002;61:1980–5.
[166] Kobayashi H, Kawamoto S, Star RA, Waldmann TA, Tagaya Y, Brechbiel MW. Micro-magnetic resonance lymphangiography in mice using a novel dendrimer-based magnetic resonance imaging contrast agent. Cancer Research 2003;63:271–6.
[167] Kobayashi H, Kawamoto S, Sakai Y, Choyke PL, Star RA, Brechbiel MW, Sato N, Tagaya Y, Morris JC, Waldmann TA. Lymphatic drainage imaging of breast cancer in mice by micro-magnetic resonance lymphangiography using a nano-size paramagnetic contrast agent. Journal of the National Cancer Institute 2004;96:703–8.
[168] Misselwitz B, Schmitt-Willich H, Michaelis M, Oellinger JJ. Interstitial magnetic resonance lymphography using a polymeric T1 contrast agent – initial experience with gadomer-17. Investigative Radiology 2002;37:146–51.
[169] Kobayashi H, Kawamoto S, Choyke PL, Sato N, Knopp MV, Star RA, Waldmann TA, Tagaya Y, Brechbiel MW. Comparison of dendrimer-based macromolecular contrast agents for dynamic micro-magnetic resonance lymphangiography. Magnetic Resonance in Medicine 2003;50:758–66.
[170] Hong GB, Yuan RX, Liang BL, Shen J, Yang XQ, Shuai XT. Folate functionalized polymeric micelle as hepatic carcinoma-targeted, MRI-ultrasensitive delivery system of antitumor drugs. Biomedical Microdevices 2008;10:693–700.
[171] Guthi JS, Yang SG, Huang G, Li SZ, Khemtong C, Kessinger CW, Peyton M, Minna JD, Brown KC, Gao JM. MRI–visible micellar nanomedicine for targeted drug delivery to lung cancer cells. Molecular Pharmaceutics 2010;7:32–40.
[172] Shubayev VI, Pisanic TR, Jin SH. Magnetic nanoparticles for theragnostics. Advanced Drug Delivery Reviews 2009;61:467–77.
[173] Lammers T, Kiessling F, Hennink WE, Storm G. Nanotheranostics and image-guided drug delivery: current concepts and future directions. Molecular Pharmaceutics 2010;7:1899–912.
[174] Vaidya A, Sun YG, Feng Y, Emerson L, Jeong EK, Lu ZR. Contrast-enhanced MRI-guided photodynamic cancer therapy with a pegylated bifunctional polymer conjugate. Pharmaceutical Research 2008;25:2002–11.
[175] Wang D, Miller SC, Liu XM, Anderson B, Wang XS, Goldring SR. Novel dexamethasone-HPMA copolymer conjugate and its potential application in treatment of rheumatoid arthritis. Arthritis Research and Therapy 2007;9. R2/1–9.
[176] Liu XM, Quan LD, Tian J, Alnouti Y, Fu K, Thiele GM, Wang D. Synthesis and evaluation of a well-defined HPMA copolymer-dexamethasone conjugate for effective treatment of rheumatoid arthritis. Pharmaceutical Research 2008;25:2910–9.
[177] Liu XM, Miller SC, Wang D. Beyond oncology – application of HPMA copolymers in non-cancerous diseases. Advanced Drug Delivery Reviews 2010;62:258–71.